

**INVESTIGATION OF LITHIUM SALT-NONIONIC  
SURFACTANT MESOPHASES AND THEIR APPLICATIONS IN  
SOLAR CELLS AS GEL ELECTROLYTE**

A THESIS

SUBMITTED TO THE DEPARTMENT OF CHEMISTRY  
AND THE GRADUATE SCHOOL OF ENGINEERING AND SCIENCE  
OF BILKENT UNIVERSITY

IN PARTIAL FULFILLMENT OF THE REQUIREMENTS

FOR THE DEGREE OF  
MASTER OF SCIENCE

By  
GÖZDE BARIM

July, 2013

I certify that I have read this thesis and that in my opinion it is fully adequate, in scope and in quality, as a thesis for the degree of Master of Science.

.....

Prof. Dr. Ömer Dağ (Advisor)

I certify that I have read this thesis and that in my opinion it is fully adequate, in scope and in quality, as a thesis for the degree of Master of Science.

.....

Prof. Dr. Nihal Aydoğan

I certify that I have read this thesis and that in my opinion it is fully adequate, in scope and in quality, as a thesis for the degree of Master of Science.

.....

Assoc. Prof. Dr. Margarita Kantcheva

Approved for the Graduate School of Engineering and Science:

.....

Prof. Dr. Levent Onural

Director of the Graduate School

## **ABSTRACT**

### **INVESTIGATION OF LITHIUM SALT-NONIONIC SURFACTANT MESOPHASES AND THEIR APPLICATIONS IN SOLAR CELLS AS GEL ELECTROLYTE**

**Gözde Barım**

**M.S. in Department of Chemistry**

**Supervisor: Prof. Dr. Ömer Dağ**

**July, 2013**

Some salts and some nonionic surfactants self-assemble together into lyotropic liquid crystalline (LLC) mesophases. The salt can be either in aqueous solution phase or in its molten phase in the self-assembly process. Concentrated aqueous solutions of lithium salts (LiCl, LiBr, or LiI) and pluronics (triblock copolymers, such as P65, P85, P103, or P123) or 10-lauryl ether ( $C_{12}H_{25}(CH_2CH_2O)_{10}OH$ , denoted as  $C_{12}EO_{10}$ ) type nonionic surfactant mesophases were investigated in this thesis work. The LLC mesophases are well ordered between 5.0 and 25.0 salt/pluronic and 2.0 and 10.0 salt/ $C_{12}EO_{10}$  mole ratios, and remain stable for months under the ambient conditions. The water molecules remain as the hydrates under open atmosphere in the LLC mesophases of lithium salts-nonionic surfactants. The lithium salt-pluronic LLC mesophases are birefringent and have a hexagonal mesophase in a broad range of salt concentrations. The unit cell of the mesophases increases and a transition from the hexagonal to a cubic mesophases occurs upon increasing the salt content of the media. Moreover the LLC mesophases are ordered and stable up to 25.0 salt to pluronic mole ratio. At higher salt content, one can observe either a disordered phase or co-existence of salt crystals and mesophase.

There is a big demand on the gel electrolytes for dye sensitized solar cells (DSSC) in order to overcome solvent problems caused by liquid electrolytes. The LLC mesophases of LiI, LiCl and LiBr salts with 10-lauryl ether ( $C_{12}EO_{10}$ ) has been

considered as gel-electrolyte for the DSSC. We demonstrate that the LiI/I<sub>2</sub> couple can be incorporated into above LLC mesophases of various lithium salt-nonionic surfactant systems. Those LLC phases, with LiI/I<sub>2</sub> couple have been characterized by means of diffraction, microscopy, spectroscopy and conductivity measurements. The LLC mesophases diffract at small angles and do not show any phase segregation upon incorporating the LiI/I<sub>2</sub> redox couple. The LLC mesophases of these systems are 2D hexagonal, and they remain stable under ambient conditions for months. In the LLC media, the iodide ion and iodine molecule react to produce triiodide ion in the media. The iodide/triiodide (I/I<sub>3</sub><sup>-</sup>) redox couples containing gel electrolytes were formed and their solar performance was investigated by using a solar simulator and a cell consisting of a dye sensitized anode (FTO-dye modified TiO<sub>2</sub>), gel-electrolyte, and a cathode (FTO-Pt nanoparticles). The LLC mesophases of various lithium salt-nonionic surfactant systems with the I/I<sub>3</sub><sup>-</sup> redox couple were characterized using POM (Polarized Optical Microscope), XRD (X-ray Diffraction), FT-IR (Fourier Transform Infrared Spectroscopy) and Raman techniques. These new LLC mesophases can be used as gel electrolytes in solar cells after incorporation of redox couple into the media and display responses as good as commonly used liquid electrolytes.

**Key Words:** Lyotropic Liquid Crystal, Mesophases, Molten Salt, Concentrated Aqueous Solution, Self-assembly, Solar Cell, Gel Electrolyte, Redox Couple

## ÖZET

### LİTYUM TUZLARININ İYONİK OLMAYAN YÜZEY AKTİFLERLE OLUŞTURDUKLARI ARAHALLER VE BU YAPILARIN GÜNEŞ HÜCRELERİNDE JEL ELEKTROLİT OLARAK UYGULAMALARI

Gözde Barım

Yüksek Lisans, Kimya Bölümü

Tez Yöneticisi: Prof. Dr. Ömer Dağ

Temmuz, 2013

Bazı tuzlar iyonik olmayan yüzey aktiflerle kendiliğinden düzenlenerek liyotropik sıvı kristal (LSK) arahaller (mesophase) oluşturur. Kendiliğinden düzenlenme sürecinde tuzlar elektrolit çözelti olarak ya da eriyik halde bulunabilirler. Bu çalışmada lityum tuzlarının derişik elektrolit çözeltilerinin (LiCl, LiBr, and LiI) iyonik olmayan yüzey aktiflerle (oligo(ethylene oksitler, yada pluronikler, üç-bloklu polietilen-polipropilen-polietilen) oluşturdukları arahaller incelenmiştir. Lityum tuzlarının pluroniklerle oluşturduğu LSK arahaller 5.0 ile 25.0 tuz/pluronik, oligo(ethylene oksit) (C<sub>12</sub>EO<sub>10</sub>) ile oluşturdukların da ise 2.0 ile 10.0 tuz/C<sub>12</sub>EO<sub>10</sub> mol oranında düzenli olduğu ve oda koşullarında aylarca karalı olduğu gösterilmiştir. Atmosfere açık lityum tuzu-Pluronik LSK arahallerinde su, hidrat bileşikleri olarak kalmaktadır. Bu sistemlerin geniş tuz yoğunlukları aralığında hegzagonal arahalde bulunduğu gözlemlenmiştir. Ortamdaki uz oranlarını arttıkça birim hücrenin büyüdüğü ve hegzagonal arahalden kübik arahale geçiş olduğu gözlemlenmiştir. 25.0 tuz/pluronik mol oranlarına kadar numunelerin düzenli ve kararlı bir yapıda oldukları daha yüksek oranlarda ise düzensiz arafazlar ve/veya tuz kristallerinin oluştuğu görülmüştür.

Jel elektrolitler, sıvı elektrolitlerde görülen sorunların giderilmesi bakımından oldukça ilgi çekmektedirler. Bu çalışmada, LiI, LiCl ve LiBr tuzlarının 10-lauryl eter (C<sub>12</sub>EO<sub>10</sub>) ile oluşturdukları lyotropik arahaller de incelenmiştir. Bu arahaller 2.0 ile 10.0 tuz/C<sub>12</sub>EO<sub>10</sub> mol oranı aralığında kararlı yapıdadırlar. LiI/I<sub>2</sub> çifti, jel elektrolit oluşturmak için çeşitli lityum tuzu-iyonik olmayan yüzey aktif sistemine katılmıştır.

LiI/I<sub>2</sub> çifti içeren LSK arahaller polarize optik mikroskopu, X-ışını kırınım yöntemi, FT-IR ve raman spektroskopileri kullanılarak incelenmiştir. Bu sistemlerin lyotropik arahallerinin 2D hegzagonal yapıda olduğu ve açık atmosferde aylarca kararlı kaldığı belirlenmiştir. Bu arahallerin düşük açıda kırınım yaptığı ve LiI/I<sub>2</sub> çifti katıldıktan sonra faz ayrımına uğranmadığı görülmüştür. Ayrıca LSK arahallerde iyodürün, iyot ile tepkime vererek tri iyodür oluşturduğu gözlenmiştir. Böylece I<sup>-</sup>/I<sub>3</sub><sup>-</sup> yükseltgenme indirgenme çifti içeren jel elektrolitler elde edilmiş ve bu elektrolitlerin performansları güneş benzetici ve oluşturulan güneş hücresi (anot-gel elektrolit-katot, anot = FTO-boya uyarılmış TiO<sub>2</sub>, katot = FTO-Pt nanoparçacıklar) kullanılarak ölçülmüştür. Bu yeni LSK sistemlerinin güneş pillerinde jel elektrolit olarak kullanılabilmesi ve bilinen sıvı elektrolitler kadar iyi performans verdiği gösterilmiştir.

**Anahtar Kelimeler:** Liyotropik Sıvı Kristaller, Arahaller, Eriyik Tuzlar, Derişik Elektrolit Çözeltiler, Kendiliğinden Düzenlenme, Güneş Hücreleri, Jel Elektrolitler, Yükseltgenme İndirgenme Çifti

## ACKNOWLEDGEMENTS

First of all, I would like to express my gratefulness to my graduate program supervisor, Professor Ömer Dağ for patiently sharing his ideas with me throughout the time of my research. From him, I got acquainted with lots of chemistry disciplines and scientific methods. He encourages collegiality and team work in all his group members. His support and positive attitude towards my studies have helped me to propel ahead, despite all the academic challenges and huddles I faced. To accomplish great things especially in such a high level of education requires effort, dedication, perseverance, optimism and most importantly a supervisor like him, who never relents until he sees you to the level you aspired to reach. Without his continuous support and supervision, the possibility of completing this demanding task would have still been a nightmare. His knowledge and wisdom will always be a fountain!

I would also thank examining committee members, Prof. Margarita Kantcheva and Prof. Nihal Aydoğan, for their time and valuable suggestions on my thesis.

I am deeply grateful to Cemal Albayrak too. He was one of the senior members in our research group whose contribution and guidance in my research cannot be overemphasized. He assisted me all sectors of my research especially in the alkali metal systems. The service he rendered to me and other members of the group have been exceptional. As a result of his generosity and selfless attitude towards us all, I sincerely wish to thank him on behalf of all the present members of the group and on my own personal behalf. I will also like to thank Cüneyt Karakaya, Ebrima Tunkara and Aykut Aydın; we have had enjoyable and fruitful discussions about our research topics. I also thank all present and former group members for their contributions, help and friendship. I would not have gone this far without the courage and confidence they instilled in me.

For success to be pronounced in anyone's academic life, there must be nice and loving batchmates around him/her, to discourse ideas with, ease their frustrations, and remained steadfast in both dying and trying moments. Therefore, if my thesis achievement is anything to go by, I would like to thank my dear friends for being the soul reason. The list includes but not limited to Özlem Ünal, Tuğçe Durgut,

Merve Dođaç, Tuba Yaşar, Yiđit Altay, Menekşe Koca, Melis Tunalı, Duygu Demirciođlu, and Merve Taner from our department. Bilkent became my home because of their sincere friendship. We all share our happiness and sorrow, joy and frustration during the last seven years. I was truly blessed having such reliable friends. Special thanks to Şeyma Ekiz, Okan Çiftçi, Elif Mercan and Batuhan Kav for their sense of humor and candid fellowship. I spent my funniest time with them both in ‘Gradhane’ and ‘International Society of Irrationality’. I will miss the conversations we used to have about anything irrational so much after going to the US.

The hardest thing in one’s life is to stay away from the people you love most: people that will never want to see you sick, poor, or underachieve. I missed my family so much for the past seven years in order to pursuit academic excellence. In that regard, I wish to sincerely thank and dedicate the thesis to my family for their encouragement, patient and motivation. It was significant for me to feel their suppot in order to complete this thesis.

# CONTENTS

<b>CHAPTER 1</b> .....	1
<b>1. INTRODUCTION</b> .....	1
<b>CHAPTER 2</b> .....	3
<b>2. BACKGROUND</b> .....	3
2.1. Liquid Crystals.....	3
2.1.1. Lyotropic Liquid Crystalline Mesophases .....	7
2.1.2. Binary Systems of Poly(ethylene oxide) Type Surfactants ( $C_mEO_n+H_2O$ ).....	10
2.1.3. Effect of the Additives on $C_mEO_n-H_2O$ Systems .....	13
2.2. Lyotropic Liquid Crystals in the Synthesis of Novel Materials.....	16
2.3. Salt-Surfactant Liquid Crystalline Systems .....	18
2.4. A New Phase Transition in LLC Systems .....	22
2.5. Effect of Deliquescence on the Stability of LLC Mesophases.....	24
2.6. Electrolytes for Dye-Sensitized Solar Cells.....	25
2.6.1. Characteristics of the Iodide/Triiodide Redox Couple.....	27
<b>CHAPTER 3</b> .....	30
<b>3. EXPERIMENT RESULTS</b> .....	30
3.1. Materials .....	30
3.2. Sample Preparation .....	30
3.2.1. Preparation of the $LiX-xH_2O-C_{12}EO_{10}$ Gel Samples.....	30
3.2.2. Preparation of Samples in the Solution Phase.....	30
3.2.3. Preparation of the Samples with Redox Couple .....	30
3.2.4. Preparation of thin LLC Films and Small Scale Gel Samples .....	31
3.3. Fabrication of Solar Cells .....	31
3.3.1. Preparation of Mesoporous Titania Films (meso- $TiO_2$ ).....	31
3.3.2. Preparation of Dye Solution and Titania Electrode .....	31
3.3.3. Preparation of Pt-deposited FTO electrode.....	31
3.3.4. Assembly of DSSCs.....	32
3.4. Instrumentation .....	33
3.4.1. The X-ray Diffraction (XRD) .....	33
3.4.2. The Polarized Optical Microscopy (POM) .....	33
3.4.3. The Fourier Transform - Infrared Spectroscopy (FT-IR).....	33
3.4.4. The micro-Raman Spectroscopy .....	33
3.4.5. The AC Impedance Spectroscopy .....	34
3.4.6. UV-vis Spectroscopy .....	34
3.4.7. The Photovoltaic Measurements.....	34

<b>CHAPTER 4</b> .....	35
<b>4. EVALUATION</b> .....	35
4.1. Lyotropic Liquid Crystalline Mesophases of Pluronics (P65, P85, P103, and P123) with LiCl and LiNO <sub>3</sub> Salts .....	35
4.1.1. Salt-water-surfactant Interactions, Spectroscopic Studies .....	50
4.1.2. Conductivities and Isotropization Temperatures of Lithium Salt-Pluronic Systems .....	56
4.2. Lil-xH <sub>2</sub> O-C <sub>12</sub> EO <sub>10</sub> - Mesophase.....	60
4.3. Effect of Anions on the Lil-I <sub>2</sub> -xH <sub>2</sub> O-C <sub>12</sub> EO <sub>10</sub> System .....	67
4.3.1. FT-IR and Raman Spectroscopic Investigations of the Li(X)-I <sub>2</sub> -xH <sub>2</sub> O-C <sub>12</sub> EO <sub>10</sub> Systems .....	70
4.4. LLC Mesophases as Gel Electrolyte for Dye-Sensitized Solar Cells .....	73
4.5. Future Work.....	78
<b>CHAPTER 5</b> .....	79
<b>5. CONCLUSION</b> .....	79
<b>BIBLIOGRAPHY</b> .....	81

## LIST OF FIGURES

<b>Figure 2.1.</b> An illustration of positional and orientiaonal order in solids, liquid crystals and liquids.....	3
<b>Figure 2.2.</b> Schematic representation of calamitic and discoitic liquid crystalline molecules.....	4
<b>Figure 2.3.</b> Schematic representation of nematic, smectic and columnar phases from left to right. <sup>4</sup> .....	5
<b>Figure 2.4.</b> Schematic representation of non-ionic, anionic, cationic and zwitterionic surfactants from top to buttom. ....	6
<b>Figure 2.5.</b> Schematic representation of surfactant molecules (left) and micelles (right) in water.....	7
<b>Figure 2.6.</b> Schematic representation of (a) simple cubic ( $I_1$ ), (b) 2D-hexagonal ( $H_1$ ), (c) bicontiuous cubic ( $V_1$ ) and (d) lamellar ( $L_\alpha$ ) mesophases. <sup>18</sup> .....	8
<b>Figure 2.7.</b> Schematic representation of a surfactant molecule as an ice-cream cone. <sup>19</sup> .....	9
<b>Figure 2.8.</b> Phase diagram of $C_{10}EO_6$ - $H_2O$ system at 1 atm. <sup>37</sup> .....	11
<b>Figure 2.9.</b> Phase diagrams of $C_{10}EO_6$ - $H_2O$ systems in the presence and the absence of salts. The salt species none (circles and straight line), LiCl (squares and dotted line), NaCl (triangles and dashed line) and CsCl (diamonds). <sup>45</sup> .....	14
<b>Figure 2.10.</b> Phase diagrams of $C_{12}EO_7$ with various $Na^+$ salts. The dashed lines corresponds to the salt free phase diagram. <sup>47</sup> .....	15
<b>Figure 2.11.</b> Two different approach in the synthesis of mesoporous materials: (A) Cooperative self-assembly and (B) True LC templating process. <sup>54</sup> .....	17
<b>Figure 2.12.</b> Schematic representation of hydrogen bonding interactions between coordinated water molecules and the ethylene oxide chain in a hexagonal LLC mesophase. <sup>48</sup> .....	19
<b>Figure 2.13.</b> Phase diagram of the $ZnX$ - $C_{12}EO_{10}$ system. <sup>68</sup> .....	20
<b>Figure 2.14.</b> XRD patterns of the $4.0LiI-xH_2O-C_{12}EO_{10}$ mesocrystal at (a) low angles, and (b) high angles. <sup>71</sup> .....	22
<b>Figure 2.15.</b> FT-IR spectra the $4.0LiI-xH_2O-C_{12}EO_{10}$ mesocrystal (top) and LLC mesophase (bottom) at different wavenumbers. <sup>71</sup> .....	23

<b>Figure 2.16.</b> POM images of 4.0CaCl <sub>2</sub> -xH <sub>2</sub> O-C <sub>12</sub> EO <sub>10</sub> mesocrystal Mesocrystal growth from (A) defect site mesophase (B)edge of the sample (magnified images on the right). <sup>71</sup> .....	23
<b>Figure 2.17.</b> Energy scheme of cis-Ru(dcbpy) <sub>2</sub> (NCS) <sub>2</sub> -sensitized TiO <sub>2</sub> solar cell with I <sup>-</sup> /I <sub>3</sub> <sup>-</sup> redox couple. <sup>84</sup> .....	28
<b>Figure 3. 1.</b> DSSCs with gel electrolyte in the form of cell. ....	32
<b>Figure 3. 2.</b> DSSC with gel electrolyte sandwiched between two electrodes. ....	32
<b>Figure 4.1.</b> The small angle XRD patterns of the LiCl-xH <sub>2</sub> O-P65 mesophases with 8.0, 12.0 and 15.0 LiCl/P65 mole ratio (from bottom to top, left), and a POM image of a sample (right). ....	37
<b>Figure 4.2.</b> The XRD patterns at small angles of LiCl-P65-nH <sub>2</sub> O system with different mole ratios. ....	38
<b>Figure 4.3.</b> The XRD patterns, at small angles, of LiCl-xH <sub>2</sub> O-P85 system with 10.0, 12.0 and 15.0 mole ratios (from bottom to top). ....	39
<b>Figure 4.4.</b> The POM images of LiCl-xH <sub>2</sub> O-P85 system with 3.0, 6.0 and 8.0 mole ratios indicating surfactant crystals (bright dots) and formation of fan texture under the surfactant crystals. ....	39
<b>Figure 4.5.</b> The XRD patterns at small angles of LiCl-P85-nH <sub>2</sub> O system with different mole ratios. ....	40
<b>Figure 4.6.</b> The POM images of the LiCl-xH <sub>2</sub> O-P103 samples with a LiCl/P103 mole ratio of 6.0 (top) and 8.0 (bottom). ....	41
<b>Figure 4.7.</b> The XRD pattern of cubic mesophase of LiCl-xH <sub>2</sub> O-P103 system with 15.0 LiCl/P103 mole ratios. The inset is a plot of the d spacing obtained from the above three diffraction lines versus 1/(h <sup>2</sup> + k <sup>2</sup> + l <sup>2</sup> ) <sup>1/2</sup> . ....	42
<b>Figure 4.8.</b> The XRD patterns at small angles of LiCl-P103-nH <sub>2</sub> O system with different mole ratios. ....	44
<b>Figure 4.9.</b> The XRD patterns at small angles of LiCl-P123-nH <sub>2</sub> O system with different mole ratios. ....	45
<b>Figure 4.10.</b> The XRD patterns of the 2D hexagonal mesophase of LiNO <sub>3</sub> -xH <sub>2</sub> O-P103 samples with 6.0, 8.0, 10.0, 12.0 and 15.0 LiCl/P103 mole ratios from bottom to top. ....	46
<b>Figure 4.11.</b> The XRD patterns at small angles of LiNO <sub>3</sub> -P103-nH <sub>2</sub> O system with different mole ratios. ....	47

<b>Figure 4.12.</b> The XRD patterns of the 2D hexagonal mesophase of LiNO <sub>3</sub> -xH <sub>2</sub> O-P123 system with 6.0, 8.0, 10.0, 12.0 and 15.0 LiCl/P123 mole ratios from bottom to top.....	48
<b>Figure 4.13.</b> The XRD patterns at small angles of LiNO <sub>3</sub> -P123-nH <sub>2</sub> O system with different mole ratios. ....	49
<b>Figure 4.14.</b> FT-IR spectra of the LiNO <sub>3</sub> - xH <sub>2</sub> O-P123 and P123 (bottom) and LiNO <sub>3</sub> - xH <sub>2</sub> O-P103 and P103 (top) with the same salt/pluronic mole ratios. ....	51
<b>Figure 4.15.</b> Micro-Raman spectra of P123 and the LiNO <sub>3</sub> -xH <sub>2</sub> O-P123 samples with 6.0, 8.0, 10.0, 12.0 and 15.0 salt/pluronic mole ratios (from bottom to top). ....	52
<b>Figure 4.16.</b> FT-IR spectra of different salt systems (as indicated on the spectra) at various salt/surfactant mole ratios, from bottom to top 6.0, 8.0, 12.0, and 15.0.....	54
<b>Figure 4.17.</b> FT-IR spectra of P123, LiCl-xH <sub>2</sub> O-P123 and LiNO <sub>3</sub> -xH <sub>2</sub> O-P123 (bottom) and P103, LiCl-xH <sub>2</sub> O-P103 and LiNO <sub>3</sub> -xH <sub>2</sub> O-P103 (top) with the 12.0 salt/Pluronic mole ratios.....	55
<b>Figure 4.18.</b> (A) Nyquist plots of various samples with 10.0 and 200.0 salt/surfactant and water/surfactant mole ratios between 1.0x10 <sup>4</sup> Hz and 0.2 Hz. (B) Resistance values were recorded at the point where Z <sub>imaginary</sub> is equals to zero.....	57
<b>Figure 4.19.</b> FT-IR spectra of sample with composition 10.0LiCl-200.0H <sub>2</sub> O-1.0P65, under 25% RH and RT with time.....	57
<b>Figure 4.20.</b> (A) Nyquist plots of samples with various water/surfactant mole ratios between 1.0x10 <sup>4</sup> Hz and 0.2 Hz, and (B) the correlation between water mole ratio and conductivity.....	58
<b>Figure 4.21.</b> Typical XRD patterns at small angles of LiI-xH <sub>2</sub> O-C <sub>12</sub> EO <sub>10</sub> system with (a) 2.0, (b) .03, (c) 4.0 and (d) 5.0 LiI to C <sub>12</sub> EO <sub>10</sub> mole ratio, and a POM image of a LiI-xH <sub>2</sub> O-C <sub>12</sub> EO <sub>10</sub> sample in the inset.....	61
<b>Figure 4.22.</b> The XRD patterns at small angles of the LiI-I <sub>2</sub> -xH <sub>2</sub> O-C <sub>12</sub> EO <sub>10</sub> mesophases (numbers correspond to mole ratio of LiI, I <sub>2</sub> , and H <sub>2</sub> O per mole of surfactant).....	62
<b>Figure 4.23.</b> The XRD patterns at small angles of LiI-I <sub>2</sub> -xH <sub>2</sub> O-C <sub>12</sub> EO <sub>10</sub> with a 0.2 I <sub>2</sub> to C <sub>12</sub> EO <sub>10</sub> and 2.0 LiI to C <sub>12</sub> EO <sub>10</sub> mole ratios and a POM image of the sample in the inset. ....	63
<b>Figure 4.24.</b> The UV-vis spectra of 2.0LiI-I <sub>2</sub> -xH <sub>2</sub> O-C <sub>12</sub> EO <sub>10</sub> system with 0.0, 0.2, 0.3, 0.4, 0.5 I <sub>2</sub> to C <sub>12</sub> EO <sub>10</sub> mole ratios from bottom to top. ....	63
<b>Figure 4.25.</b> The UV-vis spectra of LiI/I <sub>2</sub> couple in various solvents. ....	64

<b>Figure 4.26.</b> The UV-vis spectra of LiI/I <sub>2</sub> couple in various solvents and 2.0LiI-0.2I <sub>2</sub> -xH <sub>2</sub> O-C <sub>12</sub> EO <sub>10</sub> system in water. ....	65
<b>Figure 4.27.</b> Raman spectra of (a) 2.0LiI-xH <sub>2</sub> O-C <sub>12</sub> EO <sub>10</sub> and (b) 2.0LiI-0.2I <sub>2</sub> -xH <sub>2</sub> O-C <sub>12</sub> EO <sub>10</sub> systems.....	66
<b>Figure 4.28.</b> Correlation between mole ratio of iodine (0.05, 0.1, 0.15 and 0.2 I <sub>2</sub> to C <sub>12</sub> EO <sub>10</sub> mole ratio) in the LLC media and absorbance of triiodide.....	66
<b>Figure 4.29.</b> The XRD patterns at small angles of LiCl-LiI-I <sub>2</sub> -xH <sub>2</sub> O-C <sub>12</sub> EO <sub>10</sub> system with LiCl:LiI:I <sub>2</sub> mole ratios per mole of surfactant in the inset. ....	68
<b>Figure 4.30.</b> The XRD patterns at small angles of LiBr-LiI-I <sub>2</sub> -xH <sub>2</sub> O-C <sub>12</sub> EO <sub>10</sub> system with LiBr:LiI:I <sub>2</sub> mole ratios per mole of surfactant in the insets. ....	69
<b>Figure 4.31.</b> The POM images of 2.0LiI-0.2I <sub>2</sub> -xH <sub>2</sub> O-C <sub>12</sub> EO <sub>10</sub> , 2.0LiI-0.5LiCl-0.2I <sub>2</sub> -xH <sub>2</sub> O-C <sub>12</sub> EO <sub>10</sub> , and 2.0LiI-0.5LiBr-0.2I <sub>2</sub> -xH <sub>2</sub> O-C <sub>12</sub> EO <sub>10</sub> samples from left to right. ....	70
<b>Figure 4.32.</b> The FT-IR spectra of the LiI-xH <sub>2</sub> O-C <sub>12</sub> EO <sub>10</sub> samples with different salt/surfactant mole ratios, from bottom to top 1.0, 2.0, 3.0, 4.0 and 5.0. ....	71
<b>Figure 4.33.</b> The FT-IR spectra of samples with compositions: (a) 2.0LiI-0.2I <sub>2</sub> -xH <sub>2</sub> O-C <sub>12</sub> EO <sub>10</sub> , (b) 2.0LiI-0.5LiCl-0.2I <sub>2</sub> -xH <sub>2</sub> O-C <sub>12</sub> EO <sub>10</sub> , and (c) 2.0LiI-0.5LiBr-0.2I <sub>2</sub> -xH <sub>2</sub> O-C <sub>12</sub> EO <sub>10</sub> .....	72
<b>Figure 4.34.</b> Raman spectra of the samples with compositions: 2.0LiI-0.2I <sub>2</sub> -xH <sub>2</sub> O-C <sub>12</sub> EO <sub>10</sub> , 2.0LiI-0.5LiCl-0.2I <sub>2</sub> -xH <sub>2</sub> O-C <sub>12</sub> EO <sub>10</sub> , and 2.0LiI-0.5LiBr-0.2I <sub>2</sub> -xH <sub>2</sub> O-C <sub>12</sub> EO <sub>10</sub> from bottom to top. ....	72
<b>Figure 4.35.</b> UV-vis spectra of the samples with compositions: 2.0LiI-0.2I <sub>2</sub> -xH <sub>2</sub> O-C <sub>12</sub> EO <sub>10</sub> , 2.0LiI-0.5LiCl-0.2I <sub>2</sub> -xH <sub>2</sub> O-C <sub>12</sub> EO <sub>10</sub> , and 2.0LiI-0.5LiBr-0.2I <sub>2</sub> -xH <sub>2</sub> O-C <sub>12</sub> EO <sub>10</sub> . ....	73
<b>Figure 4.36.</b> I-V curves for the DSSCs employing different kinds of electrolytes under 1 sun illumination (AM1.5, 100 mW cm <sup>-2</sup> ) 2.0LiI-0.2I <sub>2</sub> -xH <sub>2</sub> O-C <sub>12</sub> EO <sub>10</sub> , 2.0LiI-0.5LiBr-0.2I <sub>2</sub> -xH <sub>2</sub> O-C <sub>12</sub> EO <sub>10</sub> , and 2.0LiI-0.5LiCl-0.2I <sub>2</sub> -xH <sub>2</sub> O-C <sub>12</sub> EO <sub>10</sub> from top to bottom. ....	75
<b>Figure 4.37.</b> I-V curves of the DSSCs by employing water-based and acetonitrile-based of electrolytes under 1 sun illumination (AM1.5, 100 mW cm <sup>-2</sup> ) using the LiI-I <sub>2</sub> -xH <sub>2</sub> O-C <sub>12</sub> EO <sub>10</sub> system.....	76
<b>Figure 4.38.</b> I-V curves for the DSSCs by employing the water-based LiI-I <sub>2</sub> -xH <sub>2</sub> O-C <sub>12</sub> EO <sub>10</sub> gel electrolyte under illumination of different sun levels. ....	77

**Figure 4.39.** I-V curves for the DSSCs by employing the water-based  $\text{LiI-I}_2\text{-xH}_2\text{O-C}_{12}\text{EO}_{10}$  gel electrolyte recorded immediately, after 24 hours, and 4 days later from top to bottom. .... 78

## LIST OF TABLES

<b>Table 2.1.</b> Critical $g$ (shape) parameters for different micellar structures. <sup>19</sup> .....	10
<b>Table 2.2.</b> Observed phases, cloud points and CMCs for various poly(ethylene oxide)monoalkylether surfactants. <sup>23</sup> .....	12
<b>Table 2.3.</b> Stability of LLC mesophases of various cation-anion couples. Roman numbers means (I) stable LLC phase, (II) no crystallization at low salt concentrations, and little structural order, (III) salt crystallizes out. The symbols indicate (-) not studied, (*) transition to mesocrystalline phase, and LS is low solubility. <sup>75</sup> .....	24
<b>Table 2.4.</b> Redox potentials of various $I/I_3^-$ systems. <sup>84</sup> .....	27
<b>Table 4.1.</b> Phase behavior of the $LiCl-xH_2O$ -Pluronics systems at RT and 22-25% RH (H =hexagonal, I = cubic).....	36
<b>Table 4.2.</b> Phase behavior of $LiCl-xH_2O$ -Pluronics systems at RT and 22-25% RH. ....	56
<b>Table 4.3.</b> Photovoltaic characteristics of various DSSCs based on different gel electrolytes. ....	74
<b>Table 4.4.</b> Photovoltaic characteristics of various DSSCs based on $LiI-I_2-xH_2O-C_{12}EO_{10}$ gel electrolyte at different time intervals. ....	77

## LIST OF ABBREVIATIONS

<b>LC</b>	Liquid Crystal
<b>LLC</b>	Lyotropic Liquid Crystal
<b>TLC</b>	Thermotropic Liquid Crystal
<b>CMC</b>	Critical Micelle Concentration
<b>CPP</b>	Critical Packing Parameter
<b>L<sub>α</sub></b>	Lamellar
<b>H<sub>1</sub></b>	Hexagonal
<b>I<sub>1</sub></b>	Cubic
<b>V<sub>1</sub></b>	Bicontinuous Cubic
<b>L<sub>1</sub></b>	Micellar
<b>HLB</b>	Hydrophilic Balance
<b>HOMO</b>	Highest Occupied Molecular Orbital
<b>LUMO</b>	Lowest Unoccupied Molecular Orbital
<b>XRD</b>	X-ray Diffractometry
<b>POM</b>	Polarized Optical Microscopy
<b>FT-IR</b>	Fourier Transform Infrared
<b>NMR</b>	Nuclear Magnetic Resonance
<b>C<sub>12</sub>EO<sub>10</sub></b>	Decaethylene glycol monododecyl ether
<b>SMC</b>	Soft Mesocrystal
<b>DRH</b>	Deliquescence Relative Humidity
<b>RT</b>	Room Temperature
<b>DSSC</b>	Dye-sensitized Solar Cell

<b>CB</b>	Conduction Band
<b>FTO</b>	Fluorine-doped Tin Oxide
<b>FF</b>	Fill Factor
<b>SDA</b>	Structure Directing Agents
<b>CTAB</b>	Cetyrimethylammonium Bromide
<b>TEOS</b>	Tetraethyl Orthosilicate
<b>TLCT</b>	True Liquid Crystalline Templating
<b>TMS</b>	Transition Metal Salt
<b>N719</b>	Di-tetrabutylammonium cis-bis(isothiocyanato)bis(2,2'-bipyridyl-4,4' dicarboxylato)ruthenium(II)

# CHAPTER 1

## 1. INTRODUCTION

Some solids can exhibit gradual phase transformation to liquid phase upon heating. At certain temperatures, there is another phase between solid phase and liquid phase for such materials. This phase is called liquid crystalline phase, and in that phase solid can be transformed either birefringed or non-refringed isotropic fluid. In the liquid crystalline phase, the fluid has physical properties between those of a crystalline solid and those of a liquid. Further increase in the temperature leads to disappearance of the birefringed property, and the liquid crystalline fluid transforms into isotropic liquid. During heating, some structural changes can be observed in which molecules still show long-range orientational order in the liquid crystalline phase. First the liquid to liquid crystalline phase transformation takes place when the liquid is cooled back, and then the crystalline solid phase is observed again.

In 1888, the liquid crystalline state of matter was discovered by Austrian botanical physiologist Friedrich Reinitzer. In his experiments, Reinitzer observed that cholesteryl benzoate had two different melting points. He realized that solid cholesteryl benzoate turned into hazy fluid upon heating, and at higher temperatures the material change into transparent liquid. After this discovery, the name liquid crystal was coined by a German physicist Otto Lehmann.

Liquid crystals have many physical properties of liquids such as high fluidity, formation and coalescence of droplets. They also have similar properties with crystalline solids. For instance, they display anisotropy in their mechanical, physical, electrical and optical properties. Liquid crystals can be found both in nature and technological applications. Thermotropic liquid crystals, which exhibit liquid crystalline phase transformation with temperature, are most widely used in liquid crystal displays. Other main application areas of this kind of liquid crystals are thermometers, optical imaging, visualization of radio frequency waves in wave guides, and light modulators. Lyotropic liquid crystals, which exhibit phase transformation with concentration, are ample in living systems such as proteins, living cells and tobacco mosaic virus. Lyotropic liquid crystals are mainly used as

electrolytes due to their conductivity. They offer many advantages such as ionic mobility, and rigidity. Therefore, they can be an alternative to solid or liquid electrolytes for solar cell applications.

Briefly, special properties of liquid crystals are still being investigated in order to provide persuasive solutions to various problems. The attention and interest on liquid crystals increases, as the new properties of these materials are investigated and researched.

## CHAPTER 2

### 2. BACKGROUND

#### 2.1. Liquid Crystals

Liquid crystals (LC) can be considered as the fourth state of matter with distinct features intermediate between solid and liquid. Atoms in crystalline solids have fixed lattice points and oriented in certain directions. As a result of the thermal motion of the atoms, there is some uncertainty in atomic positions. Crystals are optically isotropic if they have a cubic space group, and if not, they become anisotropic with distinct physical properties with respect to different directions in the crystal. In amorphous solids, atoms are spatially disordered, and it can exhibit only short-range order. On the other hand, molecules in liquids can change their positions randomly, and there are large fluctuations in atomic positions. Liquids do not exhibit any long-range orientational order, and so they are optically isotropic. Liquid crystals have similar features with both solids and liquids. In the LCs, molecules can flow like in liquids, but they also can be oriented like in solids.

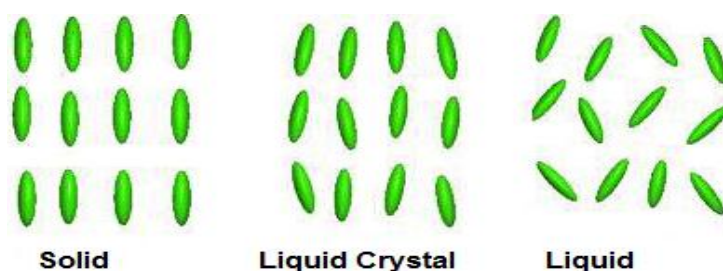


**Figure 2.1.** An illustration of positional and orientational order in solids, liquid crystals and liquids.

Intrinsic properties of molecules in LCs and temperature play a crucial role in the molecular order in liquid crystals. In contrast to solids, weak forces such as Hydrogen bonding, dipole-dipole interactions or van der Waals forces act on liquid crystals.<sup>1</sup> Thus, understanding the nature of weak forces of the soft chemistry has significance in order to figure out the self-assembly process of living organisms.

Liquid crystals can be divided into thermotropics and lyotropics. Thermotropic liquid crystals can form liquid crystalline phase at certain temperature ranges and their phase transition is a function of temperature. Calamitic (rod-like) and discotic (disk-like) are two main sub groups of thermotropic liquid crystals. Calamitic liquid crystals have a rod-shape structure in which one molecular axis is much longer than the other two. Discotic liquid crystalline mesophases are obtained with disk-like molecules where the director is perpendicular to the molecular plane.

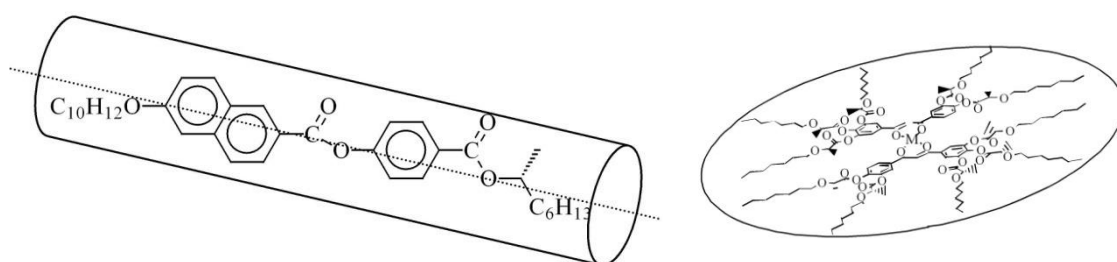


**Figure 2.2.** Schematic representation of calamitic and discotic liquid crystalline molecules.

Calamitic liquid crystals have a rigid center which maintains its alignment on the orientational direction. They have also flexible parts at each end in order to strengthen weak forces and intra-molecular interactions.

Discotics have disk-like building blocks with a rigid aromatic core and peripheral flexible chains. In contrast to calamitic liquid crystals, the z-direction of a discotic liquid crystal is shorter than the xy plane. The weak molecular interactions both in the z-direction and xy plane play crucial role in the self-assembly process of discotic liquid crystals.<sup>2</sup>

Thermotropic liquid crystals exhibit nematic (N), smectic (S) and cubic mesophases.<sup>3</sup> Calamitic liquid crystals tend to form smectic mesophases whereas discotic ones prefer to self-organize into columnar mesophases. The nematic phase is the least ordered phase in which the rod-like or disk-like molecules line up parallel to each other along a direction defined as  $n$ , and there is no long-range translational order.<sup>4</sup> In smectic phases, molecules are parallel to each other, and they are arranged in layers with long axes parallel to the layer plane. Therefore, smectic phase are positionally ordered along one direction, and

smectic phases can be found at lower temperature than the nematic phase.<sup>5</sup> In more viscous columnar phases, molecules stack on top of each other into columns, and the columns are arranged into a two-dimensional lattice.<sup>4</sup>

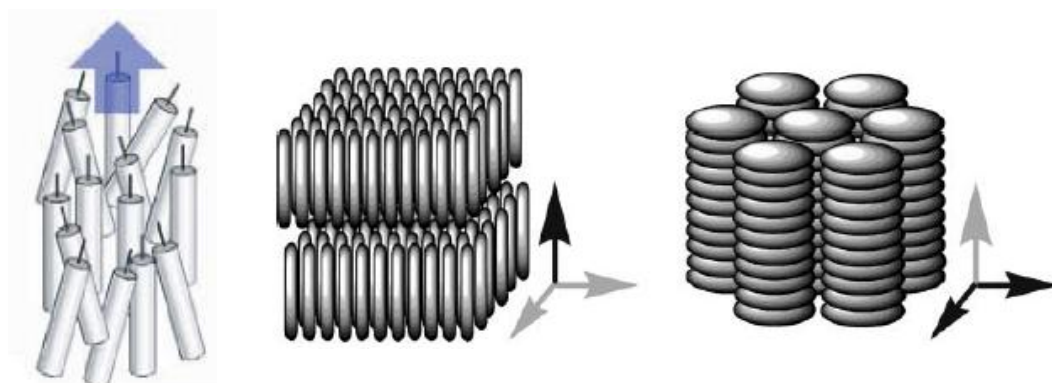


**Figure 2.3.**<sup>1</sup> Schematic representation of nematic, smectic and columnar phases from left to right.<sup>4</sup>

In contrast to thermotropics, lyotropic liquid crystals (LLC) are formed by at least two components, a surfactant and a solvent. In addition to the temperature, LLCs have another degree of freedom which is concentration. This additional degree of freedom leads to formation of a rich variety of new structures.<sup>7-11</sup> Molecules which contain both hydrophilic (water-like) and hydrophobic (lipid-like) groups can exhibit LLC behavior by forming aggregates when put into an appropriate solvent. These molecules that have both hydrophilic and hydrophobic parts are called as amphiphilic molecules. Surfactants are amphiphiles so they have a tendency to decrease surface tension of the water in an aqueous media.<sup>12</sup>

Surfactants can be classified as their charge properties; surfactants which bear no charge in a solvent is named as non-ionic surfactants, which bear charge are called as cationic, anionic or zwitterionic surfactants depending on the sign of the charge on their hydrophilic parts, see **Figure 2.4**.

---

<sup>1</sup>Reprinted from Sergeyev, S., Wojciech P., and Yves H. G., Discotic liquid crystals: a new generation of organic semiconductor *Chemical Society Reviews* 36, 1902-1929, (2007), with permission from The Royal Society of Chemistry.

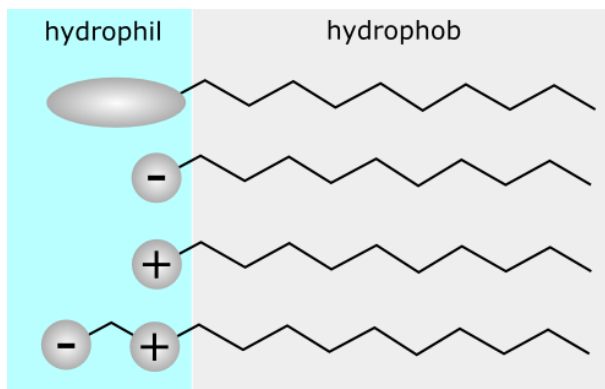


**Figure 2.4.** Schematic representation of non-ionic, anionic, cationic and zwitterionic surfactants from top to bottom.

Surfactants are surface active molecules, and they can be adsorbed at the water-air interface in order to reduce surface free energy. Surfactants can interact selectively with the different sides of the interface by using its hydrophobic and hydrophilic parts. The phase behavior of surfactants depends mainly on the concentration. At very low concentrations, surfactant molecules tend to move toward the water-air interface. The hydrophobic parts tend to stay away from the water in order to reduce interaction with water; however, the hydrophilic parts are hydrated by water molecules. When the concentration increased, the surfactant molecules start to form spherical aggregates. These aggregates are called as micelles, and the formation of micelles is related to intermolecular interactions of the surfactant molecules. The hydrophilic parts of a micelle tend to form hydrogen bonds with water molecules. This leads to disruption of the hydrogen bonding network of water molecules. As the hydrophilic regions of water molecules come close to each other, they tend to share the same shell of the hydrogen bonding network. This situation is not energetically favorable due to the presence of excess water molecules. This causes repulsion between hydrophilic parts of the surfactant, and they tend to keep away from each other. On the other hand, hydrophobic parts cannot interact with water molecules, and this causes hydrophobic interaction between alkyl chains of the surfactant.<sup>13-15</sup> As a result of both hydrophilic repulsion and hydrophobic attraction spherical micelles are formed at critical concentrations, see **Figure 2.5**.

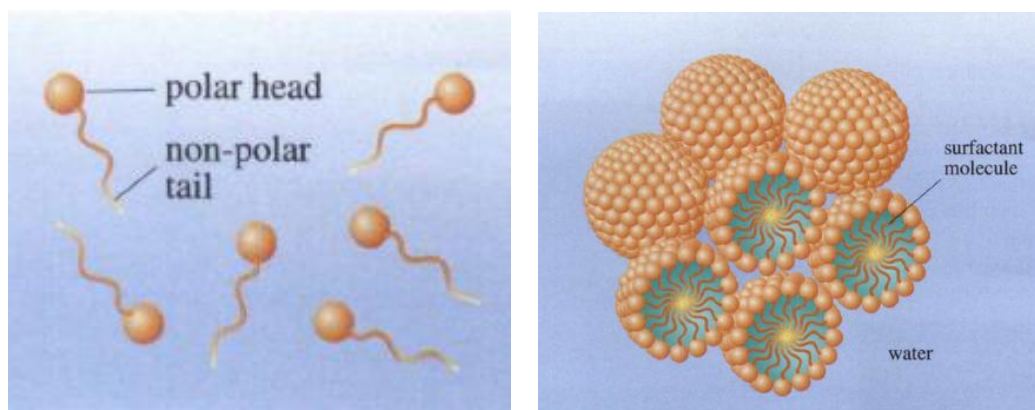


**Figure 2.5.**<sup>2</sup> Schematic representation of surfactant molecules (left) and micelles (right) in water.

The concentration where the surfactants start to form micelles is called critical micelle concentration (CMC). It depends on the nature of the surfactant, the nature of the solvent, temperature, and additives in the media. Further increase in the surfactant concentration above the CMC increases the number of micelles in the solution. At high surfactant concentrations, the micelles become densely packed, and they start to interact with each other via repulsive electrostatic forces.<sup>16</sup> As a result of intermicellar interactions, micellar domains form ordered mesostructures. Therefore, the viscosity of the solution increases drastically, and the liquid crystalline phase can be observed.

### 2.1.1. Lyotropic Liquid Crystalline Mesophases

The distance between micellar units becomes shorter with increasing surfactant concentration; thus, different lyotropic liquid crystalline phases occur due to the hydrophobic effect caused by the long-range repulsive forces between micellar interfaces. Repeating micellar units can form either lamellar ( $L_a$ ) or hexagonal ( $H_1$ ) mesophases which have planes or axes of repeating unit, respectively.<sup>17</sup> There are four different type of LLC mesophases.

The simple cubic phase ( $I_1$ ) has globular micellar structure so it is less viscous and less freely flowing than lamellar or columnar mesophases. In this phase, spherical micelles can form body-centered cubic (bcc,  $Im3m$ ), face-centered cubic (fcc,  $Fm3m$ ) or clathrate (Type I,  $Pm3n$ ) packing.<sup>17</sup>

<sup>2</sup> Reprinted from Giles Clark, *The third Dimension (The Molecular World)* (First Edition) 227 (The Open University, 2002) with permission from The Royal Society of Chemistry.

The hexagonal phase ( $\mathbf{H}_1$ ), -the subscript denotes if the phase is normal (1) or inverted (2)- is consists of dense packing of cylindrical micelles, arranged on a 2D or 3D hexagonal lattice. It can be identified by a characteristic fan texture under the polarized optical microscope because of the focal conic domains. This phase has intermediate viscosity between discrete micellar and bicontinuous cubic phases.<sup>17</sup>

The bicontinuous cubic phase ( $\mathbf{V}_1$ ) is very viscous so it can be almost solid in some cases. It exhibit cubic symmetry and does not display optical textures. This phase is structurally wrapped lamellar phases, and the network has both positively and negatively curved regions.<sup>17</sup>

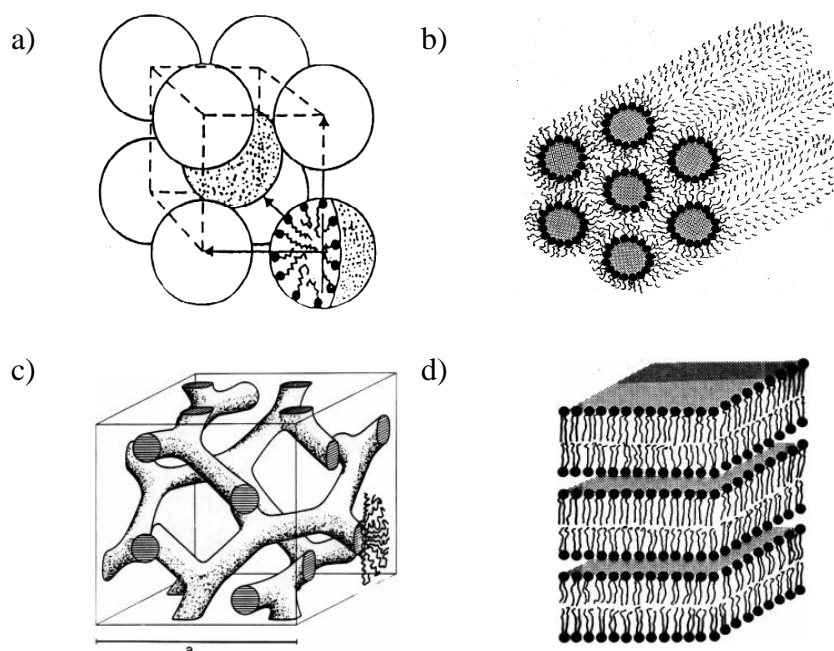


**Figure 2.6.<sup>3</sup>** Schematic representation of (a) simple cubic ( $\mathbf{I}_1$ ), (b) 2D-hexagonal ( $\mathbf{H}_1$ ), (c) bicontinuous cubic ( $\mathbf{V}_1$ ) and (d) lamellar ( $\mathbf{L}_\alpha$ ) mesophases.<sup>18</sup>

The lamellar phase ( $\mathbf{L}_\alpha$ ) has parallel surfactant bilayers that are separated by water rich regions. The  $\alpha$  subscript refers to the molten chains in this phase. It has characteristic X-ray spectra with scattering peaks in the ratio 1:2:3, related to the inter bilayer spacing. Like other anisotropic phases, it can

<sup>3</sup> Reprinted from Cevc, G., and Holger R., Lipid vesicles and membrane fusion *Advanced Drug Delivery Reviews* 38, 207-232, (1999) with permission Elsevier.

be identified by the distinct optical texture. The characteristic texture of this phase is streaky or mosaic-like.<sup>17</sup>

The transitions between these phases are in the following order with increasing surfactant concentration:  $L_1(\text{micellar}) \rightarrow I_1 \rightarrow H_1 \rightarrow V_1 \rightarrow L_a$ . The length, structure and nature of the hydrophobic chains, the nature and the charge on the hydrophilic regions, electrolyte concentration, temperature and pressure can also affect the structural preference.<sup>18</sup>

Repulsive interactions at the hydrophilic regions, attractive interactions between hydrophobic moieties at the core-shell interface in order to reduce unfavorable interactions with the solvent molecules and repulsive interactions of alkyl chains in the core are three major forces acting on the surfactant molecules.<sup>5</sup> These three forces determine the dimensionless shape parameter,  $g$ , which is very beneficial to predict morphology and topology of mesophases. Shape parameter can be defined in terms of the area per surfactant molecule at the head-group chain interface,  $a$ , the chain length of the molecule,  $l$ , and the effective hydrocarbon volume,  $v$ .<sup>5</sup>

$$g \equiv \frac{v}{al} \quad (\text{eqn. 1})$$

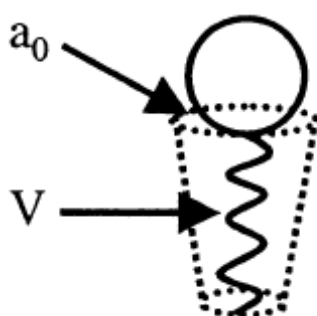


**Figure 2.7.**<sup>4</sup> Schematic representation of a surfactant molecule as an ice-cream cone.<sup>19</sup>

---

<sup>4</sup> de AA. Soler-Illia, G. J., Sanchez, C., Lebeau, B., & Patarin, J., Chemical strategies to design textured materials: from microporous and mesoporous oxides to nanonetworks and hierarchical structures *Chemical Reviews*, 102(11), 4093-4138 (2002), with permission from American Chemical Society.

The shape parameter defines the volume scaling for a fixed area as a function of the alkyl chain length, and it is characteristic for the amphiphiles in the aggregate in terms of an average block shape. Therefore, the shape parameter is defined as the critical packing parameter (CPP).<sup>16</sup> CPP is less than 1/3 for spherical micellar units, while it is 1/2 for cylinders (hexagonal phase), and it is at around 1 for lamellar structure. It is required to have higher than 1 CPP value in order to obtain inverted structures, where hydrophobic from the shell and hydrophilic groups from the core.<sup>16</sup>

**Table 2.1.**<sup>5</sup> Critical  $g$  (shape) parameters for different micellar structures.<sup>19</sup>

$g = v/l_c a_0$	structures	examples
$g < 0.33$	spherical micelles	single chain lipids with a large polar head (soaps or ionic detergents)
$g = 0.33-0.5$	cylindrical micelles	single chain lipids with a small polar head (soaps or ionic detergents in concentrated electrolyte solutions)
$g = 0.5-1$	bilayer (vesicles)	double-chain lipids
$g = 1-2$	bilayer (membranes)	
$g = 2-3$	inverse cylindrical micelles	double-chain lipids and a small polar head
$g > 3$	inverse spherical micelles	

Note that the validity of this concept depends on the complete study on various parameters including surfactant nature, pH, and presence of cosurfactants or cosolvents. Moreover, a constant temperature is required for these structural considerations, since the hydrophilicity of molecules in the micelle changes with temperature.<sup>19-22</sup>

### 2.1.2. Binary Systems of Poly(ethylene oxide) Type Surfactants (C<sub>m</sub>EO<sub>n</sub>+H<sub>2</sub>O)

The poly(ethylene oxide)monoalkylether surfactants are consist of an alkyl chain attached to a hydrophilic ethylene oxide unit. C<sub>n</sub>EO<sub>m</sub> is used as the shorthand representation for poly(ethylene oxide)monoalkylether surfactants where  $n$  represents the total number of carbon atoms in the alkyl chain, and  $m$  stands for the total number of ethylene oxide units on the hydrophilic head group.

The phase behavior of C<sub>n</sub>EO<sub>m</sub> type nonionic surfactants has been extensively investigated in various solvents such as aqueous solutions,<sup>23</sup> room temperature ionic liquids,<sup>24</sup> supercritical carbon dioxide,<sup>25,26</sup> and organic sovents.<sup>27-29</sup> Studying the phase behavior of this type surfactants is

<sup>5</sup> de AA. Soler-Illia, G. J., Sanchez, C., Lebeau, B., & Patarin, J., Chemical strategies to design textured materials: from microporous and mesoporous oxides to nanonetworks and hierarchical structures *Chemical Reviews*, 102(11), 4093-4138 (2002), with permission from American Chemical Society.

significant due to their wide application areas.<sup>30-35</sup> By changing the chain length of the alkyl and the ethylene oxide units one can control the hydrophilic balance (HLB) of the surfactants. As the number of carbon atom increase in both the alkyl chain and ethylene oxide unit, the efficiency of the surfactant increases.<sup>36</sup> Therefore, a liquid crystalline region can be observed in the phase diagrams of more efficient surfactants. Generally, micellar (normal or inverse), hexagonal (normal or inverse), cubic (normal or inverse) are common liquid crystalline phases in these diagrams.

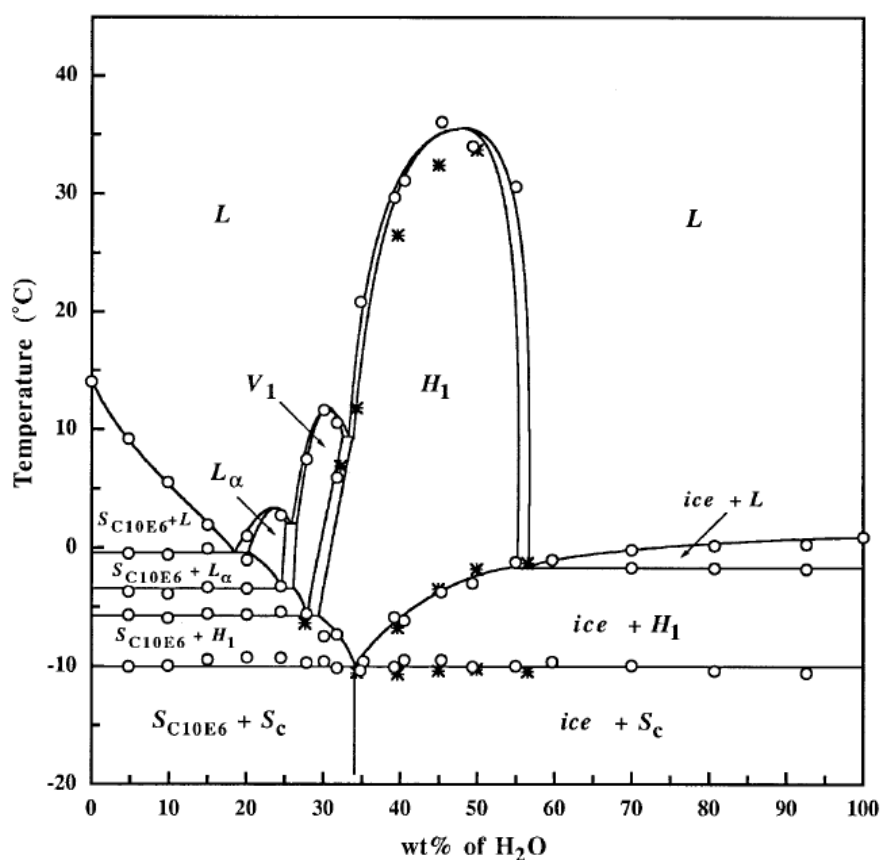


**Figure 2.8.**<sup>6</sup> Phase diagram of  $C_{10}EO_6$ - $H_2O$  system at 1 atm.<sup>37</sup>

**Figure 2.8** indicates a typical T-X phase diagram of  $C_{10}EO_6$  and  $H_2O$  mixture where various mesophases occurs with respect to changing in the CPP.  $L_1 \rightarrow H_1 \rightarrow V_1 \rightarrow L_\alpha$  transformation is observed with increasing surfactant concentration. These phase diagrams can be constructed by using

<sup>6</sup> Reprinted from Nibu, Yoshinori, and Tohru Inoue, Phase behavior of aqueous mixtures of some polyethylene glycol decyl ethers revealed by DSC and FT-IR measurements *Journal of colloid and interface science* 205, 305-315, (1998), with permission from Elsevier.

different techniques including X-ray diffractometry (XRD), polarized optical microscopy (POM), differential scanning calorimetry (DSC), Fourier transform infrared (FT-IR) spectroscopy, and nuclear magnetic resonance (NMR).

Tiddy and coworkers investigated phase diagrams of the binary C<sub>10</sub>EO<sub>6</sub>-H<sub>2</sub>O system. The chain length of the alkyl and the ethylene oxide units were varied from 8 to 16 and 3 to 12 respectively so they were able to monitor the impact of the chain length of hydrophilic and hydrophobic parts on the phase behavior.<sup>38</sup> They observed that L<sub>α</sub> phase exists for EO<sub>m</sub> where m<5, and I<sub>1</sub> phase is dominant when m>8. The reason is that increase in the ethylene oxide chain length leads to an increase in the cross-sectional area; therefore structures with higher interfacial curvatures become more favorable. On the other hand, I<sub>1</sub> → H<sub>1</sub> → V<sub>1</sub> → L<sub>α</sub> phase transitions is observed with increasing temperature since decrease in the cross-sectional area causes an increase in intermicellar repulsions. Another factor can be dehydration of ethylene oxide chain with temperature leads to breakdown of water around hydrophilic region.<sup>39-40</sup>

**Table 2.2.**<sup>7</sup> Observed phases, cloud points and CMCs for various poly(ethylene oxide)monoalkylether surfactants.<sup>23</sup>

surfactant	cmc <sup>b</sup> at 25 °C (10 <sup>-5</sup> mol·L <sup>-1</sup> )	cloud point (°C)	HLB	observed phases <sup>d</sup>	refs
C <sub>10</sub> EO <sub>3</sub>	60		9.1 <sup>e</sup>	L <sub>1</sub> ,L <sub>2</sub> ,L <sub>3</sub> ,L <sub>α</sub> ,L <sub>2</sub>	9, 25, 26
C <sub>10</sub> EO <sub>4</sub>	68	21	10.5 <sup>e</sup>	L <sub>1</sub> ,L <sub>2</sub> ,L <sub>3</sub> ,L <sub>α</sub> ,H <sub>1</sub>	2, 9, 25, 27
C <sub>10</sub> EO <sub>5</sub>	80	44	11.6 <sup>e</sup>	L <sub>1</sub> ,L <sub>α</sub> ,V <sub>1</sub> ,H <sub>1</sub>	2, 9, 25, 28
C <sub>10</sub> EO <sub>6</sub>	90	59	12.5 <sup>e</sup>	L <sub>1</sub> ,L <sub>α</sub> ,V <sub>1</sub> ,H <sub>1</sub>	2, 9, 28, 29
C <sub>10</sub> EO <sub>7</sub>	95		13.2 <sup>e</sup>	L <sub>1</sub> ,H <sub>1</sub>	30, 31
C <sub>10</sub> EO <sub>8</sub>	100	85	13.8 <sup>e</sup>	L <sub>1</sub> ,H <sub>1</sub>	25, 28, 32
C <sub>12</sub> EO <sub>2</sub>	3.3	32–35	6.4 <sup>e</sup>	L <sub>1</sub> ,L <sub>α</sub> ,L <sub>3</sub> ,V <sub>2</sub> ,L <sub>2</sub> ,	25, 33, 34
C <sub>12</sub> EO <sub>3</sub>	5.2		7.5	L <sub>1</sub> ,L <sub>3</sub> ,L <sub>α</sub> ,L <sub>2</sub>	2, 9, 25, 35, 36
C <sub>12</sub> EO <sub>4</sub>	4.3 (6.4)	6	9.0	L <sub>1</sub> ,L <sub>3</sub> ,L <sub>α</sub> ,L <sub>2</sub>	2, 9, 25, 29, 32
C <sub>12</sub> EO <sub>5</sub>	6.4	30	10.0	L <sub>1</sub> ,L <sub>3</sub> ,L <sub>α</sub> ,H <sub>1</sub> ,V <sub>1</sub> ,L <sub>2</sub>	2, 9, 30, 35, 37
C <sub>12</sub> EO <sub>6</sub>	6.8	48	11.7 <sup>e</sup>	L <sub>1</sub> ,L <sub>α</sub> ,H <sub>1</sub> ,V <sub>1</sub> ,L <sub>2</sub>	2, 9, 37, 38
C <sub>12</sub> EO <sub>7</sub>	5.0	70	12.5 <sup>e</sup>	L <sub>1</sub> ,L <sub>α</sub> ,H <sub>1</sub> ,V <sub>1</sub> ,L <sub>2</sub>	2, 9, 30, 37, 39
C <sub>12</sub> EO <sub>8</sub>	7.1	77	13.1 <sup>e</sup>	L <sub>1</sub> ,L <sub>α</sub> ,H <sub>1</sub> ,V <sub>1</sub> ,I <sub>1</sub> ,L <sub>2</sub>	2, 9, 37, 38
C <sub>12</sub> EO <sub>9</sub>	10	88	13.6 <sup>e</sup>	L <sub>1</sub> ,H <sub>1</sub> ,I <sub>1</sub> ,L <sub>2</sub>	25, 32, 37
C <sub>12</sub> EO <sub>10</sub>		96	14.1 <sup>e</sup>	L <sub>1</sub> ,H <sub>1</sub> ,L <sub>2</sub>	32, 37
C <sub>12</sub> EO <sub>12</sub>	14.0	98	14.8 <sup>e</sup>	L <sub>1</sub> ,H <sub>1</sub> ,I <sub>1</sub>	9, 38
C <sub>12</sub> EO <sub>23</sub>	17.5		16.9	L <sub>1</sub> ,I <sub>1</sub> ,L <sub>2</sub>	37, 38, 40
C <sub>14</sub> EO <sub>3</sub>		<20	7.6 <sup>e</sup>	L <sub>1</sub> ,L <sub>3</sub> ,L <sub>α</sub> ,V <sub>2</sub> ,L <sub>2</sub>	2, 9
C <sub>14</sub> EO <sub>6</sub>	0.8	42	11.0 <sup>e</sup>	L <sub>1</sub> ,L <sub>α</sub> ,H <sub>1</sub> ,V <sub>1</sub>	2, 9, 29
C <sub>14</sub> EO <sub>7</sub>	0.95	58	11.8 <sup>e</sup>		30, 41
C <sub>14</sub> EO <sub>8</sub>	0.99	70	12.4 <sup>e</sup>	L <sub>1</sub> ,L <sub>α</sub> ,H <sub>1</sub> ,V <sub>1</sub> ,I <sub>1</sub>	25, 32, 42
C <sub>16</sub> EO <sub>3</sub>		<20	7.0 <sup>e</sup>	L <sub>1</sub> ,L <sub>3</sub> ,L <sub>α</sub> ,V <sub>2</sub> ,L <sub>2</sub> ,L <sub>β</sub>	9
C <sub>16</sub> EO <sub>4</sub>		<20	8.4 <sup>e</sup>	L <sub>1</sub> ,L <sub>3</sub> ,L <sub>α</sub> ,V <sub>2</sub> ,L <sub>2</sub>	2, 9
C <sub>16</sub> EO <sub>6</sub>	0.40	37	10.4 <sup>e</sup>	L <sub>1</sub> ,L <sub>α</sub> ,L <sub>α</sub> <sup>H</sup> ,H <sub>1</sub> ,V <sub>1</sub> ,L <sub>β</sub> <sup>e</sup> ,L <sub>2</sub>	9, 43–45
C <sub>16</sub> EO <sub>7</sub>	0.30	52	11.2 <sup>e</sup>	L <sub>1</sub> ,L <sub>α</sub> ,H <sub>1</sub> ,V <sub>1</sub>	41, 43, 46
C <sub>16</sub> EO <sub>8</sub>	0.12	63	11.9 <sup>e</sup>	L <sub>1</sub> ,L <sub>α</sub> ,H <sub>1</sub> ,V <sub>1</sub> ,I <sub>1</sub> ,L <sub>2</sub>	2, 9, 25
C <sub>16</sub> EO <sub>12</sub>	0.23	92	13.7 <sup>e</sup>	L <sub>1</sub> ,L <sub>α</sub> ,H <sub>1</sub> ,V <sub>1</sub> ,I <sub>1</sub>	2, 9, 38
C <sub>16</sub> EO <sub>20</sub>	0.77		15.7 <sup>e</sup>		47

<sup>a</sup> Expanded from ref 9. <sup>b</sup> The values of cmc's are approximate due to different experimental measurements. <sup>c</sup> HLB was calculated as HLB = wt % EO/5. <sup>d</sup> Phase abbreviations are as described in the text. <sup>e</sup> L<sub>β</sub> represents a gel phase.

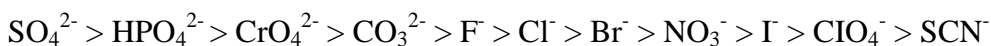
<sup>7</sup> Dong, Renhao, and Jingcheng Hao, Complex fluids of poly (oxyethylene) monoalkyl ether nonionic surfactants *Chemical reviews* 110, 4978, (2010), with permission from American Chemical Society.

### 2.1.3. Effect of the Additives on C<sub>m</sub>EO<sub>n</sub>-H<sub>2</sub>O Systems

An additive can be considered as a variable which changes the  $g$  parameter. Generally, the head group repulsions between the ionic surfactants decrease by the addition of ions into the solution. On the other hand, the effect of electrolytes is quite different for nonionic surfactant systems, and this effect generally follows the Hofmeister series of ions.

In 1881, Hofmeister and Lewith indicate that the precipitation of proteins with various salts related to concentration of ions, and anions have greater impact than the cations.<sup>42</sup> However, there is not any certain explanation for the behavior of the anions in the molecular level.

For the anions:



For the cations:



The ions on the left side of the Hofmeister series are called kosmotropes, and they reduce the solubility of organic compounds in water (salting-out) due to their tendency to enhance hydrogen bonding network of water.<sup>43</sup> Therefore, kosmotropes are considered as structure-makers. However, the ions on the right side tend to break down water clusters so water molecules hydrate the hydrophilic segments, and the overall solubility increases (salting-in). These ions are called chaotropes or structure-breakers.

The Hofmeister series has also strong effect on the solubility of many organic compounds including surfactants in addition to proteins. For instance, the CMC and cloud point of poly(ethylene oxide) surfactants follow the Hofmeister series. The cloud points of C<sub>m</sub>EO<sub>n</sub> surfactants decrease with the order:  $\text{F}^- > \text{Cl}^- > \text{Br}^-$ .<sup>44-45</sup> The reason is that water molecules that are closer to the hydrophilic part have a tendency to interact with each other instead of forming hydrogen bonds with hydrophilic ethylene oxide units if the water structure does not break down. Thus, the kosmotropes lead to an extension in the dehydration of ethylene oxide units, and so the cloud points drop.

The effect of cations on the phase behavior of C<sub>12</sub>EO<sub>7</sub>-H<sub>2</sub>O system was investigated by Zheng and coworkers.<sup>46</sup> By mixing 1.0 M of LiCl, NaCl and CsCl salts with C<sub>12</sub>EO<sub>7</sub> various percent of salt solutions were obtained, and

different phase diagrams were plotted on the same graph, see **Figure 2.9**. The presence of smaller cations causes the expansion of  $L_\alpha$  phase. The influence of the cations is related to the hydration capability of the ions.

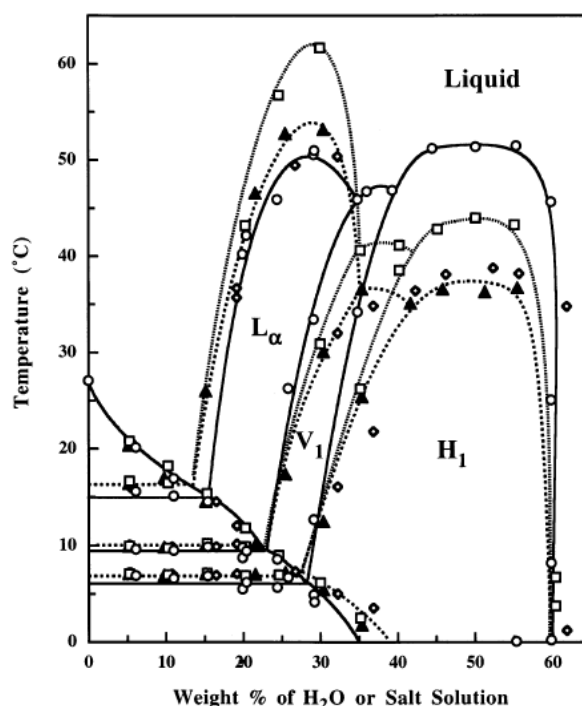


**Figure 2.9.**<sup>8</sup> Phase diagrams of  $C_{10}EO_6$ - $H_2O$  systems in the presence and the absence of salts. The salt species none (circles and straight line), LiCl (squares and dotted line), NaCl (triangles and dashed line) and CsCl (diamonds).<sup>45</sup>

$Li^+$  has the strongest hydration due to its smaller size, but the weakest hydration is expected for  $Cs^+$ . Thus, the largest amount of water is required for the hydration of  $Li^+$ , and the hydration of the ethylene oxide units follows this trend:  $Cs^+ < Na^+ < Li^+$ . The effective cross sectional area reduces with the dehydration of the ethylene oxide chains so CPP of the surfactant molecules increases. As a result, the region that belongs to  $L_\alpha$  phase expands in the diagram with higher CPP values.

The anion effect on the phase behavior of  $C_{12}EO_7$  system was investigated by Inoue and coworkers.<sup>47</sup> In this case, 1.0 M of NaCl, NaI and NaSCN salts

<sup>8</sup> Peprinted from Zheng, Li Qiang, et al., "Effect of inorganic salts on the phase behavior of an aqueous mixture of heptaethylene glycol dodecyl ether" *Langmuir* 19, 10487-10494 (2003), with permission from American Chemical Society.

were mixed with surfactants at different weight percent of salt solutions. It was observed that  $H_1$  region expands with  $ClO_4^-$  and  $I^-$  anions, but it shrinks with  $Cl^-$  ion, see **Figure 2.10**. This observation is related to the dehydration of the ethylene oxide chains. The effective cross sectional area per surfactant molecule decreases as a result of the dehydration of ethylene oxide units which is caused by the structure-maker ions, and the structure-breaker ions have the opposite impact.

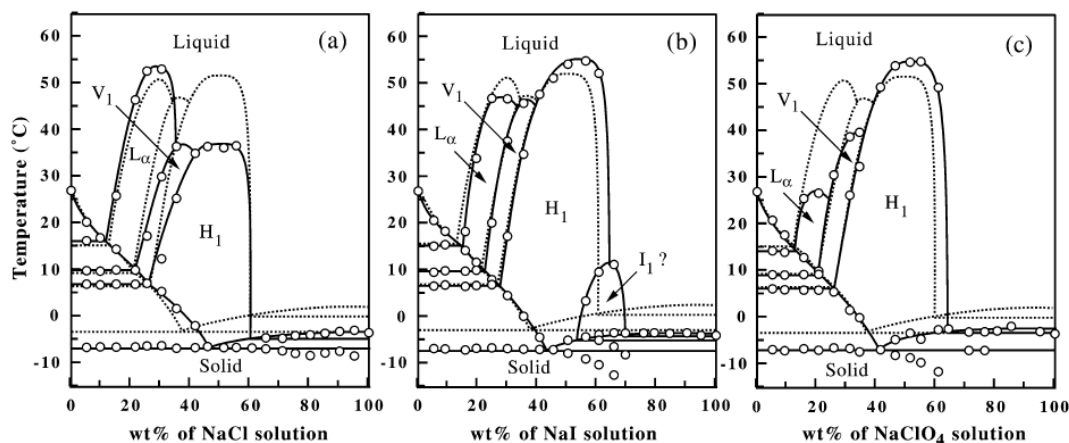


**Figure 2.10.**<sup>9</sup> Phase diagrams of  $C_{12}EO_7$  with various  $Na^+$  salts. The dashed lines corresponds to the salt free phase diagram.<sup>47</sup>

In the investigation of phase behavior of nonionic surfactants, the salts were usually considered as additives, and their influence on the phase behavior and the cloud points were studied generally at low concentrations. A detailed study of LLC mesophases at high salt concentrations have never been performed until 2001.<sup>48</sup> On the other hand, salts can be the main component of surfactant self-assembly at high concentrations. This argument will be investigated on the upcoming chapters.

<sup>9</sup> Reprinted from Inoue, Tohru, Yusuke Yokoyama, and Li-Qiang Zheng, Hofmeister anion effect on aqueous phase behavior of heptaethylene glycol dodecyl ether. *Journal of colloid and interface science* 274, 349-353 (2004), with permission from American Chemical Society.

## 2.2. Lyotropic Liquid Crystals in the Synthesis of Novel Materials

According to IUPAC definition, inorganic solids having pore size in the range of 2 to 50 nm are called mesoporous materials.<sup>49</sup> Ordered mesoporous materials have high functionality as a result of their high surface area (ca. 1500 m<sup>2</sup>/g).<sup>50</sup> Therefore, they become great candidates as catalysts or adsorbents for selective chemical reactions. They can also be considered as anti-quantum dots or anti-quantum rods due to their nano-scale geometries. Therefore, they represent transport properties and size effects which make them as good candidates for novel optical, electrical and magnetic devices.<sup>51</sup>

In 1992, Kresge and coworkers discovered ordered mesoporous silica.<sup>52</sup> Hexagonal (MCM41), cubic (MCM-48), and lamellar (MCM-50) mesoporous materials were produced via cetyrimethylammonium bromide (CTAB) as structure directing agents (SDA) and tetraethylortosilicate (TEOS) as the polymerizing component.<sup>53</sup> Hydrophilic surface of the micelles provide a reaction media for the silica precursor. During the reaction, silica particles surround these micelles, and newly formed binary structure condenses to form mesostructured materials. The surfactant molecules are removed by calcinations in order to form the porous structure.

There are two main approaches in the synthesis of mesostructured and mesoporous materials, see **Figure 2.11**. The first approach is cooperative self-assembly (CSA) method where the inorganic precursors and surfactants are mixed and self-assembled into an ordered pseudo-LC phase. After the formation of LC phase, further polymerization and condensation of the inorganic species are required to form more rigid framework that can be calcined to obtain mesoporous materials.<sup>54</sup> The second approach is true liquid crystalline templating (TLCT) method. A solution of surfactants, inorganic precursor and solvent is spread over a glass substrate and LLC film is obtained by the evaporation of the solvent. In this approach, the inorganic framework exactly mimics the liquid crystalline template. However, in the cooperative self-assembly approach the final structure cannot be predicted since the final structure is constituted via coactions of the initial precursors. This is the main difference between these two approaches. Another main difference is that in the

CSA method the reaction carried out in a dilute micelle solution, while in the TLCT method the synthesis is directed by the LLC phase.<sup>54</sup>

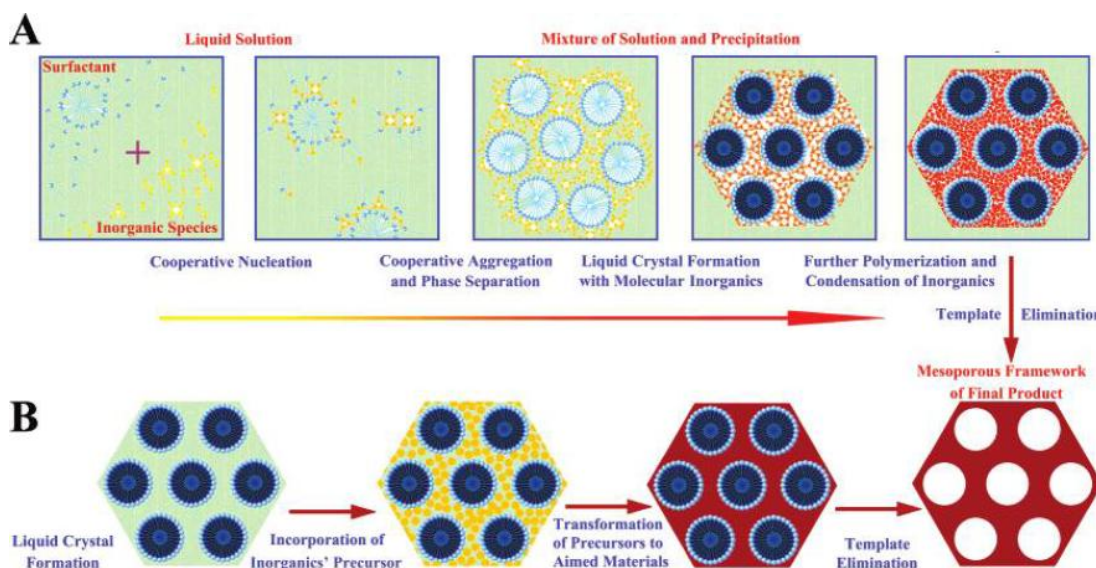


**Figure 2.11.**<sup>10</sup> Two different approach in the synthesis of mesoporous materials: (A) Cooperative self-assembly and (B) True LC templating process.<sup>54</sup>

In 1995, TLCT method was introduced first by Attard and coworkers,<sup>55</sup> and the pathway was extended to block copolymer type surfactants.<sup>56</sup> Hydrogen-bonding network of interactions between the polymerizing inorganic species and ethylene oxide groups of the self-assembled surfactant domains stabilized the LLC mesophase, and further condensation of the inorganics in the hydrophilic domains of the LLC phase makes the mesophase into mesostructured solid. Therefore, strong interactions between inorganic precursors and surfactant molecules are required in order to assemble metal containing structures, otherwise the metal precursors can be leach out or phase separate into surfactant rich domains and salt crystals.<sup>55</sup>

Mesoporous silica synthesis has attracted much attention since it has unique properties and well-known sol-gel chemistry of silica allowed controlled synthesis.<sup>50</sup> In contrast, nonsilicaeous materials are more difficult to synthesis and the synthesis mechanism is not well understood. For example, LLC films are

<sup>10</sup> Reprinted from Wan, Ying, and Dongyuan Zhao On the controllable soft-templating approach to mesoporous silicates. *Chemical Reviews* 107, 2821-2860, (2007), with permission from American Chemical Society.

exposed to H<sub>2</sub>S gas in order to synthesize metal sulfides.<sup>57,58</sup> In the reaction, nanoparticles of metal sulfide is produced which can mimic the LLC template. High metal concentrations in the LLC phase are necessary to synthesize a macroscopic film of the mesoporous material. Therefore, it is important to explore the salt-surfactant LLC mesophases for the synthesis of new and advanced porous materials.

### 2.3. Salt-Surfactant Liquid Crystalline Systems

The transition metal nitrate salt (TMS, [M(H<sub>2</sub>O)<sub>n</sub>](NO<sub>3</sub>)<sub>2</sub>) and nonionic surfactant (oligo(ethylene oxides) or pluronics, triblock-copolymers) lyotropic liquid crystalline phases have been discovered in 2001 by our group.<sup>48,59</sup> The first row transition metal ions such as Co<sup>2+</sup>, Ni<sup>2+</sup>, and Zn<sup>2+</sup> and some second row transition metal ions such as Cd<sup>2+</sup> in their hexa- or tetra-aqua complexes were used to form LLC mesophases with various counter-ions (X<sup>-</sup>) such as chloride, perchlorate and nitrate. The new salt-surfactant LLC mesophases have significantly high metal ion concentration when compared to water-salt-surfactant systems.<sup>48</sup> Stable salt-surfactant LLC phase can be obtained up to 3.2 salt/surfactant mole ratio with many nitrate salts. The difference is nearly 4 folds between these salt-surfactant systems and the water-salt-surfactant systems. The salt content of these systems can be as much as 60 w/w%, and it can be further increased by adding a charged surfactant<sup>60</sup> or using pluronic type surfactants instead of oligo(ethylene oxides).<sup>59</sup>

The strong hydrogen bonding between the coordinated water molecules of the TMS species and hydrophilic ethylene oxide chain of the surfactant is the driving force for the formation of the LLC phase, see **Figure 2.12**.<sup>48</sup> This interaction is considerably higher than the one in the water-surfactant systems.<sup>48</sup> As a result of this strong hydrogen bonding interaction, the salt-surfactant systems have higher isotropization temperatures where the **H<sub>1</sub>** phase can be observed up to 110 °C.

Controlling the quantity of the salt and the type of counter ion allows one to control the structure of the salt-surfactant LLC mesophases. Generally, the nitrate salts form an hexagonal LLC phase, whereas the perchlorates usually form cubic mesophase.<sup>59-61</sup> In the nitrate systems, the overall charge decreases

due to the coordination of nitrate to the metal centers and so the solubility increases.<sup>48</sup> On the other hand, only  $\text{Co}^{2+}$  can form an LLC mesophase with chlorides. In this system, the tetrachlorocobaltate ion ( $\text{CoCl}_4^{2-}$ ) is formed as a result of coordination of chlorides to the metal center.<sup>61</sup> The LLC mesophases, where the counter ion is sulfate are not common since the sulfate salts are insoluble in small amount of water in the LLC media.<sup>48</sup>

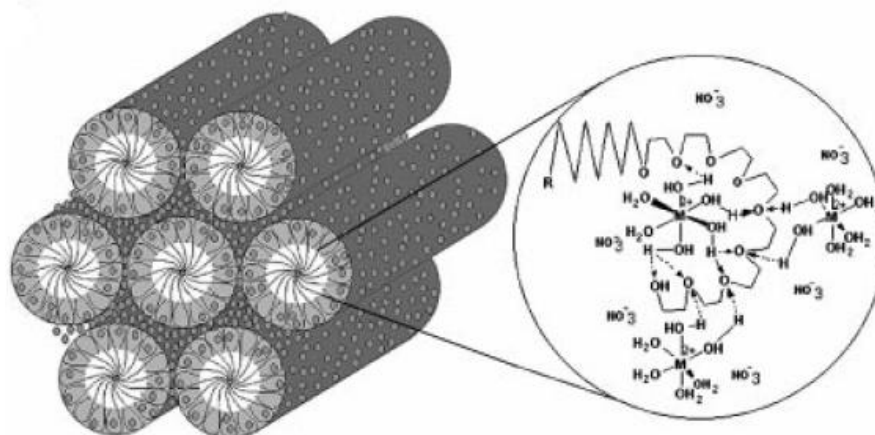


**Figure 2.12.**<sup>11</sup> Schematic representation of hydrogen bonding interactions between coordinated water molecules and the ethylene oxide chain in a hexagonal LLC mesophase.<sup>48</sup>

In 2005, Dag et. al. extended the salt-surfactant LLC mesophases to Pluronic type triblock copolymers  $(\text{OH}(\text{CH}_2\text{CH}_2\text{O})_n-(\text{CH}(\text{CH}_3)\text{CH}_2\text{O})_m-(\text{CH}_2\text{CH}_2\text{O})_n-\text{H})$ .<sup>59</sup> The pluronic-salt mesophases have larger variety of phases including tetragonal and lamellar in addition to hexagonal and cubic phases.<sup>59</sup> A phase separation was observed in the  $\text{Co}^{2+}$  systems of pluronics due to oxidation of the surfactant.<sup>62</sup> Pluronic, in the cobalt salt-pluronic mesophases, undergo slow oxidation in the presence of  $\text{Co}^{2+}$  and oxygen and cause phase separation as salt rich LLC mesophase and an disordered salt free macro domains. All other metal salts form stable LLC mesophases with pluronics. The salt-surfactant mesophases have also been used as templates for the synthesis of mesoporous materials.<sup>58,63-65</sup>

<sup>11</sup> Reprinted from Özgür Çelik, and Ömer Dag, A new lyotropic liquid crystalline system: oligo(ethylene oxide) surfactants with  $[\text{M}(\text{H}_2\text{O})_n]\text{X}_m$  transition metal complexes. *Angewandte Chemie-International Edition* 40, 3800, (2001), with permission from John Wiley & Sons.

The salt-surfactant-water ternary mixtures were also used as templates in the synthesis of mesostructured silica monoliths. In these systems, the salts were chosen among noble metals such as  $\text{H}_2\text{PtCl}_6$ ,  $\text{AgNO}_3$  and  $\text{HAuCl}_4$ .<sup>68</sup> Metal nanoparticles were produced by the reduction of noble metal in the silica network. Moreover, the mesostructured metal sulfide films were produced by exposing spin coated LLC samples over a glass substrate to  $\text{H}_2\text{S}$  gas.<sup>57,58</sup> Later, Dag and coworkers increased the metal-uptake of the salt-surfactant systems up to 80 w/w% of salt by using charged surfactants such as cetyltrimethylammonium bromide (CTAB) or sodium dodecylsulfate (SDS).<sup>60,67</sup> In these mesophase, the charged surfactants do not leached out as a result of the long-range columbic interaction between the salt species and the charged core-shell interface of the mesophase. Therefore, it is possible to synthesize stable mesostructures metal sulfide films having higher salt ratios.<sup>64</sup>

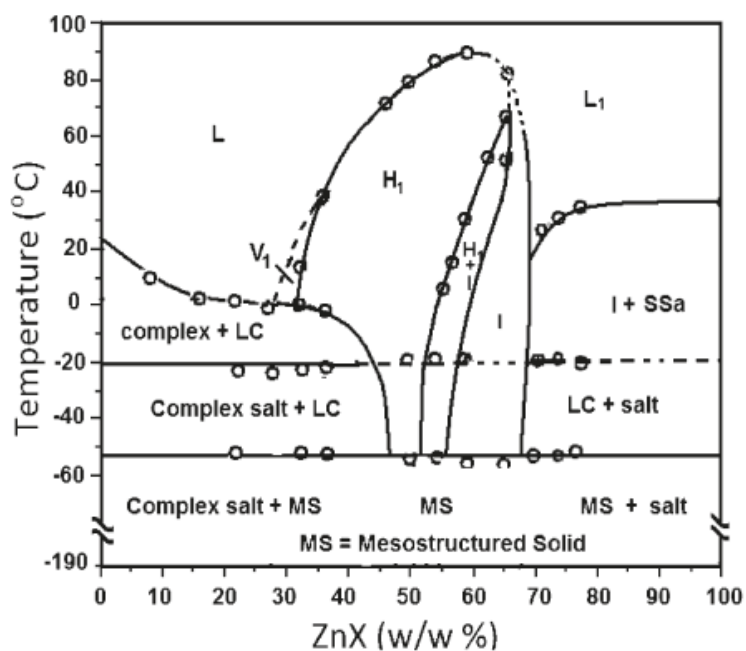


**Figure 2.13.**<sup>12</sup> Phase diagram of the  $\text{ZnX-C}_{12}\text{EO}_{10}$  system.<sup>68</sup>

The  $[\text{Zn}(\text{H}_2\text{O})_6](\text{NO}_3)_2\text{-C}_{12}\text{EO}_{10}$  mesophase has been investigated extensively in order to clarify the perspective on the salt-surfactant systems of

<sup>12</sup> Reprinted from C. Albayrak, N. Özkan, and Ö. Dag. Origin of Lyotropic Liquid Crystalline Mesophase Formation and Liquid Crystalline to Mesostructured Solid Transformation in the Metal Nitrate Salt-Surfactant Systems. *Langmuir* 27, 870-873, (2010), with permission from American Chemical Society.

the first row transition metals.<sup>68</sup> The phase diagram of the  $[\text{Zn}(\text{H}_2\text{O})_6](\text{NO}_3)_2$ - $\text{C}_{12}\text{EO}_{10}$  was constructed by using DSC, POM and XRD techniques, see **Figure 2.13**.<sup>68</sup>

The phase diagram of the salt-surfactant and water-surfactant are very similar. The **V<sub>1</sub>**, **H<sub>1</sub>**, **I<sub>1</sub>** and **L<sub>1</sub>** phases were observed with increasing the salt concentration. However, the salt-surfactant mesophase shows an unusual behavior at low temperatures, and it displays glass transition at  $-52\text{ }^\circ\text{C}$ .<sup>68</sup> Furthermore, the LLC mesophase freezes into a mesostructured solid below the glass transition temperature.<sup>68</sup> This work proved that in the  $[\text{Zn}(\text{H}_2\text{O})_6](\text{NO}_3)_2$ - $\text{C}_{12}\text{EO}_{10}$  system, the salt species are in the molten phase and they act as solvent in the media.<sup>68</sup>

In 2012, Dag and coworkers further extended salt-surfactant mesophases to non-transition metal salts. They proved that the  $\text{LiNO}_3$ ,  $\text{LiCl}$  and  $\text{LiClO}_4$  salts can also form LLC mesophases with the oligo(ethylene oxide) type surfactants in the presence of a small amount of water.<sup>69</sup> In these mesophases, the hydrated alkali metal salts acts as a solvent in the assembly process. Therefore, the highly concentrated solution of electrolyte can be regarded as an analogue of a molten salt.<sup>68</sup> In the LLC mesophase of  $\text{LiNO}_3$ , the salt to water mole ratio can be nearly 2 times lower than the one in the saturated  $\text{LiNO}_3$  aqueous solution.<sup>69</sup> The reason of this is due to the interaction between the salt-water couple and ethylene oxide chain, and confinement effect (the melting point depression of the salts in the confined hydrophilic domains of the mesophases). The confinement effect enforces the formation of the LLC mesophase through hydrogen bonding ( $\text{M-OH}_2\cdots(\text{OCH}_2\text{CH}_2)_x\text{-R}$ ) and more importantly depress the melting point of the salt that acts as a good solvent in the media.<sup>69</sup> Moreover, the hydrated alkali salt-surfactant LLCs display high ionic conductivity ( $7.0 \times 10^{-3}\text{ S cm}^{-1}$ ) so they can be considered as good electrolytes for the non-water-sensitive electrochemical applications.<sup>69</sup>

## 2.4. A New Phase Transition in LLC Systems

In the LLC mesophases of hydrated salt-surfactant systems of LiI, CaCl<sub>2</sub> and MgCl<sub>2</sub> another unusual phase transition from LLC mesophase to soft mesocrystal (SMC) phase was observed under ambient condition by our group.<sup>70-71</sup> The mesocrystals are usually solid materials that are formed as a result of self-assembly process of colloidal nanocrystals.<sup>72</sup> They can be synthesized through several steps; by chemical reactions to form nanoparticles,<sup>73</sup> and then directed and organized by the organic directing agents.<sup>74</sup> Recently, we also observed the formation of soft mesocrystals (SMC) from these three salt systems. The SMC samples display both small and high angle diffractions, and unit cell of the samples becomes larger than those of their LLC mesophases, see **Figure 2.14**.

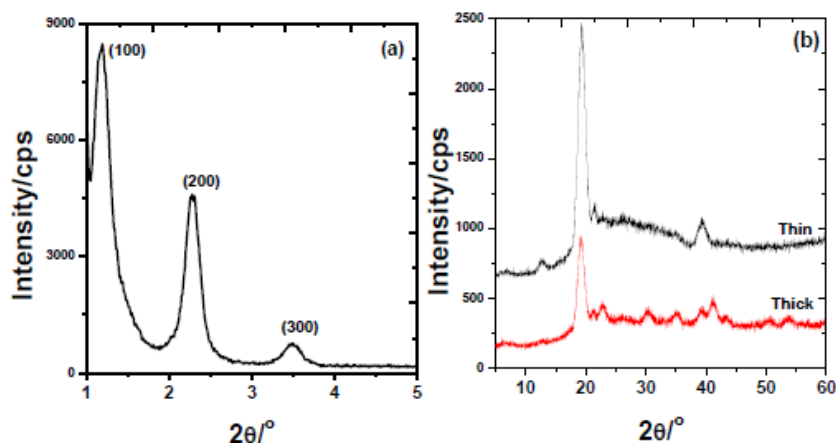


**Figure 2.14.** XRD patterns of the 4.0LiI-xH<sub>2</sub>O-C<sub>12</sub>EO<sub>10</sub> mesocrystal at (a) low angles, and (b) high angles.<sup>71</sup>

The FT-IR spectra of the mesocrystalline samples have some distinct properties when compared to the spectra of the LLC mesophases, **Figure 2.15**. All the peaks in the spectra become sharper; in addition to that, some of the surfactant peaks split into two, and some new peaks arise.

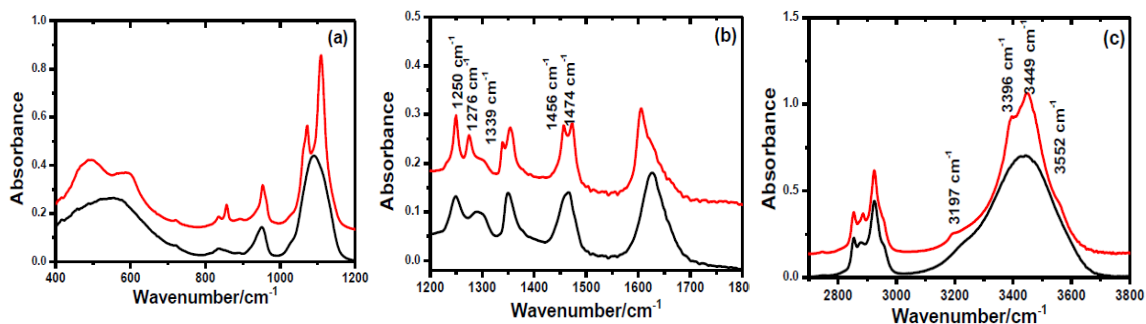


**Figure 2.15.** FT-IR spectra the 4.0Li-xH<sub>2</sub>O-C<sub>12</sub>EO<sub>10</sub> mesocrystal (top) and LLC mesophase (bottom) at different wavenumbers.<sup>71</sup>

Two new peaks arise at 1274 and 1339 cm<sup>-1</sup> which correspond to the CH<sub>2</sub> twisting mode and CH<sub>2</sub> rocking mode of the trans C-O bond in the ethylene oxide domain, respectively. This has been regarded as the expansion of the surfactant domains upon phase transition from LLC mesophase to SMC phase, and it is consistent with the changes in the XRD patterns of these samples. The water peaks get sharper and the intensity of 4 resolved water signals demonstrate that the SMC samples do not lose water during phase transition.<sup>71</sup>

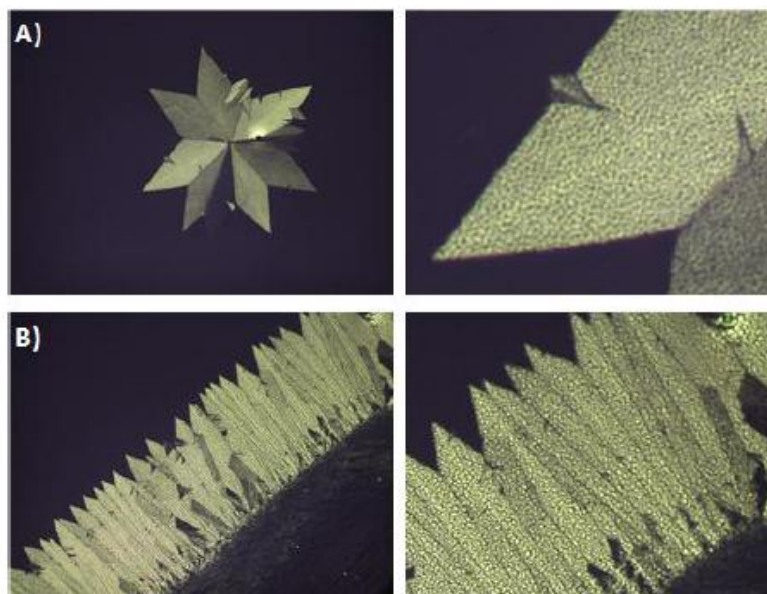


**Figure 2.16.** POM images of 4.0CaCl<sub>2</sub>-xH<sub>2</sub>O-C<sub>12</sub>EO<sub>10</sub> mesocrystal Mesocrystal growth from (A) defect site mesophase (B)edge of the sample (magnified images on the right).<sup>71</sup>

The POM images of mesocrystal samples display birefringent and sharp edged texture like in the crystal textures, see **Figure 2.16**. In contrast to normal crystal texture, there is some sponge like texture in the birefringent domains.

According to our recent investigation, the mesocrystal formation is related to the temperature and relative humidity in the air. Above 25% RH mesocrystals transform into LLC phase at RT. At higher salt concentrations, the mesocrystal formation is observed at lower RH. For example, in the 5.0-8.0 mole ratios, the mesocrystal are stable at 20 % RH; however, between 3.0 and 5.0 mole ratios 15% RH is required to observe mesocrystals both at RT.<sup>76-77</sup> These samples can change birefringency, and be used as humidity sensors due to their sensitivity toward relative humidity.

## 2.5. Effect of Deliquescence on the Stability of LLC Mesophases

There is a strong relationship between the formation and stability of LLC mesophases and the deliquescence relative humidity (DRH) of the salts.<sup>76</sup> According to our recent findings, the salts can be categorized into three different groups: type I salts can form stable LLC phase because of their low DRH, type II salts have intermediate DRH and form LLC mesophases with little or no structural order, and Type III salts leach out salt and surfactant, and cannot form stable LLC mesophase due to their high DRH.<sup>70,75</sup> Therefore, the DRH is a critical value for the salts, where the salt spontaneously absorbs water in the air and dissolves.<sup>76</sup>

**Table 2.3.** Stability of LLC mesophases of various cation-anion couples. Roman numbers means (I) stable LLC phase, (II) no crystallization at low salt concentrations, and little structural order, (III) salt crystallizes out. The symbols indicate (-) not studied, (\*) transition to mesocrystalline phase, and LS is low solubility.<sup>75</sup>

Cation/Anion	CH <sub>3</sub> CO <sub>2</sub> <sup>-</sup>	Cl <sup>-</sup>	Br <sup>-</sup>	I <sup>-</sup>	NO <sub>3</sub> <sup>-</sup>	ClO <sub>4</sub> <sup>-</sup>	SCN <sup>-</sup>	F <sup>-</sup>
Li <sup>+</sup>	-	I	I	I*	I	III	-	LS
Na <sup>+</sup>	III	III	III	II	III	II	III	-
K <sup>+</sup>	-	III	-	III	III	LS	II	-
Ca <sup>2+</sup>	-	I*	-	-	I	-	-	-
Mg <sup>2+</sup>	-	I*	-	-	III	-	-	-

**Table 2.3** shows that the LiCl, LiNO<sub>3</sub>, LiBr, LiI, CaCl<sub>2</sub>, CaNO<sub>3</sub> and MgCl<sub>2</sub> salts can form stable LLC mesophase with non-ionic surfactants although the CaCl<sub>2</sub>-nH<sub>2</sub>O-C<sub>12</sub>EO<sub>10</sub>, LiI-nH<sub>2</sub>O-C<sub>12</sub>EO<sub>10</sub> and MgCl<sub>2</sub>-nH<sub>2</sub>O-C<sub>12</sub>EO<sub>10</sub> mesophases undergo mesocrystalline phase transformation upon aging. However, the Na(I) salts, K(I) salts, and Mg(II) salts, are unstable and crystallize rapidly upon spin coating, except NaI, NaClO<sub>4</sub>, KSCN and MgCl<sub>2</sub>. LiClO<sub>4</sub> salt cannot form stable mesophase with C<sub>12</sub>EO<sub>10</sub> surfactant, but it can form stable LLC mesophase with C<sub>18</sub>EO<sub>10</sub> between 1.0 and 3.0 salt to surfactant mole ratios.<sup>75</sup>

The trends among different salts depend on the deliquescence relative humidity of the salts. Li(I) salts have lower DRH values than Na(I) and K(I) salts. The DRH levels of Li(I) salts are lower than 20%, which is below the experimental conditions, 20-25%.<sup>75</sup> This may explain the stability of LLC mesophase containing Li(I) salts. The chloride salts of Ca(II) and Mg(II) have lower DRH (33%-31%) compared to nitrate salts (52%-51%). Therefore, the Mg(NO<sub>3</sub>)<sub>2</sub>-C<sub>12</sub>EO<sub>10</sub> samples crystallize rapidly after spin coating, whereas the LLC mesophase of the Ca(NO<sub>3</sub>)<sub>2</sub>-C<sub>12</sub>EO<sub>10</sub> is stable. This indicates that the interactions between the divalent cation and hydrophilic part of the surfactant are stronger compared to monovalent cations.<sup>75</sup> Other factors such as the salt concentration, temperature, pressure, hydrophilicity, and relative humidity can also affect the phase behavior of hydrated salt-surfactant systems. For this reason, further investigation is required to completely elucidate the nature of such systems and their stability.

## 2.6. Electrolytes for Dye-Sensitized Solar Cells

Dye-sensitized solar cells (DSSCs) are photovoltaic devices that provide a maximum power conversion efficiency of around 12%.<sup>77,78</sup> They attract significant attention since they can be produced with a lower cost than their solid-state alternatives, and they are more environment-friendly.

The working principle of the dye-sensitized solar cells is based on using photons to separate charges (electron-hole pairs). A dye that is attached to a

wide band gap semiconductor ( $\text{TiO}_2$  or  $\text{ZnO}$ ) absorbs a photon under illumination. As a result of photon absorption, an electron is excited from the highest occupied molecular orbital (HOMO) of the dye into lowest unoccupied molecular orbital (LUMO) level. This electron is transferred to the conduction band (CB) of the nanostructured semiconductor, then to a transparent fluorine-doped tin oxide (FTO), and then to the counter electrode, where the reduction process takes place. Simultaneously, a redox couple that is present in the electrolyte between these two electrodes supplies the electrons to replenish the electron deficient dye back to its original state. This completes the circuit, as a result the solar energy is converted into the electrical energy.<sup>79</sup>

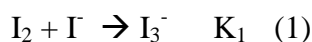
Generally, an  $\text{I}/\text{I}_3^-$  redox couple is used as the redox couple between the working and counter electrodes, and plays a significant role in the regeneration of oxidized dye molecules and determination of the photovoltage of the cell.<sup>80</sup> Conventionally, organic-solvent-based liquid electrolytes such as acetonitrile or 3-methoxypropionitrile are used in DSSCs. The usage of this kind of electrolytes has some drawbacks, such as being toxic or explosive which are obstacles for their practical applications. Hence, water-based electrolytes can be better alternative to prevent performance degradation due to the water entrance into the cell via poor sealing.<sup>80-81</sup>

On the other hand, liquid electrolytes have some disadvantages in terms of long-term operation since the volatile nature of solvents leads to leakage and evaporation of electrolytes. Moreover, corrosion of Pt counter electrode, desorption of dye molecules, and photodegradation in the desorbed state are other factors which reduce efficiency and long-term stability of DSSCs where the liquid electrolytes are used. To solve these problems, gel electrolytes attract considerable attention due to their long-term stability and superior mechanical properties.<sup>82-83</sup> If one could combine the advantages of water-based electrolytes and gel electrolytes, it would be possible to produce environment-friendly, efficient, low-cost DSSCs with a long-term stability. However, energy conversion efficiencies of the gel electrolytes are usually lower than that achieved by using the liquid electrolytes, caused by the low conductivity of the gel electrolytes compared to liquid ones.

### 2.6.1. Characteristics of the Iodide/Triiodide Redox Couple

The redox couple is one of the key components of DSSCs because it regenerates the oxidized dye. The redox couple also determines the electrochemical potential of the wide band gap semiconductor by the recombination kinetics of electrons in the semiconductor and oxidized redox species.<sup>84</sup> Iodide/triiodide is the most preferred redox couple since it has good solubility and suitable redox potential, does not absorb too much light, leads to rapid regeneration of dye molecules.<sup>84</sup> The standard redox potential of I<sup>-</sup>/I<sub>3</sub><sup>-</sup> couple is 0.35 V (versus normal hydrogen electrode, NHE), and oxidation potential of the standard Ru-based dye sensitizer is 1.1 V. Therefore, the driving force for the reduction of oxidized dye molecules is about 0.75 V.<sup>84</sup>

In solution, the iodine and iodide from triiodide:



Polyiodide species such as I<sub>5</sub><sup>-</sup>, I<sub>7</sub><sup>-</sup> and I<sub>9</sub><sup>-</sup> may also be formed, if the iodine concentration is too high in the solution, but only I<sub>3</sub><sup>-</sup> is significant for DSC electrolytes.<sup>84</sup> The redox potential of the electrolyte can be calculated from the Nernst equation:

$$E_{\text{redox}} = E^{0'} + \frac{RT}{2F} \ln \frac{[I_3^-]}{[I^-]^3} \quad (2)$$

Where  $E^{0'}$  is the formal potential,  $R$  the gas constant,  $T$  the absolute temperature, and  $F$  Faraday constant. **Table 2.4** summarizes redox potentials of iodide/triiodide systems in different solvents.

**Table 2.4.**<sup>13</sup> Redox potentials of various I<sup>-</sup>/I<sub>3</sub><sup>-</sup> systems.<sup>84</sup>

solvent	$E^0$ (I <sub>3</sub> <sup>-</sup> /I <sup>-</sup> )	$E^0$ (I <sup>*</sup> /I <sup>-</sup> )	$E^0$ (I <sub>2</sub> <sup>-*</sup> /I <sup>-</sup> )	$E^0$ (I <sub>3</sub> <sup>-</sup> /I <sub>2</sub> <sup>-*</sup> )
water	+0.536	+1.33 <sup>6</sup>	+1.03 <sup>6</sup>	+0.04 <sup>b</sup>
acetonitrile <sup>a</sup>	+0.29 <sup>c</sup> +0.354 <sup>5</sup>	+1.23 <sup>7</sup>	<+0.93 <sup>7</sup>	>-0.35

<sup>a</sup> Values reported vs Fc<sup>+</sup>/Fc are converted to NHE by addition of 0.63 V. <sup>b</sup> A value of +0.21 V for  $E^0$ (I<sub>2</sub><sup>-\*</sup>/I<sup>-</sup>) is reported by Stanbury.<sup>6</sup> <sup>c</sup> Average value from studies summarized in ref 7.

<sup>13</sup> Reprinted from Boschloo, Gerrit, and Anders Hagfeldt. Characteristics of the iodide/triiodide redox mediator in dye-sensitized solar cells. *Accounts of Chemical Research* 42, 1819-1826, (2009), with permission from American Chemical Society.

**Figure 2.17** shows schematic representation of energy levels of a DSSC. For the standard Ru-based such as N719 the oxidization potential toward NHE is 1.10 V. This value is the same for absorbed dye onto a conducting tin oxide glass (ITO). The potential difference between  $E^{0'}(D^+/D)$  and  $E^{0'}(I/I_3^-)$  is about 0.75 V. This potential is the driving force the forward reaction the DSSC.

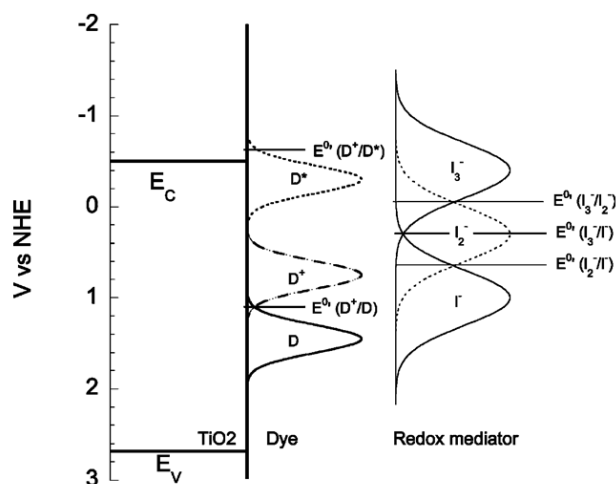


**Figure 2.17.**<sup>14</sup> Energy scheme of cis-Ru(dcbpy)<sub>2</sub>(NCS)<sub>2</sub>-sensitized TiO<sub>2</sub> solar cell with I<sup>-</sup>/I<sub>3</sub><sup>-</sup> redox couple.<sup>84</sup>

The oxidized dye is reduced by I<sup>-</sup> in the electrolyte, and the half-time for regeneration of dye molecules is in the range of 100 ns to 10 μs in the presence of 0.5 M iodide and 0.05 M iodine. The nature of the cation (such as Li<sup>+</sup>) has also great impact on the regeneration half-time. Pelet et al. reported faster regeneration time by using cation containing electrolytes.<sup>85</sup> Cations are absorbed at the TiO<sub>2</sub> surface, and this leads to an increase in the local concentration of iodide near TiO<sub>2</sub>/electrolyte surface.

At the counter electrode, the I<sub>3</sub><sup>-</sup> ion must be reduced to I<sup>-</sup> efficiently so the counter electrode must be catalytically active in order to provide fast reaction and low overpotential.<sup>84</sup> The charge transfer resistance,  $R_{ct}$ , is related to the overpotential,  $\eta$ , that is required to drive reaction at creation current density,  $J$ .<sup>84</sup>

<sup>14</sup> Reprinted from Boschloo, Gerrit, and Anders Hagfeldt. Characteristics of the iodide/triiodide redox mediator in dye-sensitized solar cells. *Accounts of Chemical Research* 42, 1819-1826, (2009), with permission from American Chemical Society.

$$R_{ct} = \eta/J \quad (3)$$

$R_{ct}$  act as a series resistance in DSSCs, and it should be down to about  $1 \text{ } \Omega/\text{cm}^2$  to avoid huge loses. For this purpose, counter electrodes made by Pt deposited conducting glass electrodes are suitable. However, low Pt loadings are necessary in order to keep electrodes transparent.<sup>84</sup>

The iodide/triiodide couple is one of the best redox mediators for DSSCs. The recombination rate of electrons in the  $\text{TiO}_2$  and triiodide in the electrolyte is very slow compared to the other redox couples. Moreover, the regeneration rate of the oxidized dye is fast, however, this is caused by the potential loss of  $0.75 \text{ V}$ .<sup>84</sup>

This thesis involves the investigation of LLC mesophases of lithium salts with nonionic surfactants. Iodide/triiodide redox couple was incorporated into these LLC mesophases in order to create a gel electrolyte for DSSCs.

## CHAPTER 3

### 3. EXPERIMENT RESULTS

#### 3.1. Materials

All chemical were obtained from Sigma Aldrich. Tap water was distilled and further purified using Millipore Synergy 185 water purifier.

#### 3.2. Sample Preparation

##### 3.2.1. Preparation of the $\text{LiX-xH}_2\text{O-C}_{12}\text{EO}_{10}$ Gel Samples

The samples were prepared by mixing the surfactant and the salts of metal ions in water with required amounts, and they were homogenized in sealed glass vials by constant shaking in a water bath at 70° C for 24 hours. For instance, a sample with the composition  $3.0\text{LiI-9.0H}_2\text{O-1.0C}_{12}\text{EO}_{10}$  was prepared by weighing  $\text{C}_{12}\text{EO}_{10}$  (1.00 g), LiI (0.64 g) and  $\text{H}_2\text{O}$  (0.26 g) in a 20 ml glass vial. The closed vial was constantly shaken in a water bath at 70 °C for at least 24 hours. The remaining amount of water in the LLC media under ambient conditions depends on the temperature, RH and the salt composition in the mesophase. However, it is enough to assure stability of the LLC mesophase.

##### 3.2.2. Preparation of Samples in the Solution Phase

The required amounts of the surfactant and salt were weighted and mixed in glass vials using a stirrer for at least 6 hours for homogenization. The solution phase does not require heating. For example, in preparation of  $4.0\text{LiCl-1.0C}_{12}\text{EO}_{10}\text{-excessH}_2\text{O}$ , 0.27 g of LiCl, 1.00 g of  $\text{C}_{12}\text{EO}_{10}$  and 5 ml of  $\text{H}_2\text{O}$  were mixed and stirred 6 hours. The homogenous solutions were ready for further treatment.

##### 3.2.3. Preparation of the Samples with Redox Couple

The preparation of these samples requires the steps mention in section 3.2.1 and 3.2.2. for gel samples and samples in the solution phase respectively. However, acetonitrile was used instead of  $\text{H}_2\text{O}$ , and only 3 drops of  $\text{H}_2\text{O}$  was added to the solutions. For instance, a sample with the composition of  $1.0\text{LiBr-3.0LiI-0.3I}_2\text{-1.0-xH}_2\text{O-C}_{12}\text{EO}_{10}$  in excess

acetonitrile was prepared by weighing LiBr (0.140 g), LiI (0.364 g), I<sub>2</sub> (0.120 g), C<sub>12</sub>EO<sub>10</sub> (1.000 g). 5 ml of acetonitrile and 3 drops of water were added for the preparation of the samples in the solution phase or 0.26 g of acetonitrile was added for those of the gel samples. After addition of 3 drops of H<sub>2</sub>O, the samples were homogenized as mentioned in section 3.2.1 and 3.2.2.

#### **3.2.4. Preparation of thin LLC Films and Small Scale Gel Samples**

The LLC thin films were prepared by spin coating the homogenized samples in the solution phase on glass slides or silicon wafers. The speed of the spin coater was kept between 1500 and 500 rpm depending on the purpose. Small scale gel samples were prepared by dropping 1-2 drops of the homogenized solution on a glass slide or silicon wafer. The LLC samples were formed by the evaporation of the excess water. However, evaporation of water in this way caused the concentration gradient along the sample. The spin coated samples are more homogeneous due to the rapid evaporation of the excess water.

### **3.3. Fabrication of Solar Cells**

#### **3.3.1. Preparation of Mesoporous Titania Films (meso-TiO<sub>2</sub>)**

3.5 g of P25 (titania) was dispersed into 15 ml of ethanol and sonicated 30 minutes. 0.5 ml of Ti(IV) isopropoxide was added into the suspension, and mixed until the suspension becomes uniform. In advance, the FTO glass was first spin coated with the solution of 5 ml of ethanol, 0.25 g of Ti(BuO)<sub>4</sub> and 0.5 ml of HNO<sub>3</sub> with 200 rpm, and heated at 450 °C for 15 minutes. Then the suspension was spread over the pre-coated FTO, and then calcined at 450° C for an hour, denoted as meso-TiO<sub>2</sub>.

#### **3.3.2. Preparation of Dye Solution and Titania Electrode**

20 ml of 1 mM dye solution was prepared by dissolving 0.024 g of N719 dye in ethanol. The titania electrode, which was prepared as mentioned in **section 3.3.1**, was dipped into the dye solution for 24 hours.

#### **3.3.3. Preparation of Pt-deposited FTO electrode**

A 5 mM H<sub>2</sub>PtCl<sub>6</sub> solution was prepared in 2-propanol. Then a few drops of the solution were spread on FTO glass, and heated up to 450 °C for 1

hour. These electrodes were used as counter electrode in the dye-sensitized solar cells device.

### 3.3.4. Assembly of DSSCs

DSSCs were fabricated either using cells or sandwiching gel electrolyte between electrodes.

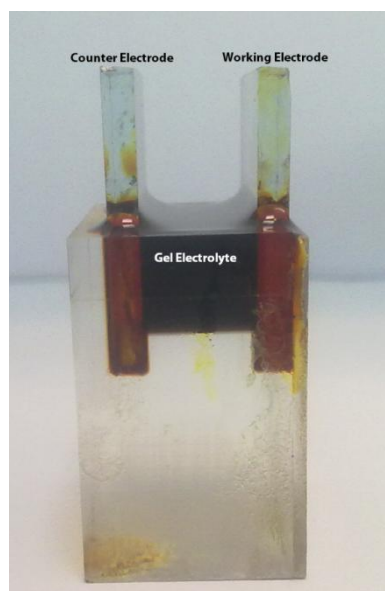


**Figure 3. 1.** DSSCs with gel electrolyte in the form of cell.

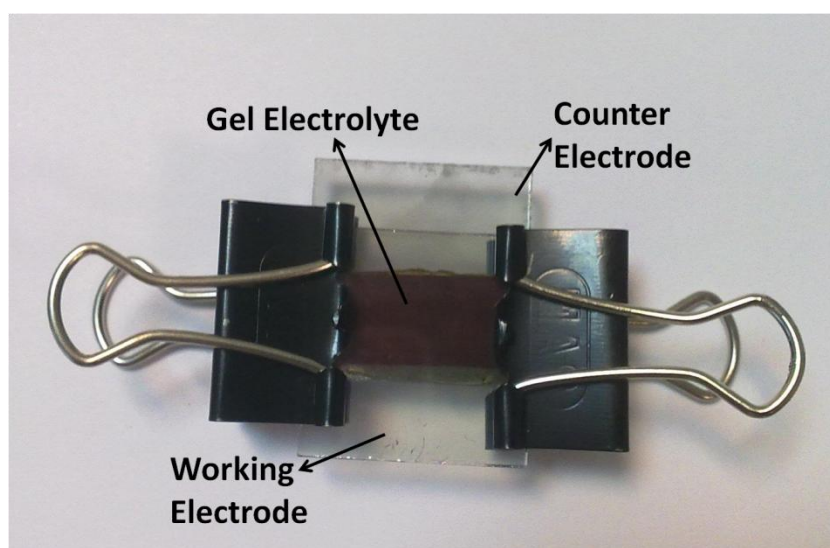


**Figure 3. 2.** DSSC with gel electrolyte sandwiched between two electrodes.

**Figure 3.1.** and **3.2.** show two different DSSC assemblies. In the cell form, working and counter electrodes were placed into the holes of cell as

parallel to each other. The vicinity between two electrodes was filled with the gel electrolyte. In the sandwich form, the gel electrolyte (solution phase of our LiI LLC mesophase) was dropped onto the dye coated TiO<sub>2</sub> electrode and kept at 80° C for 1 hour in order to ensure sufficient penetration of gel into pores of the TiO<sub>2</sub> electrode (anode). Then the counter electrode was placed onto the gel-containing working electrode.

### **3.4. Instrumentation**

#### **3.4.1. The X-ray Diffraction (XRD)**

The XRD patterns were recorded on a Rigaku Miniflex diffractometer using a high power Cu-K<sub>α</sub> source operating at 30kV/15mA and a wavelength of 1.5405 Å. The measurements were carried out by spreading the samples on glass slides by spin-coating. The measurements were done at various scan rates (ranging from 0.1 Θ/min to 1 Θ/min) at 0.01 data intervals.

#### **3.4.2. The Polarized Optical Microscopy (POM)**

The POM images were obtained in transmittance mode by using a ZEISS Axio Scope.A1 polarizing optical microscope with a Linkam LTS350 temperature controlling stage attached to the microscope. The temperature control was performed by using a LinkamT95-LinkPad temperature programmer attached to the stage.

#### **3.4.3. The Fourier Transform - Infrared Spectroscopy (FT-IR)**

The FT-IR spectra were recorded using a Bruker Tensor 27 model FTIR spectrometer. A Digi Tect TM DLATGS detector was used with a resolution of 4.0 cm<sup>-1</sup> in the 400-4000 cm<sup>-1</sup> range. The spectra were recorded by either spreading the samples on silicon wafers or sandwiching them between two silicon wafers in order to prevent the evaporation of water. The FT-IR spectra of the samples were collected using 128 scans.

#### **3.4.4. The micro-Raman Spectroscopy**

The micro Raman spectra were recorded on a LabRam confocal Raman microscope with a 300 mm focal length. The spectrometer is equipped with a Ventus LP 532, 50 mW, diode pumped solid-state laser operator at 20

mW, with a polarization ratio of 100:1, a wavelength of 532.1 nm, and a 1024x256 element CCD camera. The signal collected was transmittance via a fiber optic cable into a spectrometer with 600 g/mm grating. The Raman spectra were collected by manually placing the probe tip on the desired point of the sample over the glass or silicon wafer.

#### **3.4.5. The AC Impedance Spectroscopy**

The conductivity measurements were performed by using Gamry G750 potentiostat/galvanostat with a homemade conductivity cell equipped with two stainless-steel electrodes. The cell constant for the conductivity cell was determined by using standard solution of KCl at RT. The measurements at RT were performed by immersing the conductivity cell in a water bath. Resistance data were recorded for all conductivity measurements after the equilibration of the sample temperature with the bath temperature.

#### **3.4.6. UV-vis Spectroscopy**

The UV-vis spectroscopy were recorded using a Varian Carry 5 and Thermo Specific Evolution 160 double beam spectrophotometer with a 600 nm/min speed and 0.2 nm resolution over a wavelength range from 190 nm to 900 nm. Samples were spin coated on quartz substrates for measurements.

#### **3.4.7. The Photovoltaic Measurements**

Solar performance measurements employed an AM 1.5 solar simulator equipped with a 300 W xenon lamp (Model N0. 81172, Oriel). The light intensity was adjusted to  $100\text{mWcm}^{-2}$  by using a reference Si photodiode. I-V curves were obtained by applying an external bias to the cell and measuring the generated photocurrent with a Keithley model 2400 digital source meter.

## CHAPTER 4

### 4. EVALUATION

Since the discovery of the lyotropic liquid crystalline (LLC) phase of transition metal nitrate salts ( $[M(H_2O)_n](NO_3)_2$ , TMS) and non-ionic surfactants,<sup>48</sup> the LLC mesophases of TMS and triblock poly(ethylene oxide)-poly(propylene oxide)-poly(ethylene oxide) copolymers (known as pluronics,  $HO-(CH_2CH_2O)_n(CH(CH_3)CH_2O)_m(CH_2CH_2)_n-H$ , represented  $EO_nPO_mEO_n$  or PX, where X is a number related to the molecular weight and percent ethylene oxide of the polymer and P65, P85, P103 and P123 have been used in this work) have been extensively investigated in our group.<sup>59,62</sup> The coordinated water molecules of the TMS and confinement effects (drop in the melting point of the salts in a small space) are the two driving forces for the formation and stability of the LLC mesophases. In this chapter, we will demonstrate that concentrated solutions of alkali metal salts can also organize the surfactants molecules into the LLC mesophases like transition metal salts.

#### 4.1. Lyotropic Liquid Crystalline Mesophases of Plurionics (P65, P85, P103, and P123) with LiCl and LiNO<sub>3</sub> Salts

The LLC mesophases of LiCl and LiNO<sub>3</sub> salts with the P65 ( $EO_{20}PO_{30}EO_{20}$ ), P85 ( $EO_{26}PO_{40}EO_{26}$ ), P103 ( $EO_{17}PO_{55}EO_{17}$ ), and P123 ( $EO_{20}PO_{70}EO_{20}$ ) triblock copolymers have been investigated over a range of salt concentrations in the presence of a small amount of water in the media. The LLC mesophases were observed in the LiCl-xH<sub>2</sub>O-P65, LiCl-xH<sub>2</sub>O-P85, LiCl-xH<sub>2</sub>O-P103, and LiCl-xH<sub>2</sub>O-P23 systems between 6.0 and 25.0, 10.0 and 25.0, 6.0 and 20.0, and 8.0 and 25.0 LiCl/pluronic mole ratios, respectively, see **Table 4.1**. At low salt concentration, the samples leached out surfactant crystals since the amount of salt was not sufficient to organize surfactant molecules into mesophases. On the other hand, at very high salt concentrations the systems leached out the salt crystals slowly over time. The fresh samples with intermediate composition form homogenous and stable mesophases for months

(salt crystals were not observed over six months by means of XRD, microscopy and spectroscopy).

The LiCl-xH<sub>2</sub>O-Pluronic mesophases were identified using XRD patterns and POM images of the samples that are either spin coated over a glass surface or drop casted the homogenized LiCl, water, and pluronic solutions on desired substrates. **Table 4.1** summarizes the phase behavior of the samples of various pluronics (P65, P85, P103, and P123) with LiCl and LiNO<sub>3</sub> salts. The **H** stands for the hexagonal mesophase and **I** represents the cubic phase. All other compositions could not be identified using XRD and POM techniques.

**Table 4.1.** Phase behavior of the LiCl-xH<sub>2</sub>O-Pluronic systems at RT and 22-25% RH (H =hexagonal, I = cubic).

	MOLE RATIOS							
	5.0	6.0	8.0	10.0	12.0	15.0	20.0	25.0
<b>P65-LiCl</b>	-	H	H	H	H	H	I	-
<b>P85-LiCl</b>	-	-	H	H	H	H	I	-
<b>P103-LiCl</b>	H	H	H	H	H	I	-	-
<b>P123-LiCl</b>	-	H	H	H	H+I	H+I	I	I
<b>P103-LiNO<sub>3</sub></b>	-	H	H	H	I	I	I	-
<b>P123-LiNO<sub>3</sub></b>	-	H	H	H	H	I	I	I

The LiCl-xH<sub>2</sub>O-P65 samples display small angle diffraction lines in the 2 $\theta$  range of 1.0-5.0° with a broad range of LiCl concentrations. **Figure 4.1** shows the small angle XRD patterns of the LiCl-xH<sub>2</sub>O-P65 samples and a representative POM image under the ambient conditions. The diffraction patterns are characteristic for the 2D hexagonal LLC mesophase with a unit cell parameter *a* of 87.1 Å.

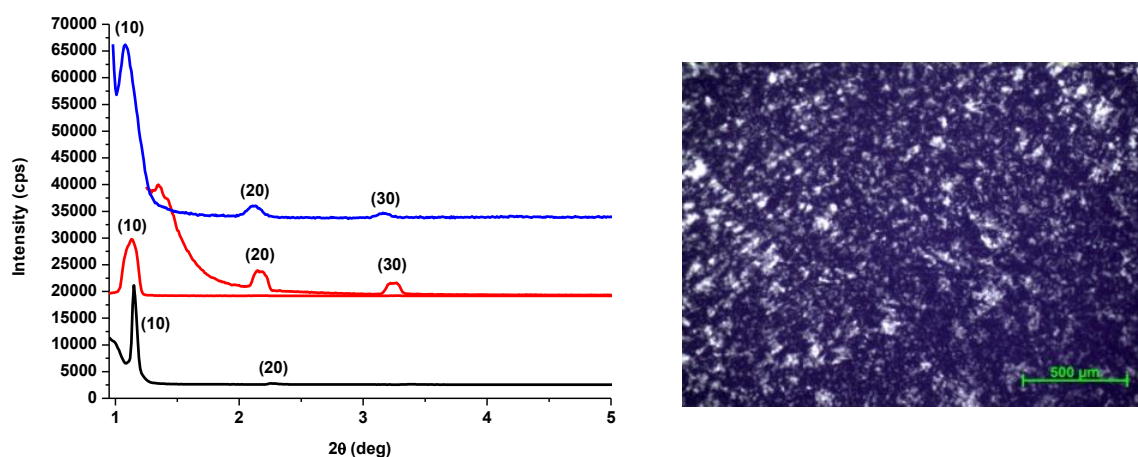


**Figure 4.1.** The small angle XRD patterns of the LiCl-xH<sub>2</sub>O-P65 mesophases with 8.0, 12.0 and 15.0 LiCl/P65 mole ratio (from bottom to top, left), and a POM image of a sample (right).

The unit cell parameter increases with increasing salt concentration, and it was calculated as 96.7 Å for the 15.0 LiCl/P65 mole ratio. The 2D hexagonal LLC mesophase is observed between 6.0 and 15.0 LiCl to P65 mole ratios. The cubic mesophase exists above 15.0 and extends up to 25.0 LiCl to P65 mole ratio. Above 25.0 mole ratio, the mixture is still gel-like but does not diffract at small angles (see **Figure 4.2**), indicating a disordered mesophase, therefore this region is not investigated (due to lack of measurement tools).

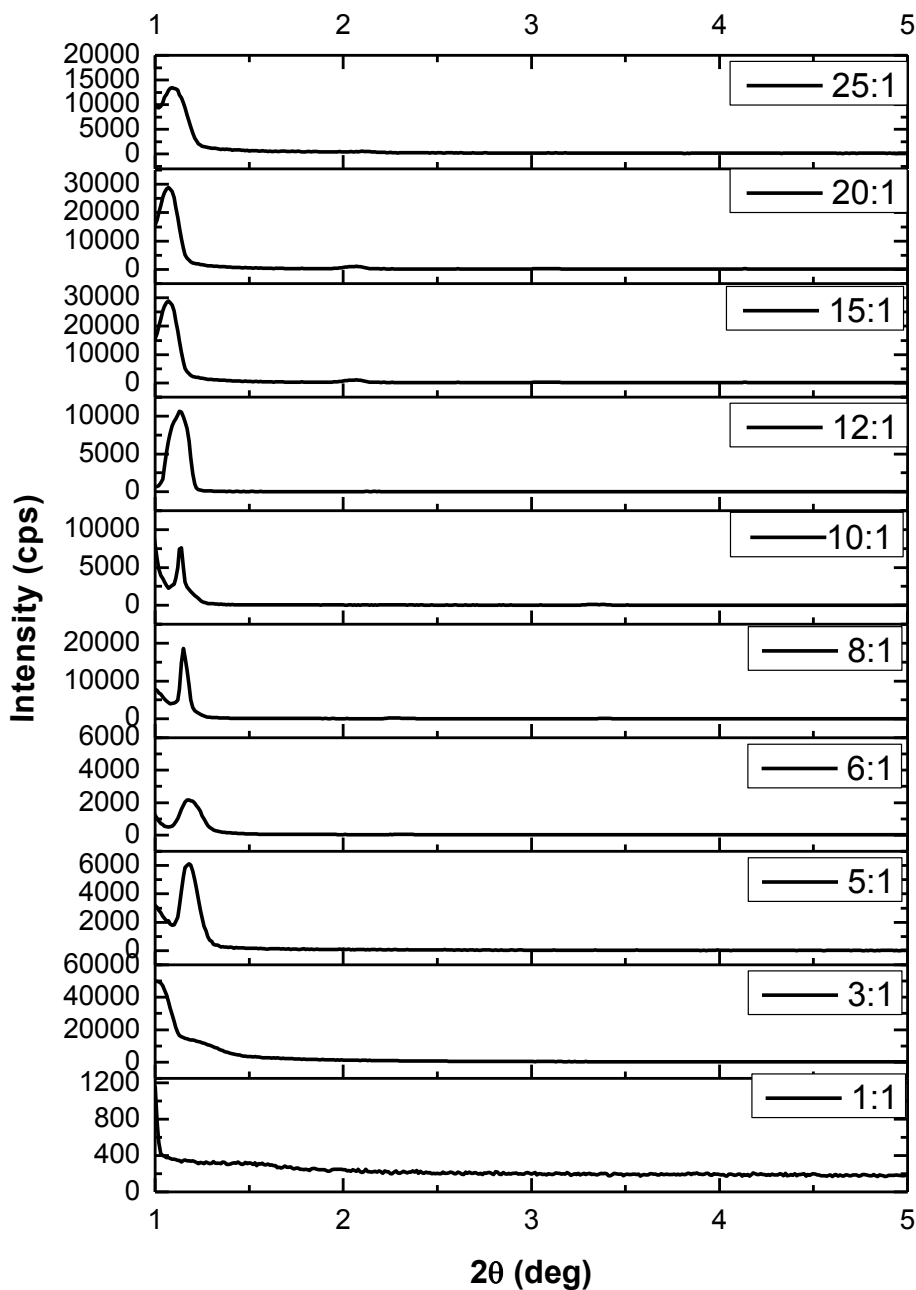


**Figure 4.2.** The XRD patterns at small angles of LiCl-P65-nH<sub>2</sub>O system with different mole ratios.

**Figure 4.3** displays the XRD patterns of the LLC mesophases of the LiCl-xH<sub>2</sub>O-P85 system at different salt to surfactant mole ratios. The first diffraction line corresponds to the (100) plane of the hexagonal mesophase and provides a unit cell parameter  $a$  of about 90.1 Å. The hexagonal mesophase was observed between 8.0 and 15.0 LiCl/P85 mole ratios.

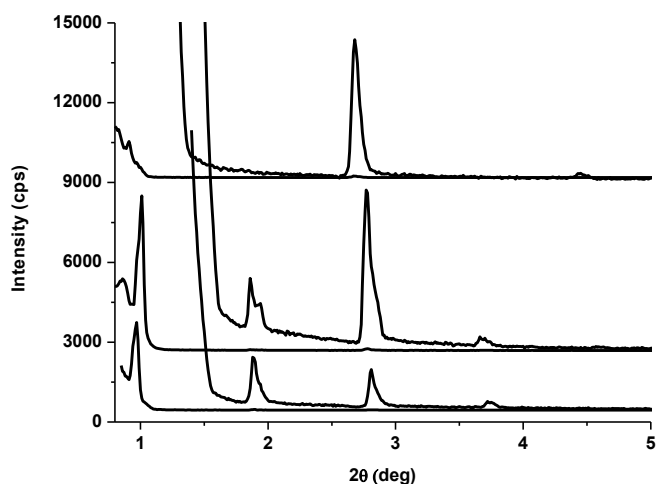


**Figure 4.3.** The XRD patterns, at small angles, of LiCl-xH<sub>2</sub>O-P85 system with 10.0, 12.0 and 15.0 mole ratios (from bottom to top).

Under a salt to surfactant mole ratio of 8.0, some surfactant molecules crystallized and were leached out. However, the characteristic fan texture of the LLC hexagonal mesophase was observed under the surfactant crystals, see **Figure 4.4**.

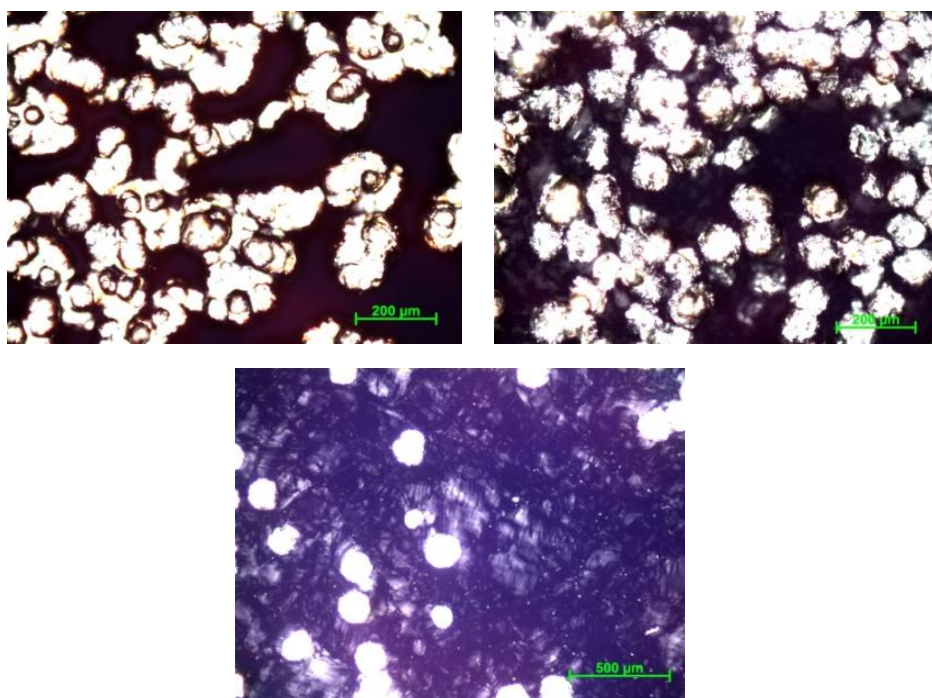


**Figure 4.4.** The POM images of LiCl-xH<sub>2</sub>O-P85 system with 3.0, 6.0 and 8.0 mole ratios indicating surfactant crystals (bright dots) and formation of fan texture under the surfactant crystals.

This indicates that the salt concentration is not enough to organize surfactant molecules into an LLC mesophase below 8.0 LiCl/P85 mole ratios. The mixtures undergo a phase separation into a salt free (pure surfactant) and salt rich (LLC) domains at low salt concentrations, demonstrating that the mesophase is one of the stable phases of the salt-surfactant mixtures.

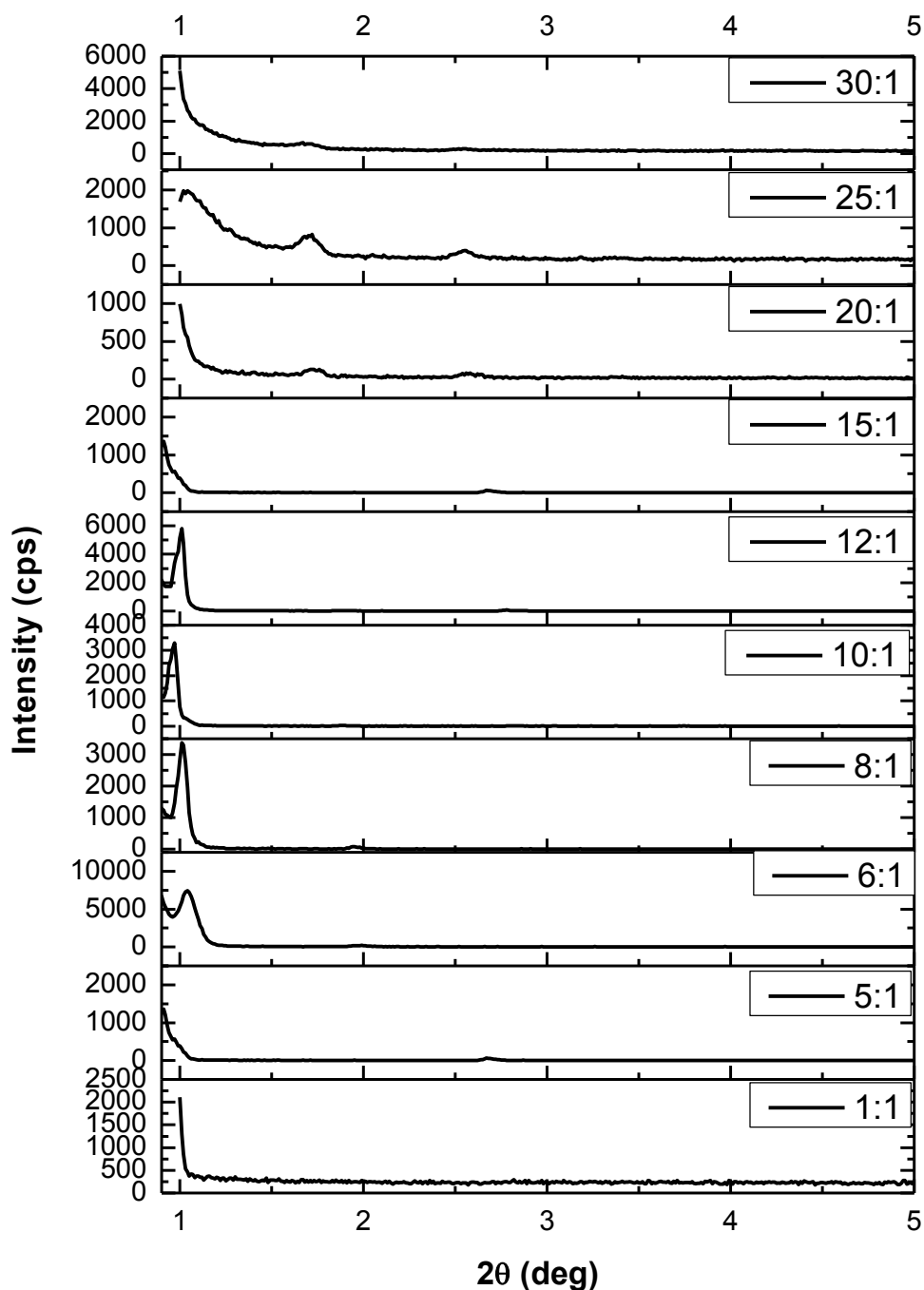


**Figure 4.5.** The XRD patterns at small angles of LiCl-P85-nH<sub>2</sub>O system with different mole ratios.

The LLC mesophase of the  $\text{LiCl-xH}_2\text{O-P103}$  samples also display birefringent texture, in a broad range of salt concentration, under the polarized optical microscope, which indicates the presence of hexagonal mesophase, see **Figure 4.6**. The XRD patterns of the samples display small angle diffraction lines, but it is difficult to index unambiguously to a particular mesostructure due to lack of enough information (one needs more diffraction lines to correctly assign and index the diffraction lines). However, combining the XRD data with the POM images provides insights on the structure of the mesophases. The first diffraction line is most probably below  $1.0^\circ$  of  $2\theta$  so the first diffraction line cannot be detected in our XRD patterns (we cannot measure below  $1^\circ$ ,  $2\theta$  with our set up, unless if the signal below  $1^\circ$  is very intense, a few hundred thousand cps), see **Figure 4.7**. This is an expected result since the surfactant P103 is much larger than both P65 and P85, therefore the unit cell is larger in the P103 samples.

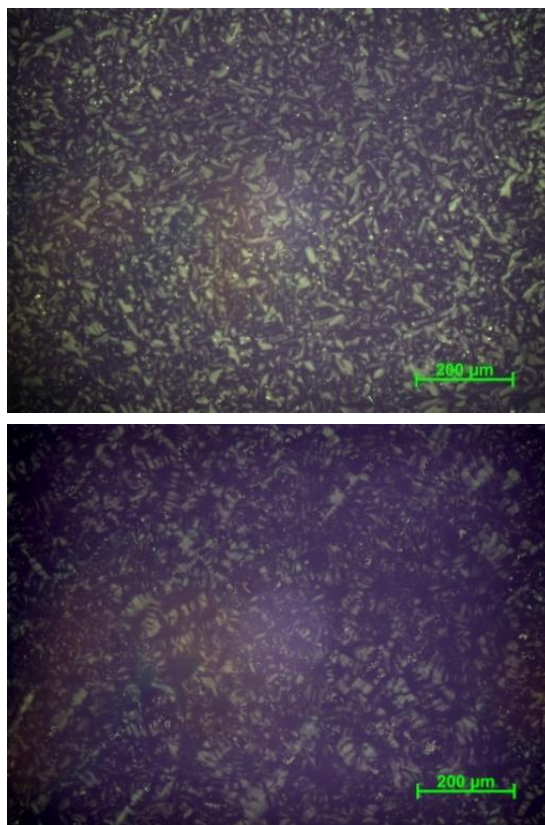


**Figure 4.6.** The POM images of the  $\text{LiCl-xH}_2\text{O-P103}$  samples with a  $\text{LiCl/P103}$  mole ratio of 6.0 (top) and 8.0 (bottom).

The POM images and XRD patterns are used together to identify the structure of the  $\text{LiCl-xH}_2\text{O-P103}$  samples, and the data show the presence of hexagonal mesophase between 6.0 and 12.0 salt to surfactant mole ratios. The samples display small angle diffraction line(s) up to 20.0  $\text{LiCl/P103}$  mole ratios; therefore, lyotropic liquid crystalline mesophase of  $\text{LiCl-xH}_2\text{O-P103}$  system is also stable at higher salt concentrations, see **Figure 4.8**. Notice also that there is no surfactant separation in the  $\text{LiCl-xH}_2\text{O-P103}$  mesophases at low salt concentrations. Origin of surfactant separation, at low salt concentrations, can be due to the percent EO units of the pluronics. Notice that both P65 and P85 have 50% ethylene oxide blocks compared to 30% in P103 and P123. Therefore surfactants with more EO units (such as in P65 and P85) requires more salts to minimize the surfactant-surfactant interactions through EO blocks for the phase separation.

The XRD patterns of the  $\text{LiCl-xH}_2\text{O-P103}$  samples usually display two or three diffraction lines at small angles, see **Figure 4.7** and **4.8**. The hexagonal mesophase was observed between 5.0 and 12.0 salt to surfactant mole ratios. The POM images of these samples display fan texture under the ambient conditions, indicating the presence of the hexagonal LLC mesophase. At higher salt concentrations, the mesophase is usually cubic and displays no texture under the POM.

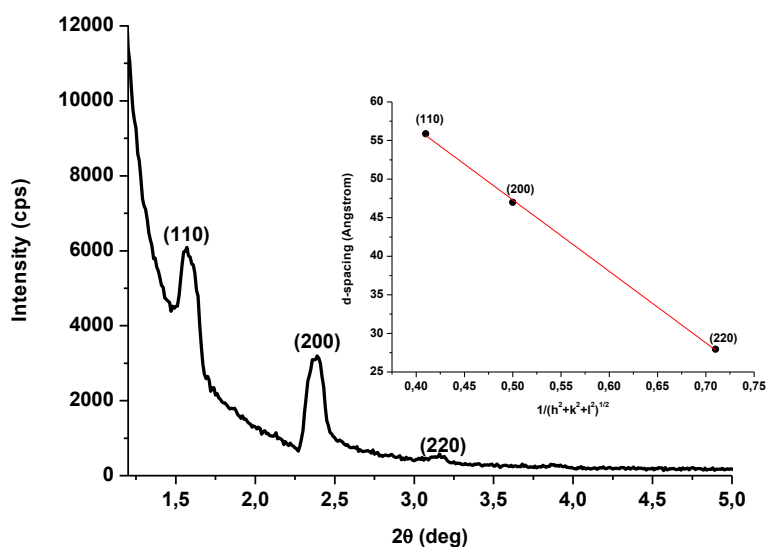


**Figure 4.7.** The XRD pattern of cubic mesophase of  $\text{LiCl-xH}_2\text{O-P103}$  system with 15.0  $\text{LiCl/P103}$  mole ratios. The inset is a plot of the d spacing obtained from the above three diffraction lines versus  $1/(h^2 + k^2 + l^2)^{1/2}$ .

**Figure 4.7** displays the diffraction pattern of the LiCl-xH<sub>2</sub>O-P103 sample with a 15.0 LiCl to P103 mol ratio. According to the data, the sample has three diffraction lines that can be indexed to (110), (200) and (220) planes of the cubic mesophase with a cell parameter  $a$  of about 78.8 Å.

The polarized optical microscopy images of the LiCl-xH<sub>2</sub>O-P103 sample with a 15.0 LiCl/P103 mole ratio do not display any texture so this confirms the presence of cubic mesophase. The diffraction lines disappears at around 20.0 LiCl/P103 mole ratio; therefore, ordered LLC mesophase was not observed at higher salt concentrations, although the samples were still gel-like, see **Figure 4.8**.

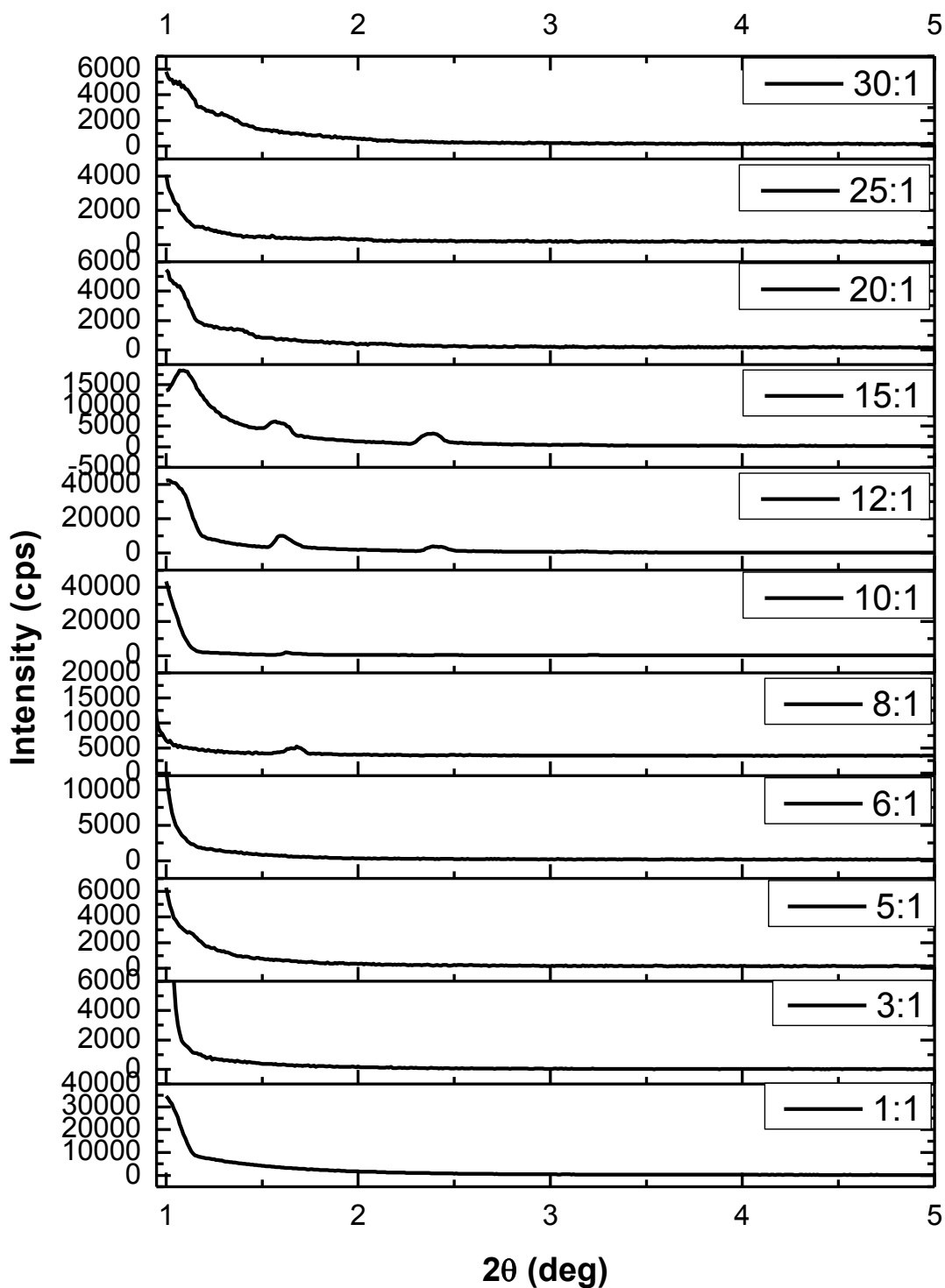


**Figure 4.8.** The XRD patterns at small angles of LiCl-P103-nH<sub>2</sub>O system with different mole ratios.

The XRD patterns of the LiCl-xH<sub>2</sub>O-P123 samples, between 6.0 and 30.0 LiCl to P123 mole ratios, display diffraction lines at small angles. The patterns display two or three diffraction lines under ambient conditions. The samples between 6.0 and 15.0 LiCl/P123 mole ratios are birefringent and display fan

texture under the polarized optical microscope, indicating the presence of the hexagonal mesophase. At higher salt concentrations, the diffraction lines shift to higher angles, and the characteristic fan texture disappears. This means that there is a phase change at around 15.0 salts to surfactant mole ratio, see **Figure 4.9**. The diffraction lines disappear at around 30.0 LiCl/P123 mole ratios in the diffraction patterns. Hence, there is no stable LLC mesophase at higher salt concentrations or the phase is completely disordered (and not further investigated).

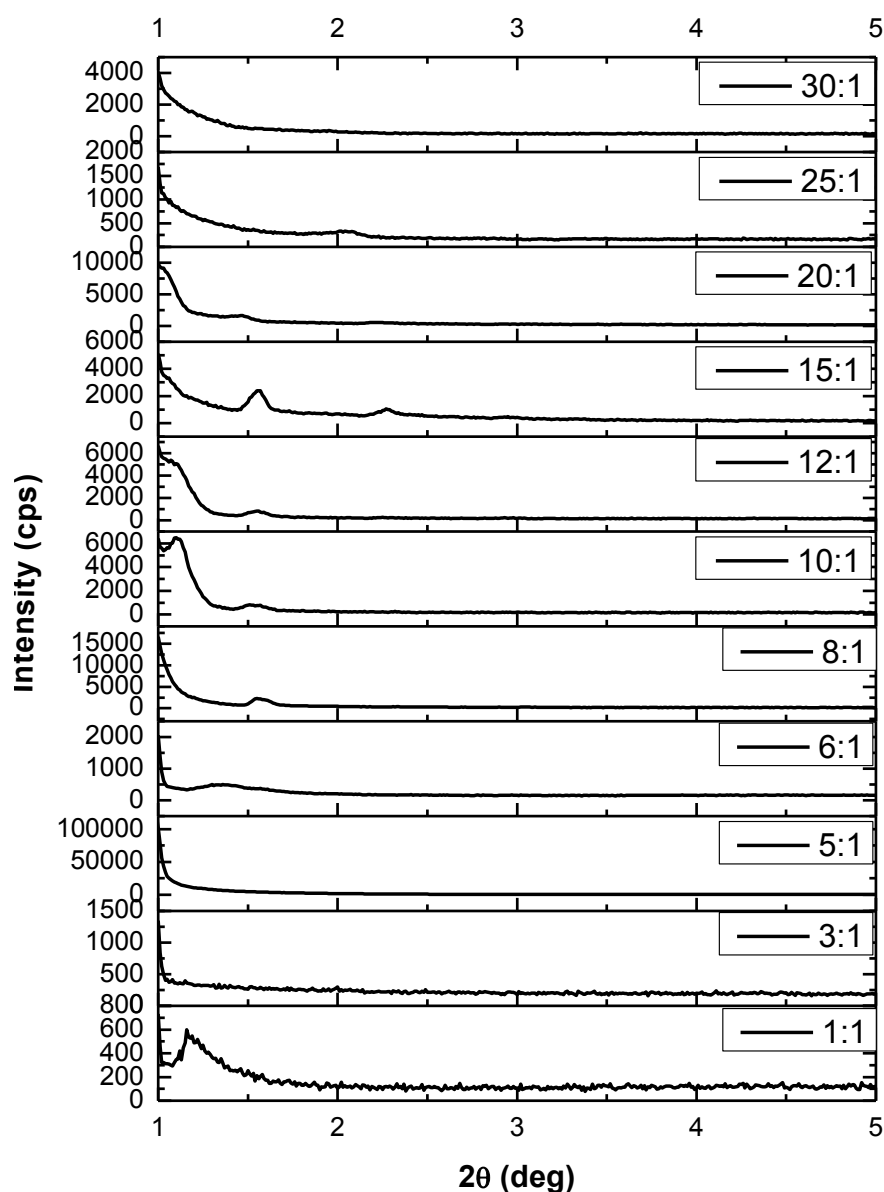


**Figure 4.9.** The XRD patterns at small angles of LiCl-P123-nH<sub>2</sub>O system with different mole ratios.

In all pluronics, the mesophases are hexagonal in the intermediate LiCl/surfactant mole ratios and undergo phase change, at higher LiCl mole ratios, from a hexagonal to cubic mesophase, and from cubic to a disordered phase. Both hexagonal and cubic mesophases diffract at small angles. There are no diffraction lines in the disordered phase. The LiCl/pluronic mole ratio can be increased up to 30.0. The mesophase at low salt concentration leaches out the excess surfactants in the P65 and P85 cases, where the ethylene oxide block is 50% of the polymer. However, no phase separation was observed in the P103 and P123 samples.

To extend the salt-pluronic systems, we also investigated the  $\text{LiNO}_3\text{-}x\text{H}_2\text{O}$ -P103 and  $\text{LiNO}_3\text{-}x\text{H}_2\text{O}$ -P123 samples using XRD and POM imaging techniques. The  $\text{LiNO}_3\text{-}x\text{H}_2\text{O}$ -P103 samples display small angle diffraction patterns, where the first diffraction line is observed at around  $2.0^\circ$ ,  $2\theta$ . The intensity of the first diffraction line decreases, and shifts to lower angles with increasing salt concentration, see **Figure 4.10**.

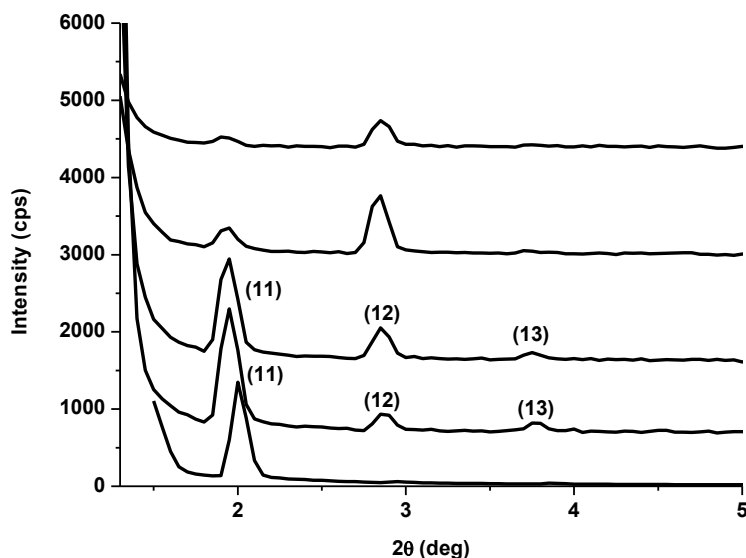


**Figure 4.10.** The XRD patterns of the 2D hexagonal mesophase of  $\text{LiNO}_3\text{-}x\text{H}_2\text{O}$ -P103 samples with 6.0, 8.0, 10.0, 12.0 and 15.0 LiCl/P103 mole ratios from bottom to top.

The diffraction patterns of the samples have three different diffraction lines that can be indexed to (11), (12), and (13) planes of the 2D hexagonal mesophase. The samples between 8.0 and 10.0 salt to surfactant mole ratios display 2D hexagonal mesophase with a cell parameter  $a$  of  $94.1 \text{ \AA}$ . The

mesophase of the samples with 12.0 and 15.0  $\text{LiNO}_3/\text{P103}$  mole ratios cannot be indexed due to the absence of a third diffraction line in the diffraction pattern, see **Figure 4.11**. However, the POM images of the samples which have salt to surfactant mole ratios between 6.0 and 15.0 display characteristic fan texture. This demonstrates that the 2D hexagonal phase exist between 6.0 and 15.0  $\text{LiNO}_3/\text{P103}$  mole ratios in the  $\text{LiNO}_3\text{-xH}_2\text{O-P103}$  samples.

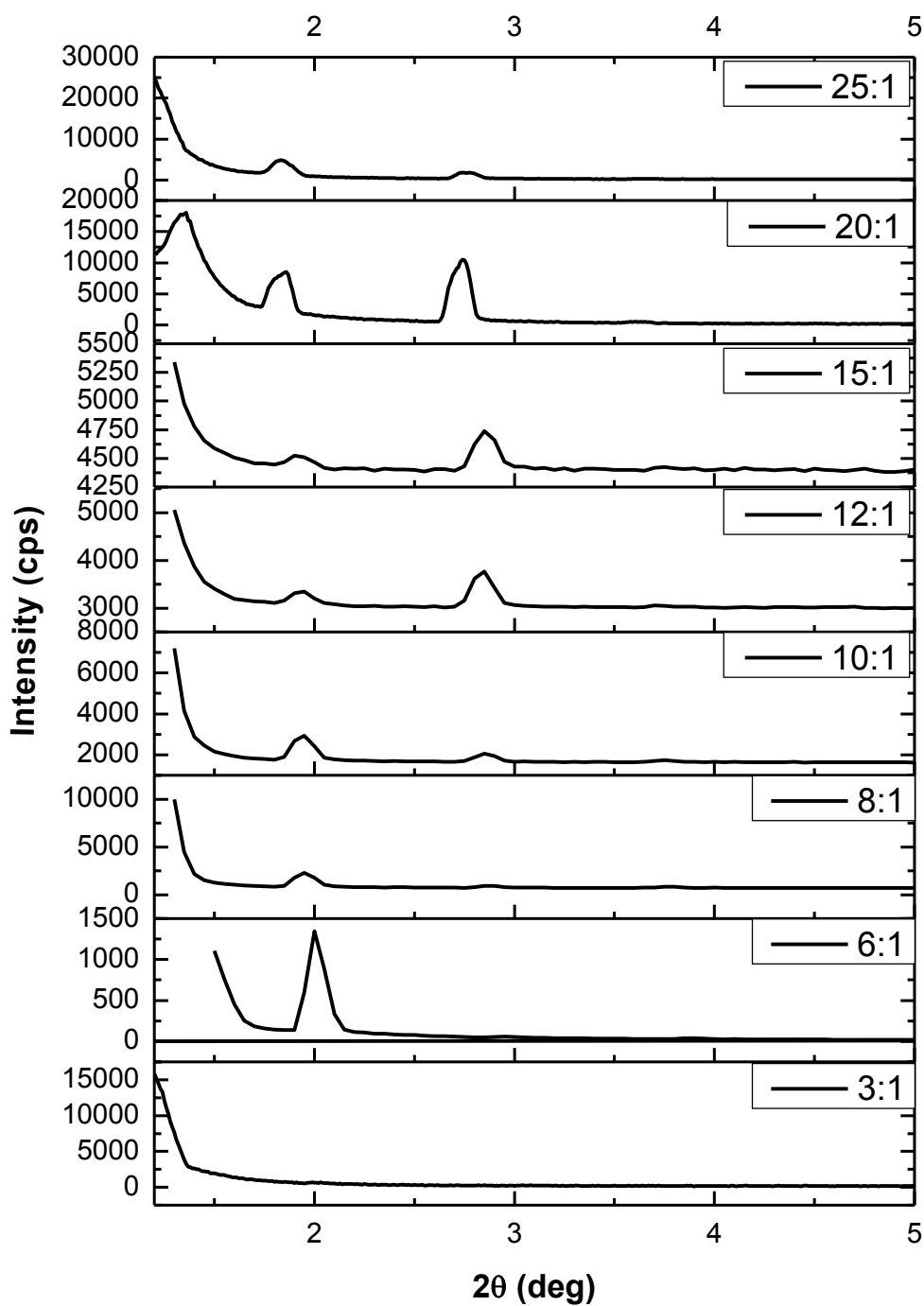


**Figure 4.11.** The XRD patterns at small angles of  $\text{LiNO}_3\text{-P103-nH}_2\text{O}$  system with different mole ratios.

**Figure 4.12** displays the diffraction pattern of the  $\text{LiNO}_3\text{-xH}_2\text{O-P123}$  samples under ambient conditions. The diffraction pattern is characteristic of a 2D hexagonal LLC mesophase with a unit cell parameter  $a$  of about 107.4 Å. The patterns have three diffraction lines that can be indexed to (11), (12) and (13) planes of the 2D hexagonal mesophase. The unit cell is about 10-15 % larger in the  $\text{LiNO}_3\text{-xH}_2\text{O-P123}$  compared to  $\text{LiNO}_3\text{-xH}_2\text{O-P103}$ , likely due to larger size of the P123 micelle domains.

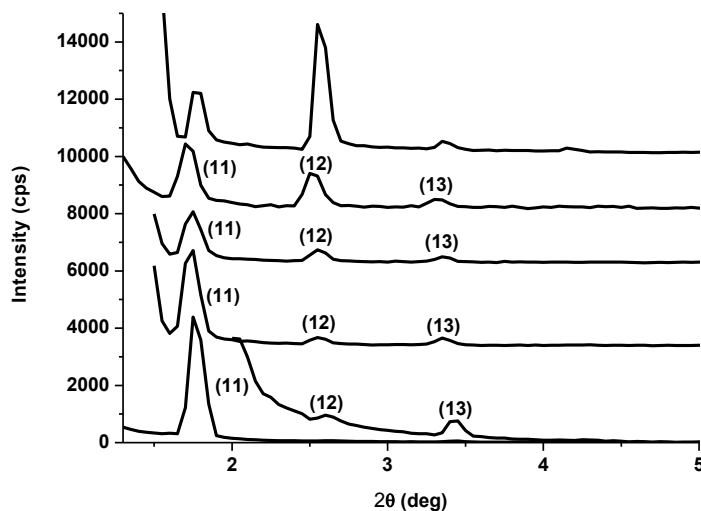


**Figure 4.12.** The XRD patterns of the 2D hexagonal mesophase of  $\text{LiNO}_3\text{-xH}_2\text{O-P123}$  system with 6.0, 8.0, 10.0, 12.0 and 15.0  $\text{LiCl/P123}$  mole ratios from bottom to top.

The diffraction lines in the  $\text{LiNO}_3$  systems also shift to smaller angles with increasing salt to surfactant mole ratio, indicating an increase in the unit cell parameter. This means that the inter micelle spacing increases with increasing salt concentration, see **Figure 4.13**. The additional salt species in the mesophase require more space, thus the expansion is expected. However, the diffraction lines shift to higher angles starting from 15.0  $\text{LiNO}_3/\text{P123}$  mole ratios and the characteristic fan texture of the hexagonal LLC mesophase disappears at high salt concentrations. This demonstrates that the phase transition from the hexagonal to cubic LLC mesophase occurs at around 15.0 salts to surfactant mole ratio. The LLC mesophase of the  $\text{LiNO}_3\text{-P123}$  is stable and ordered up to 25.0  $\text{LiNO}_3/\text{P123}$  mole ratios.

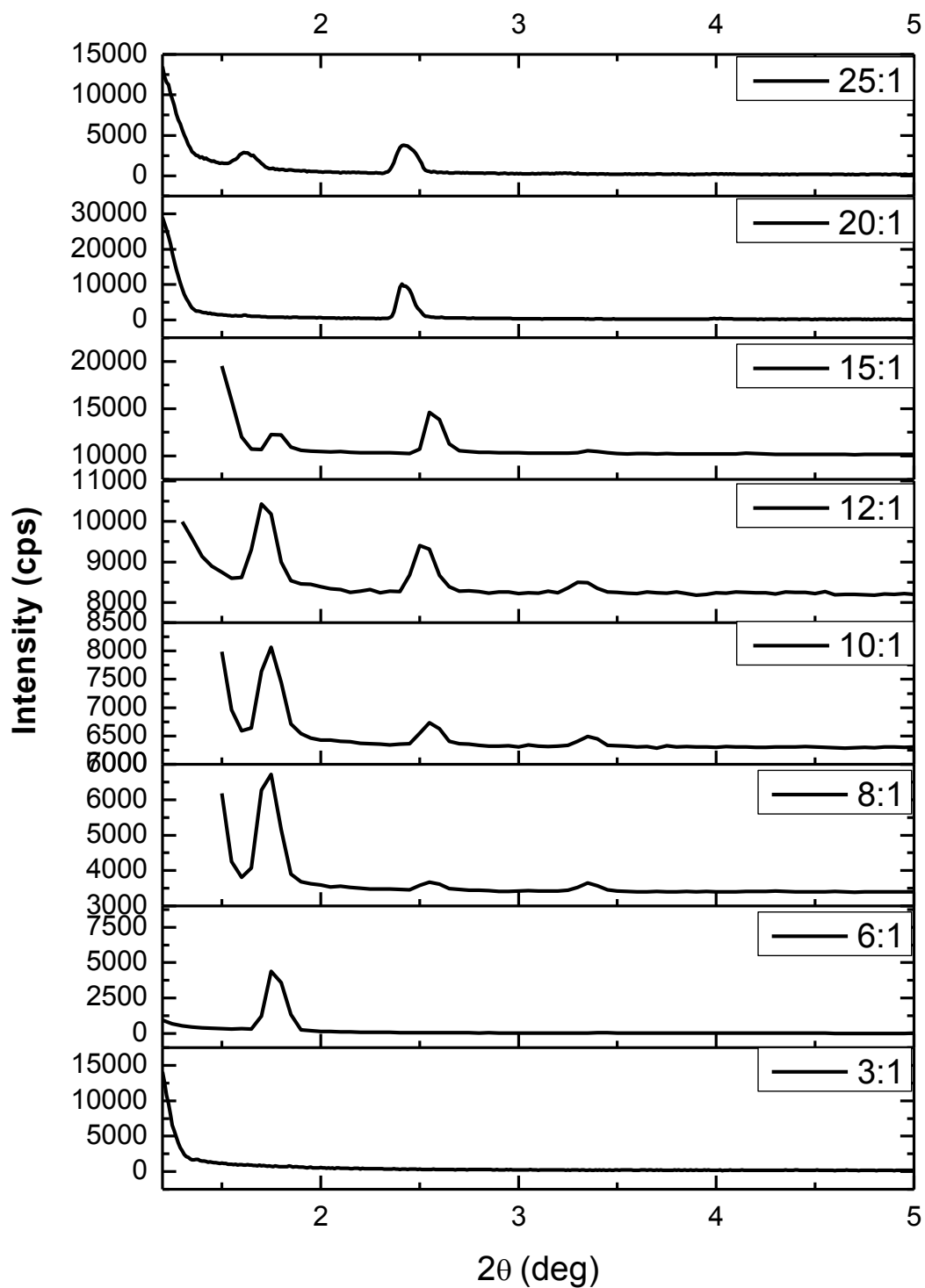


**Figure 4.13.** The XRD patterns at small angles of  $\text{LiNO}_3\text{-P123-nH}_2\text{O}$  system with different mole ratios.

According to XRD and POM data, the  $\text{LiCl-xH}_2\text{O-pluronic}$ s samples display hexagonal mesophases in a broader range of the salt concentration than the  $\text{LiNO}_3\text{-xH}_2\text{O-pluronic}$ s system. Moreover, the hexagonal to cubic phase

transition occurs at lower salt concentration in the  $\text{LiNO}_3\text{-xH}_2\text{O}$ -pluronics systems. This trend is related to Hofmeister series. The  $\text{NO}_3^-$  ion has more structure breaking character than  $\text{Cl}^-$  so that it is less hydrated with water molecules. For this reason, it can increase interfacial curvature due to the higher ability to penetrate in the vicinity of hydrophobic regions. Similarly, the  $\text{NO}_3^-$  ion leads to increase the hydration of hydrophilic ethylene oxide units, and interfacial curvature increases again. Therefore, increase in the concentration of structure breaker ions leads to an increase in the repulsive forces between the hydrophilic units. As a result, the hexagonal mesophase exists in a narrower range of salt concentration for the  $\text{LiNO}_3\text{-xH}_2\text{O}$ -pluronics mesophases.

#### 4.1.1. Salt-water-surfactant Interactions, Spectroscopic Studies

The interactions among the salt, water and surfactants in the  $\text{LiCl}$  (or  $\text{LiNO}_3$ )- $\text{xH}_2\text{O}$ -pluronics samples have also been investigated by using FT-IR and micro-Raman spectroscopy. The samples were prepared by either spin coating on silicon wafers or drop casting on glass substrates for the measurements. The spectra were recorded under ambient laboratory conditions at RT and 22-25 % relative humidity (RH). The nitrate ion in the  $\text{LiNO}_3\text{-xH}_2\text{O}$ -pluronics systems interacts with the lithium ion and the corresponding peak related to the nitrate ion broadens at around  $1370\text{ cm}^{-1}$  and dominates the FT-IR spectra, see **Figure 4.14**. The broad peak(s) in this region is the antisymmetric stretching mode of the nitrate ions.

**Figure 4.14** shows the FT-IR spectra of the pure pluronics (P103 and P123),  $\text{LiNO}_3\text{-xH}_2\text{O}$ -P103 and  $\text{LiNO}_3\text{-xH}_2\text{O}$ -P123 samples with 12.0 salts to surfactant moles ratio. The major spectral changes take place in the  $\text{NO}_3^-$  related peaks.

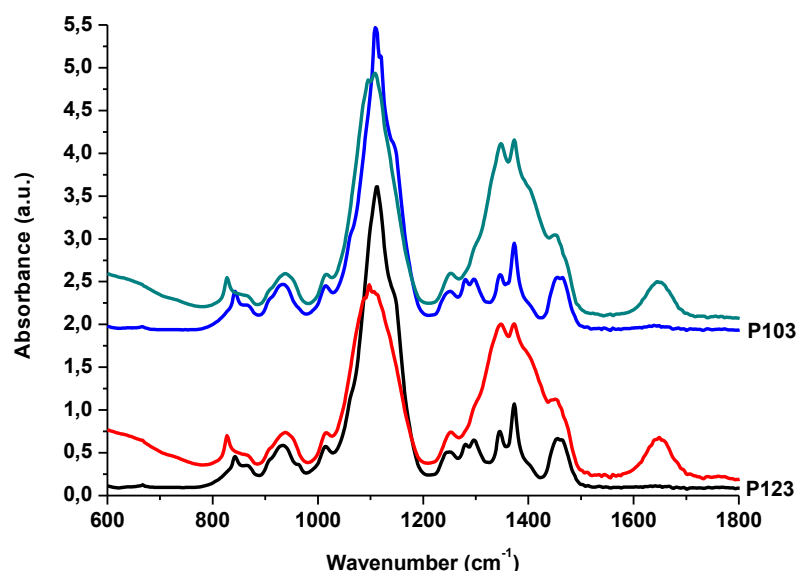


**Figure 4.14.** FT-IR spectra of the  $\text{LiNO}_3\text{-}x\text{H}_2\text{O-P123}$  and P123 (bottom) and  $\text{LiNO}_3\text{-}x\text{H}_2\text{O-P103}$  and P103 (top) with the same salt/pluronic mole ratios.

Note that in the TMS LLC systems, the doubly degenerate antisymmetric stretching mode of nitrate ion at around  $1360\text{ cm}^{-1}$  splits into two non-degenerate modes as a result of coordination. The reason is that the symmetry group of the free nitrate ion changes from  $D_{3h}$  to  $C_{2v}$  upon coordination to the metal.<sup>48,67</sup> However, this splitting is not strong in  $\text{LiNO}_3$  systems since  $\text{LiNO}_3$  does not undergo ligand exchange with water molecules due to the lack of strong interactions.<sup>48-67</sup> In the  $\text{LiNO}_3$  system, the nitrate anions and lithium cations form ion-pairs. As a result of the weaker interactions, compared to coordination of the nitrate ions to transition metal ion, the bond strength does not change much. Therefore, the splitting is much smaller than those in the TMS LLC mesophases. On the other hand, some minor changes in the pluronic region were observed, showing that the surfactant molecules also display conformational changes due to the addition of salt into the media. The C-O stretching region of the surfactant shifts to lower wavenumbers in the salted systems. This demonstrates that there is a hydrogen-bonding interaction between the hydration sphere of the ions ( $\text{Li}^+$  and  $\text{NO}_3^-$ ) and the ethoxy groups of the surfactant molecules.

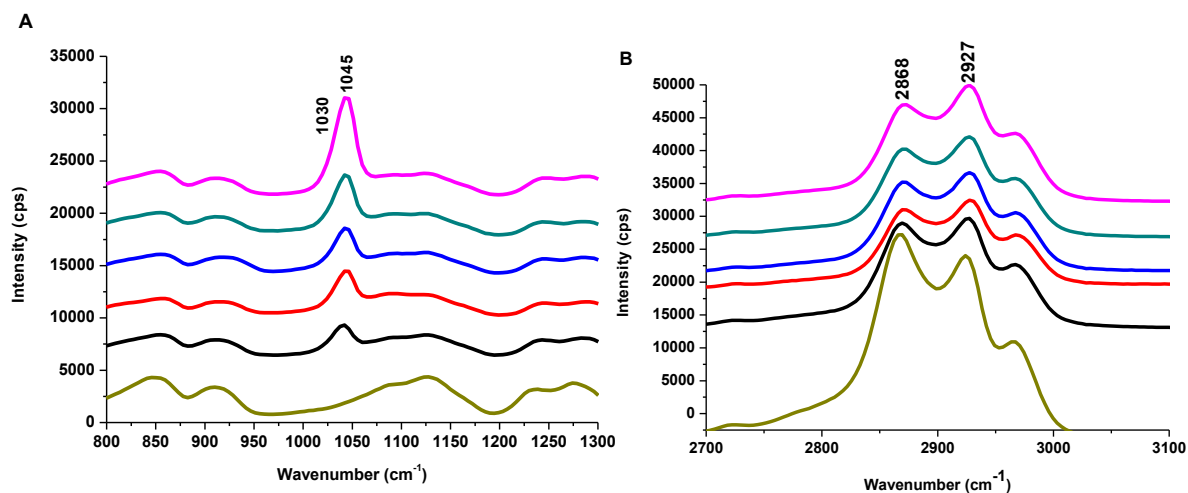


**Figure 4.15.** Micro-Raman spectra of P123 and the  $\text{LiNO}_3\text{-}x\text{H}_2\text{O-P123}$  samples with 6.0, 8.0, 10.0, 12.0 and 15.0 salt/pluronic mole ratios (from bottom to top).

The  $\text{LiNO}_3\text{-}x\text{H}_2\text{O-pluronic}$  mesophases were also investigated using micro-Raman spectroscopy. The peaks at 1030 and 1045  $\text{cm}^{-1}$  are due to the hydrated ion-pair and hydrated nitrate ions respectively, see **Figure 4.15**. The intensity of the free nitrate ion is much higher compared to the intensity of the ion paired nitrate ions. Moreover, the intensity of free nitrate ion peak increases with increasing salt concentration in the media, indicating that the majority of the ions are free ions in the media. This can be beneficial for the ionic conductivity of the mesophases (see the conductivity section). The stretching modes of the  $\text{CH}_2$  and  $\text{CH}_3$  groups of surfactants also respond to addition of salt into the media. The sharp signals at 2868 and 2927  $\text{cm}^{-1}$  get broader with the addition of salt species, see **Figure 4.15**. These peaks correspond to the stretching modes of  $\nu\text{-CH}_2$  and  $\nu\text{-CH}_3$ , respectively. The ratios of the intensities of these two peaks  $I(\text{CH}_2)/I(\text{CH}_3)$  decreases with increasing salt concentration in the media. This indicates the conformational changes of ethoxy and propoxy units of the surfactants. This is a reasonable explanation when we consider the unit cell of the mesophases that also show response to the salt concentration. The change in the unit cell dimensions, phase changes and change in the FT-IR intensities of the  $\nu\text{-CH}_2$  and  $\nu\text{-CH}_3$

stretching modes are all related to the conformational changes in the EO units of the pluronics in the mesophases.

The FT-IR spectra were also collected at various salts to surfactant mole ratios in order to understand the effect of anions on the phase behavior. **Figure 4.16** indicates the FT-IR spectra of different systems with increasing salt concentration. The intensity of  $\nu$ -OH band of water at around 3100-3700  $\text{cm}^{-1}$  increases with increasing salt concentration. This means that, the salt concentration determines the amount of water kept (hydration water) in the LLC mesophase. Ions are hydrated in the LLC mesophase, where the excess water evaporates. Only a required amount of water can stay in the mesophase as a result of strong interactions (ion-dipole type interactions) with the salt species. Hence, the amount of water is directly proportional with the mole ratio of the salt in the media. Moreover, most of the water species in the media are in the form of hydration water.

The amount of water kept in the mesophases is larger in the LiCl system compared to the  $\text{LiNO}_3$  system. Note also that the ion-pairs are observed in the  $\text{LiNO}_3$  system that can be monitored using the nitrate signals, however in the  $\text{Cl}^-$  case this is not possible. For this reason, in contrast to nitrate anion, the LiCl salt species cannot be detected in the FT-IR spectra. Therefore, the relative impact of the LiCl species on the surfactant and water signals can be discussed. On the other hand, increasing the salt concentration has no effect on the position of the maxima for  $\nu$ -OH band of water in the LiCl systems. This indicates that the only water source is the hydration water, which increases with increasing LiCl in the media. In contrast, the  $\nu$ -CO stretching mode of surfactant head groups at around 1100  $\text{cm}^{-1}$  shift to lower wavenumbers in all spectra. This is caused by the increase in the extent of interactions between the salt species and surfactant molecules. Note also that there is no change in the other regions of the spectra other than these two regions.

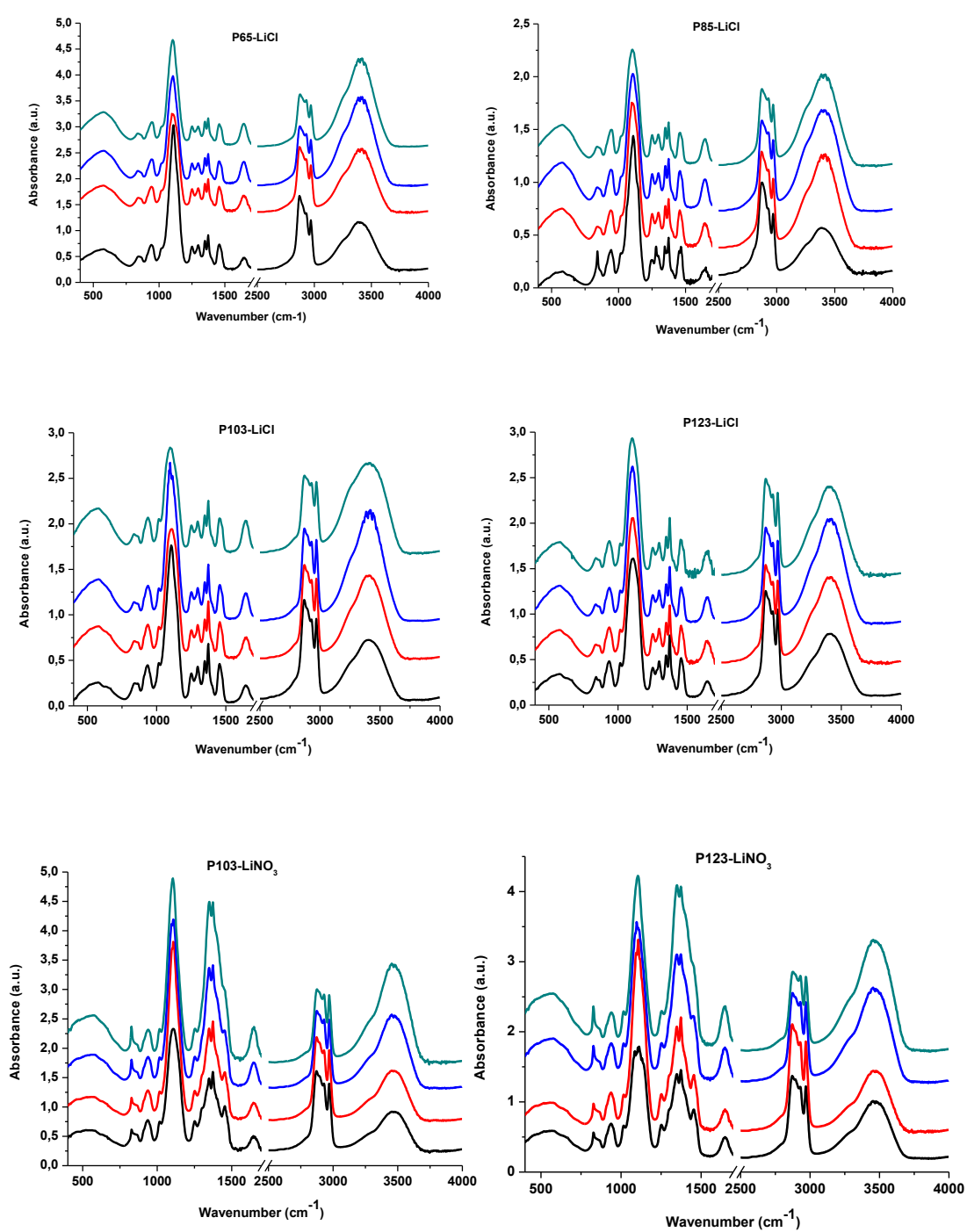


**Figure 4.16.** FT-IR spectra of different salt systems (as indicated on the spectra) at various salt/surfactant mole ratios, from bottom to top 6.0, 8.0, 12.0, and 15.0.

**Figure 4.17** shows the combined FT-IR spectra of the LiCl and LiNO<sub>3</sub> salts with the P123 and P103 surfactants and pure (molten) surfactants. The molten surfactants have a  $\nu$ -CO stretching maxima at around 1120 cm<sup>-1</sup>. This band shifts to 1104 cm<sup>-1</sup> and 1100 cm<sup>-1</sup> in the LiCl and LiNO<sub>3</sub> systems, respectively. The reason of this shift is that the addition of chaotropic ions into the media increases the hydration of the hydrophilic ethylene oxide units in the mesophase. These ions lead to the rupture of water structure, and so they can penetrate to the core-shell interface (hydrophilic ethoxide and hydrophobic propoxide of the pluronics).

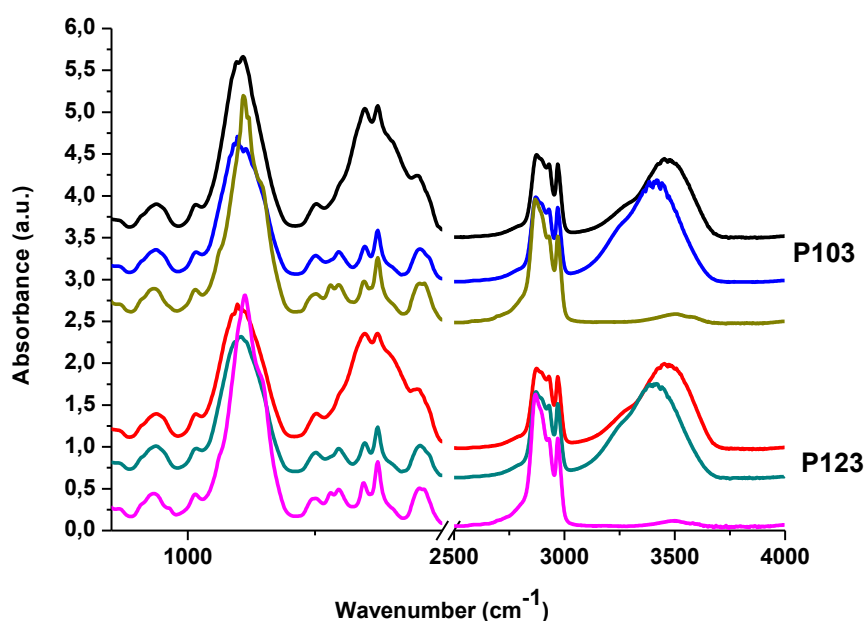


**Figure 4.17.** FT-IR spectra of P123, LiCl- $x$ H<sub>2</sub>O-P123 and LiNO<sub>3</sub>- $x$ H<sub>2</sub>O-P123 (bottom) and P103, LiCl- $x$ H<sub>2</sub>O-P103 and LiNO<sub>3</sub>- $x$ H<sub>2</sub>O-P103 (top) with the 12.0 salt/Pluronic mole ratios.

The amount of water in the LLC mesophase also depends on the anion. The maxima of the  $\nu$ -OH stretching band are at around 3400 cm<sup>-1</sup> in the spectra of LiCl- $x$ H<sub>2</sub>O-P123 and LiCl- $x$ H<sub>2</sub>O-P103 systems. However,  $\nu$ -OH stretching maxima are at around 3460 cm<sup>-1</sup> in the pure surfactant spectra. This red-shift in the LiCl systems indicates that the interaction between Cl<sup>-</sup> anions and water species is stronger than those between NO<sub>3</sub><sup>-</sup> anions and water.

#### 4.1.2. Conductivities and Isotropization Temperatures of Lithium Salt-Pluronic Systems

The ionic conductivities of the LLC mesophases of various lithium salt-pluronic systems were also measured by using AC impedance spectroscopy. Samples were prepared with the same salt and water mole ratios (10.0 mole of salt and 200.0 mole of water per mole of surfactant). During the measurements, the working electrode was connected to the one probe, and counter and reference electrodes were connected to the other probe. The stainless-steel electrodes were used with a diameter of 4 mm, and the electrodes were 2.3 mm far away from each other. The cell constant was measured as  $0.62 \text{ cm}^{-1}$  by using 0.01 M KCl solution at RT. Conductivities were calculated by converting the measured resistances with the following formula:

$$\sigma = KR^{-1}$$

where K is the cell constant and R is the measured resistance.

**Table 4.2.** Phase behavior of LiCl-xH<sub>2</sub>O-Pluronic systems at RT and 22-25% RH.

	Isotropization T.	Cloud P.	Melting P.	Resistance	Conductivity
P65-LiCl	52 °C	59 °C	64 °C	25.7 Ω	21 mS/cm
P85-LiCl	69 °C	73 °C	76 °C	332.2 Ω	1.87 mS/cm
P103-LiCl	56 °C	72 °C	89 °C	286.7 Ω	1.97 mS/cm
P123-LiCl	76 °C	80 °C	92 °C	315.4 Ω	2.18 mS/cm
P103-LiNO <sub>3</sub>	78 °C	97 °C	105 °C	150.2 Ω	4.1 mS/cm
P123-LiNO <sub>3</sub>	83 °C	104 °C	113 °C	2790 Ω	0.22 mS/cm

**Figure 4.18** indicates Nyquist plots of various samples where the imaginary part of the impedance is equal to zero at the high frequency region. The ionic conductivities of various LiCl-xH<sub>2</sub>O-pluronic systems were recorded in the range of 21 mS/cm and 1.87 mS/cm. The highest conductivity was obtained for the LiCl-xH<sub>2</sub>O-P65 system as 21 mS/cm, see **Table 4.2**.

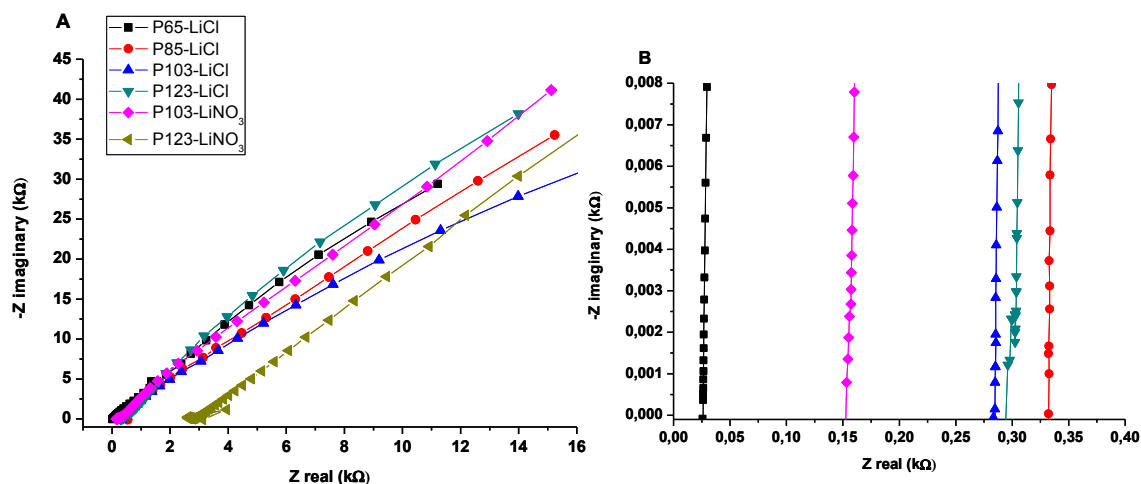


**Figure 4.18.** (A) Nyquist plots of various samples with 10.0 and 200.0 salt/surfactant and water/surfactant mole ratios between  $1.0 \times 10^4$  Hz and 0.2 Hz. (B) Resistance values were recorded at the point where  $Z_{\text{imaginary}}$  is equals to zero.

Nyquist plot shows the variation of the real and imaginary components of impedance. The sample resistance at  $Z_{\text{imaginary}} = 0$  was taken as  $Z_{\text{real}}$  in the Nyquist plot, see **Figure 4.18**. The difference between conductivities of various systems is related to the amount of water in the LLC mesophase.

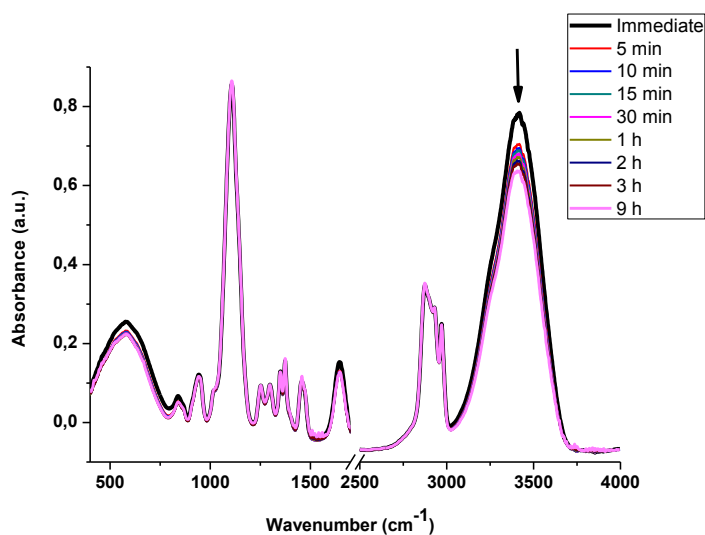


**Figure 4.19.** FT-IR spectra of sample with composition 10.0LiCl-200.0H<sub>2</sub>O-1.0P65, under 25% RH and RT with time.

Although all the samples were prepared with the same water to salt mole ratio, the amount of water in the mesophase changes before the conductivity

measurements. The excess amount of water evaporates immediately, and the samples become stable in terms of water amount at the end, see **Figure 4.19**. According to the time-dependent FT-IR spectra of 10.0LiCl-200.0H<sub>2</sub>O-1.0P65 sample, 13.2% amount of water evaporates in 5 minutes, and the total amount of water decreases to 77.6% at the end of 9 hours. This means that the mole ratio of water decreases to 155.6 from 200.0 in 9 hours.

**Figure 4.20** indicates the conductivities of P65-LiCl samples with increasing salt concentration. According to data, conductivity is proportional to the amount of water in the LLC mesophase. The conductivities of samples with 50.0, 75.0, 100.0 and 150.0 water/surfactant mole ratios were recorded immediately. The highest conductivity was obtained for the sample which contains the highest amount of water. As the water amount decreases in the sample the resistance increases and so the conductivity decreases. This demonstrates that there is a direct relation between water amounts of LLC media and conductivity.

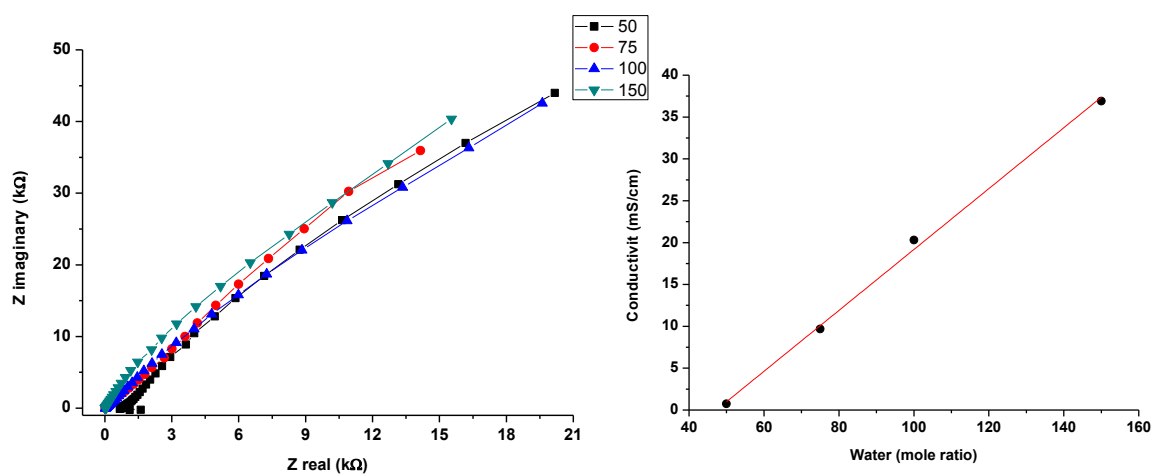


**Figure 4.20.** (A) Nyquist plots of samples with various water/surfactant mole ratios between  $1.0 \times 10^4$  Hz and 0.2 Hz, and (B) the correlation between water mole ratio and conductivity.

The LLC mesophases of LiCl- $x$ H<sub>2</sub>O-pluronic and LiNO<sub>3</sub>- $x$ H<sub>2</sub>O-pluronic were further characterized by determining the temperature that the mesophases becomes isotropic. The isotropization temperature can be regarded as the melting point in some composition, but it can also be a hexagonal to cubic or disordered phase change in some other composition. To

fully elucidate the nature of isotropization temperature in every composition, the phase diagram of each system needs to be constructed. However, the construction of phase diagrams is outside the scope of this thesis.

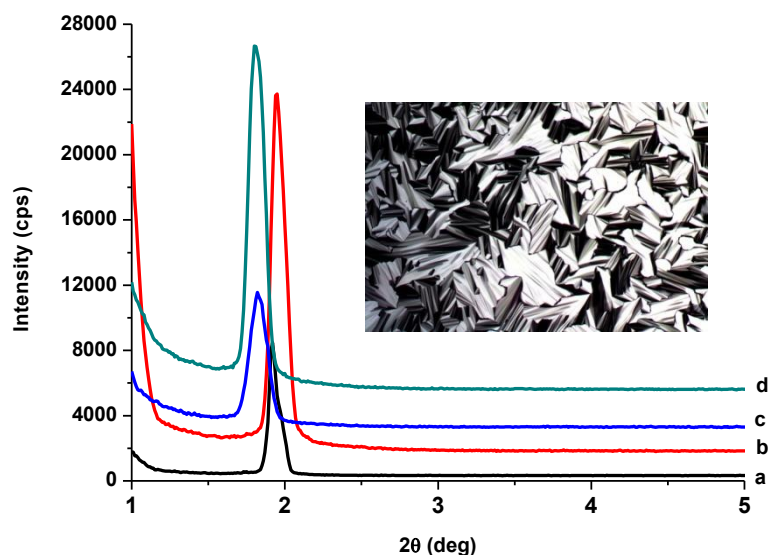
The isotropization temperatures of the samples with 10.0 salts to surfactant mole ratio in all systems were determined by heating and cooling and monitored using polarized optical microscope. Little amount of sample was put on a microscope slide and sealed with a cover glass and Scotch tape in order to prevent evaporation of water from the mesophase during heating. The isotropization temperature was recorded as the point where the characteristic fan texture of hexagonal mesophase disappeared, and totally dark image was observed. Since the cubic phase is also isotropic, it displays completely dark images under the POM. The isotropization temperatures of LiCl samples were obtained in the range of 52 °C to 67 °C, where as the LiNO<sub>3</sub> samples have 78 °C and 83 °C of isotropization temperature, see **Table 4.2**. It is obvious that LiCl systems have lower isotropization temperatures than those of LiNO<sub>3</sub> systems with the same surfactants. This is also related to Hofmeister's series where Cl<sup>-</sup> has higher kosmotropic character than the NO<sub>3</sub><sup>-</sup> ion. Therefore, Cl<sup>-</sup> has higher tendency to increase hydrogen bonding network structure of water. This leads to increase in the hydrophobic moieties since the interaction between water and solute decreases so the isotropization temperature is lower for LiCl systems. Similar trends were also observed for melting points and cloud points. Cloud point is the temperature where the solutes are not completely soluble, and their precipitation gives a cloudy appearance to the substance.<sup>86</sup> The LiNO<sub>3</sub> systems have cloud points higher than 95 °C and melting points higher than 100 °C, which are much higher than those of LiCl samples, see **Table 4.2**. The origin of these observations can be considered as the same for the isotropization temperature.

Since LLC mesophases of lithium salts with pluronics display cloud point at certain temperature it is tedious to homogenize samples. It also affects solar performance of the gel electrolytes negatively. For this reasons, a shorter surfactant, oligo(ethylene oxide), was used instead of pluronics in order to achieve better solar performance.

## 4.2. $\text{LiI-xH}_2\text{O-C}_{12}\text{EO}_{10}$ -Mesophase

In this part of the thesis, we have studied the phase behavior of LiI and oligo(ethylene oxide) type surfactant (10-lauryl ether,  $\text{C}_{12}\text{EO}_{10}$ ). A highly concentrated aqueous solution of an alkali metal salt can also be considered as an analogue of a molten salt, and it can act as a solvent in the assembly process of non-ionic surfactants. The mesophase is formed as a result of collaborative assembly of hydrated salt species and surfactant molecules. The structure of the LLC mesophase and the interactions among the metal ion, surfactant and water were investigated by using microscopy (POM), diffraction (XRD), and spectroscopy (FT-IR and micro-Raman) techniques. We will use the abbreviation of  $\text{LiI-xH}_2\text{O-C}_{12}\text{EO}_{10}$  for the LiI systems with different salt concentrations. Under the ambient conditions, the amount of water in the samples depends on the amount of salt, temperature and relative humidity.

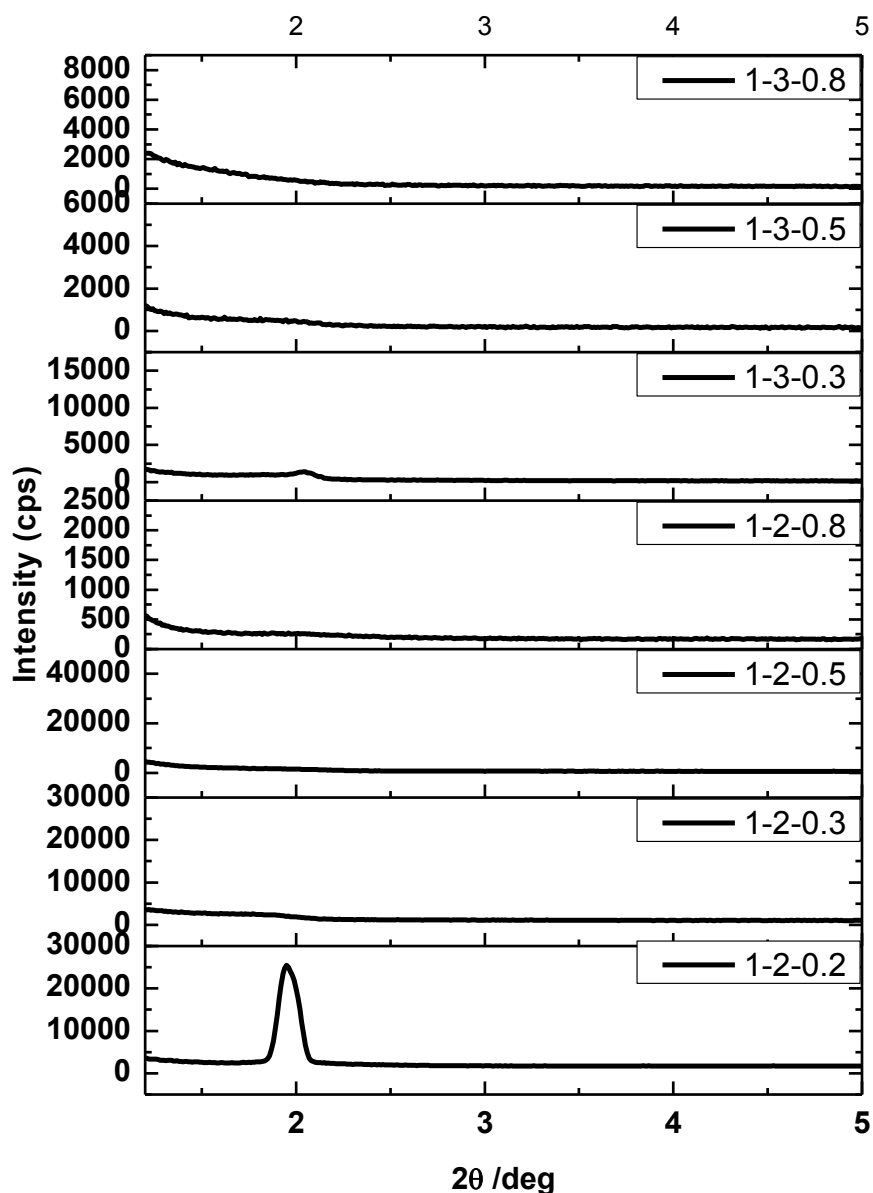
The first diffraction line in **Figure 4.21** corresponds to the (100) plane of the hexagonal mesophase, and the inset in the figure shows a polarized optical microscopy image of a sample with a classical fan texture of a hexagonal mesophase. The samples with 2.0 and 3.0 salts to surfactant mole ratios exhibit similar fan texture, but other samples with 4.0 and 5.0  $\text{LiI/C}_{12}\text{EO}_{10}$  mole ratios do not show any texture. Therefore, the hexagonal mesophase exists between 2.0 and 3.0  $\text{LiI/C}_{12}\text{EO}_{10}$  mole ratio, and above the 3.0 salt to surfactant mole ratio the mesophase is cubic in this system. It can be deduced from the XRD patterns that the  $\text{LiI-xH}_2\text{O-C}_{12}\text{EO}_{10}$  mesophase is highly ordered in a broad range of salt to surfactant mole ratios, 2.0-6.0 and loses the ordered-mesostructure at around 10.0 salt/surfactant mole ratio. The first diffraction line at around  $1-2\ 2\theta$  shifts to lower angles with increasing salt concentration after 4.0  $\text{LiI/C}_{12}\text{EO}_{10}$  mole ratio. This indicates a structural change due to the transition from  $\mathbf{H}_1$  to  $\mathbf{I}_1$  phase. The shift can also be related to an increase in the intermicellar spacing between the surfactant domains in the mesophase with increasing salt concentration. The additional salt species in the mesophase requires more space, thus the expansion is expected.



**Figure 4.21.** Typical XRD patterns at small angles of  $\text{LiI-xH}_2\text{O-C}_{12}\text{EO}_{10}$  system with (a) 2.0, (b) .03, (c) 4.0 and (d) 5.0 LiI to  $\text{C}_{12}\text{EO}_{10}$  mole ratio, and a POM image of a  $\text{LiI-xH}_2\text{O-C}_{12}\text{EO}_{10}$  sample in the inset.

The wide angle diffraction pattern shows no diffraction line indicating that there is no crystallization of the salt species under the specified conditions. However, the samples that have more than 3.0 salt to surfactant mole ratio can exhibit mesocrystal formation below 20% RH, and the system loses its mesostructure above 10.0 salt to surfactant mole ratio. The samples with 4.0 or above salt/surfactant mole ratios exhibit a new phase transformation from LLC mesophase to a mesocrystalline phase. In the mesocrystalline phase, some significant changes were observed in the FT-IR spectra and XRD diffraction patterns (see **Section 2.4**).

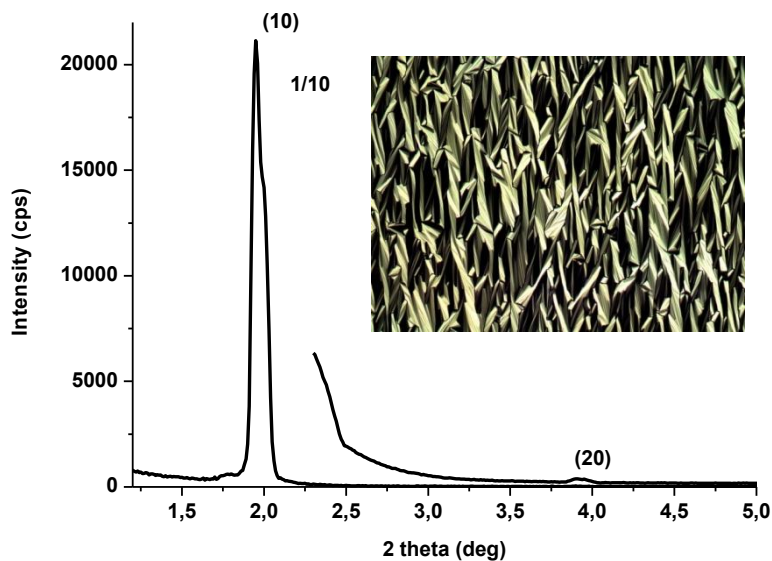
The effect of iodine into the LLC mesophases was also investigated by using XRD technique. LiI can be directly assembled into LLC mesophases in the presence of a minimum amount of water, and  $\text{I}_2$  can be incorporated into the LLC phase without disturbing the mesophase up to 0.2 iodine to surfactant mole ratio for the  $\text{LiI-xH}_2\text{O-C}_{12}\text{EO}_{10}$  system, see **Figure 4.22**.



**Figure 4.22.** The XRD patterns at small angles of the  $\text{LiI-I}_2\text{-xH}_2\text{O-C}_{12}\text{EO}_{10}$  mesophases (numbers correspond to mole ratio of LiI,  $\text{I}_2$ , and  $\text{H}_2\text{O}$  per mole of surfactant).

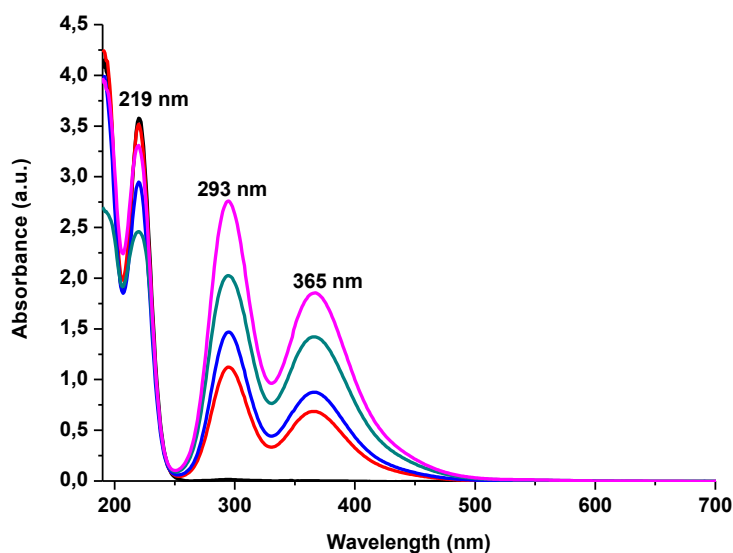
The first diffraction line corresponds to (10) plane of the 2D hexagonal mesophase with a unit cell parameter of about  $52.0 \text{ \AA}$  for the  $2.0\text{LiI-}0.2\text{I}_2\text{-xH}_2\text{O-C}_{12}\text{EO}_{10}$  sample. Incorporation of  $\text{I}_2$  into the mesophase results a second diffraction line, but still can be indexed to the normal hexagonal ( $\text{H}_1$ ) mesophase, see **Figure 4.23**. The iodine molecules can also be incorporated to the LLC mesophases of  $3.0\text{LiI-I}_2\text{-xH}_2\text{O-C}_{12}\text{EO}_{10}$  sample up to 0.3 mole ratio of iodine to surfactant. Further increase in the mole ratio of iodine leads to

disappearance of the first diffraction line, indicating the formation of a disordered phase.



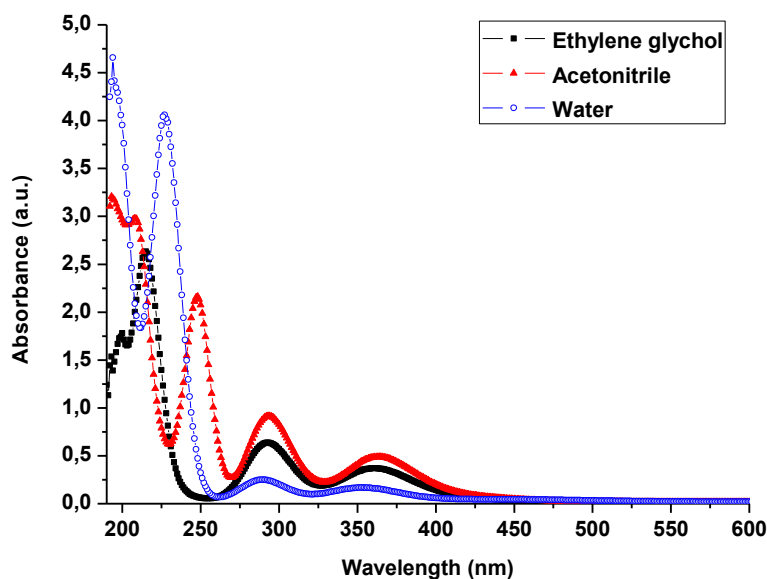
**Figure 4.23.** The XRD patterns at small angles of  $\text{LiI-I}_2\text{-xH}_2\text{O-C}_{12}\text{EO}_{10}$  with a 0.2  $\text{I}_2$  to  $\text{C}_{12}\text{EO}_{10}$  and 2.0  $\text{LiI}$  to  $\text{C}_{12}\text{EO}_{10}$  mole ratios and a POM image of the sample in the inset.

The POM image of  $\text{LiI-I}_2\text{-H}_2\text{O-C}_{12}\text{EO}_{10}$  samples display a focal conic fan texture, characteristic for a 2D hexagonal mesophase. The LLC phase remains 2D hexagonal upon addition of  $\text{I}_2$  to the mesophases.



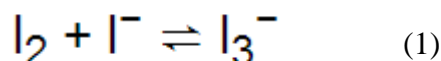
**Figure 4.24.** The UV-vis spectra of  $2.0\text{LiI-I}_2\text{-xH}_2\text{O-C}_{12}\text{EO}_{10}$  system with 0.0, 0.2, 0.3, 0.4, 0.5  $\text{I}_2$  to  $\text{C}_{12}\text{EO}_{10}$  mole ratios from bottom to top.

The iodine ( $I_2$ ) and iodide ( $I^-$ ) react in the media to form triiodide ( $I_3^-$ ). The iodide and triiodide related species can be identified using UV-vis absorption spectroscopy.<sup>87</sup> In the UV-Vis spectra, the peak at 219 nm indicates the presence of  $I^-$  and the other two peaks at 293 and 365 nm show the formation of  $I_3^-$  ion. There is no absorbance at around 500 nm that originates from  $I_2$ . Therefore it demonstrates that  $I_2$  is almost completely transformed to the  $I_3^-$  like in many other solvents, and its concentration can be increased by the addition of  $I_2$  into the LLC media, see **Figure 4.24**.



**Figure 4.25.** The UV-vis spectra of LiI/ $I_2$  couple in various solvents.

The equilibrium constant of the  $I^-$ ,  $I_2$  with  $I_3^-$  mixture highly depends on the solvent, and it was reported to be larger than  $10^7 \text{ M}^{-1} \text{ cm}^{-1}$  in acetonitrile<sup>88</sup> and  $800 \text{ M}^{-1} \text{ cm}^{-1}$  in water.<sup>89</sup> The position of the absorbance peak also strongly depends on the solvent, and it shifts to higher wavelength in acetonitrile. The ratio of absorbance at 219 nm to 367 nm gives information about the equilibrium constant of the reaction (equation 1). The ratios of the absorbance at 219 nm to 367 nm were found as 4.3, 7.2 and 23.9 in acetonitrile, ethylene glycol and water respectively, see **Figure 4.25**. This means that the conversion of iodine to triiodide is more favorable in acetonitrile, but the least favorable in water among these three different media.



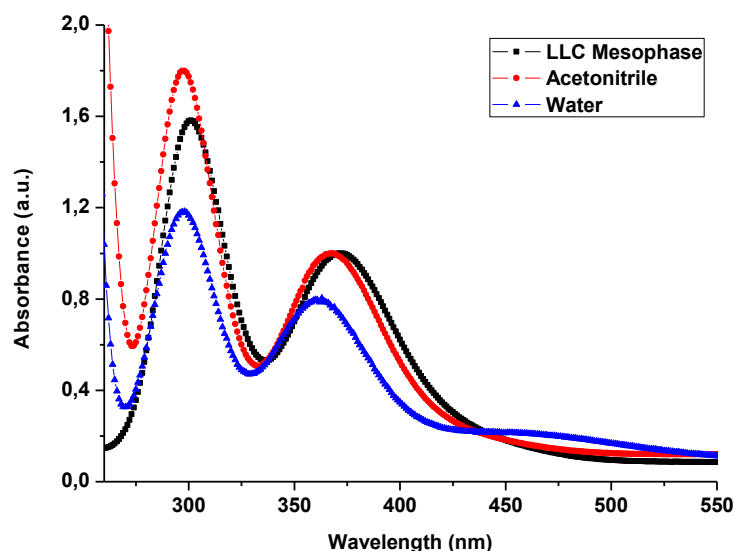


**Figure 4.26.** The UV-vis spectra of LiI/I<sub>2</sub> couple in various solvents and 2.0LiI-0.2I<sub>2</sub>-xH<sub>2</sub>O-C<sub>12</sub>EO<sub>10</sub> system in water.

The I<sub>2</sub> molecule is a strong oxidizing agent and causes corruptions on the electrodes upon using in a solar cell. For this reason, it is also crucial to increase the conversion of iodine to triiodide in the LLC mesophases. The shoulder at around 500 nm indicates presence of iodine in the media, see **Figure 4.26**. In the UV-vis spectra of LiI/I<sub>2</sub> there is no observable absorbance at around 500 nm when acetonitrile is used as the solvent. Similarly, the LLC mesophase of the 2.0LiI-0.2I<sub>2</sub>-xH<sub>2</sub>O-C<sub>12</sub>EO<sub>10</sub> sample does not display any absorbance in the same region when the hydrated salt is the solvent. This demonstrates that in the LLC mesophases the iodine is almost completely converted into triiodide, therefore the electrode corrosion caused by the presence of iodine can be diminished.

The mesophases were further analyzed using Raman spectroscopy. The peak at 117 cm<sup>-1</sup> is assigned to the symmetric stretching mode of triiodide ion. Even in the absence of iodine in the LLC media, the formation of triiodide was observed in the Raman spectra, see **Figure 4.27**. When the iodine is added to the mesophase, the formation of triiodide increases, such that the intensity of the peak which corresponding to the symmetric stretching mode of I<sub>3</sub><sup>-</sup> masks the surfactant peaks.

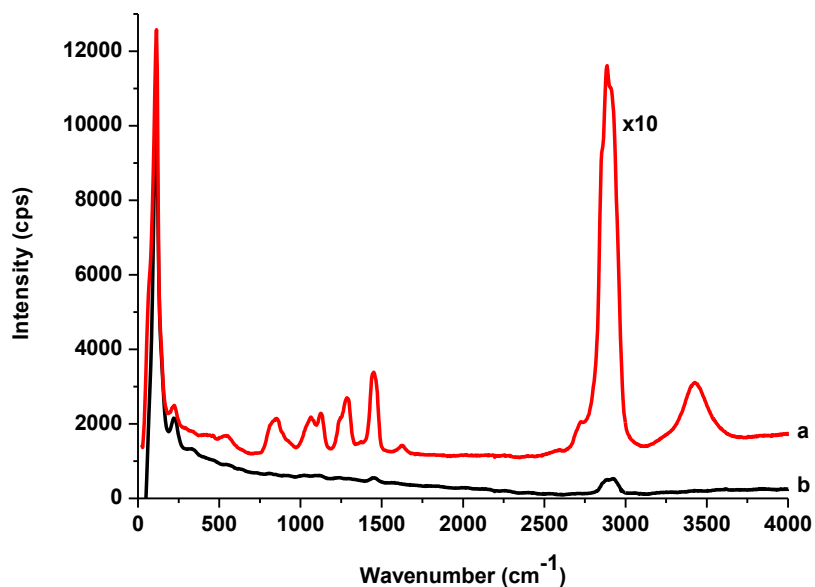


**Figure 4.27.** Raman spectra of (a)  $2.0\text{LiI}-x\text{H}_2\text{O}-\text{C}_{12}\text{EO}_{10}$  and (b)  $2.0\text{LiI}-0.2\text{I}_2-x\text{H}_2\text{O}-\text{C}_{12}\text{EO}_{10}$  systems

Both the Raman and UV-vis spectra confirm that there is a direct relationship between the amount of iodine in the LLC media and the formation of triiodide anion. According to the UV-vis data, as the mole ratio of iodine in the LLC phase of  $\text{LiI}-\text{I}_2-x\text{H}_2\text{O}-\text{C}_{12}\text{EO}_{10}$  increases, the intensity of triiodide at 367 nm also linearly increases, see **Figure 4.28**.

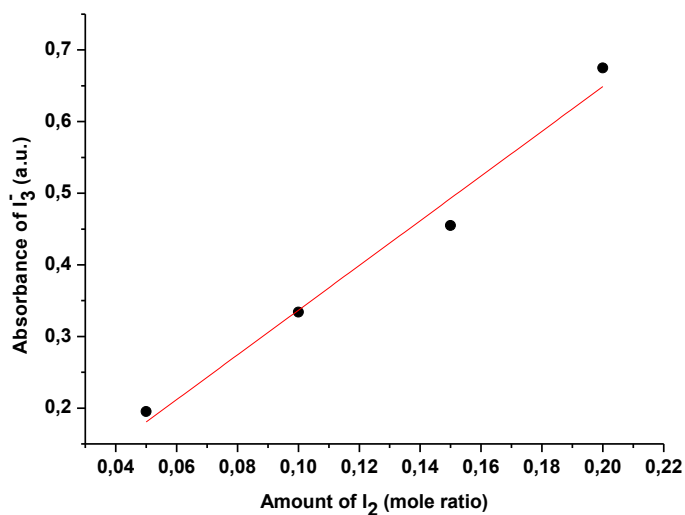


**Figure 4.28.** Correlation between mole ratio of iodine (0.05, 0.1, 0.15 and 0.2  $\text{I}_2$  to  $\text{C}_{12}\text{EO}_{10}$  mole ratio) in the LLC media and absorbance of triiodide.

This indicates that in the liquid crystalline mesophase of  $\text{LiI}-\text{I}_2-\text{C}_{12}\text{EO}_{10}-x\text{H}_2\text{O}$ , the  $\text{I}^-$  anion can be converted into the  $\text{I}_3^-$  ion that its concentration can be

increased by the addition of I<sub>2</sub> into the LLC media. Therefore, one can create I<sup>-</sup>/I<sub>3</sub><sup>-</sup> redox couple in the LLC mesophase by the incorporation of iodine, and so LLC mesophases may be used as a gel-electrolyte for dye-sensitized solar cells.

#### 4.3. Effect of Anions on the LiI-I<sub>2</sub>-xH<sub>2</sub>O-C<sub>12</sub>EO<sub>10</sub> System

The LiCl and LiBr salts were added into the LLC mesophases of LiI-I<sub>2</sub>-xH<sub>2</sub>O-C<sub>12</sub>EO<sub>10</sub> system in order to have an idea on the effect of different anions on the phase behavior and ionic conductivities of the system. The samples were prepared by mixing 5 ml of water, 1.0 g of surfactant and required weight of salts. The homogenized samples were spin coated on glass slides at 1500 rpm and allowed to equilibrate under open atmosphere at RT and 20-25 % RH. The samples were kept under open atmosphere in the laboratory in order to carry measurements at constant humidity.

The LLC mesophases of LiI-xH<sub>2</sub>O-C<sub>12</sub>EO<sub>10</sub>, LiCl-xH<sub>2</sub>O-C<sub>12</sub>EO<sub>10</sub>, and LiBr-xH<sub>2</sub>O-C<sub>12</sub>EO<sub>10</sub> are well ordered with a salt/surfactant mole ratio between 1.0 and 6.0, 2.0 and 10.0, and 2.0 and 7.0, respectively. These systems lose their mesostructure at around 10.0-12.0 mole ratio. The first diffraction line between 1.0 and 2.0 degrees corresponds to the (10) plane of 2D hexagonal mesophase for the LiI, LiCl, and LiBr systems. The XRD patterns of these systems with I<sup>-</sup>/I<sub>3</sub><sup>-</sup> redox couple shows that the I<sub>2</sub> can be incorporated into the LLC phase without disturbing the mesophase up to 0.3 mole ratio for LiI system, and 0.4 mole ratio for the LiCl and LiBr systems. The amount of LiCl and LiBr salts can be increased up to 10.0, and 7.0 salt to surfactant mole ratio, respectively, in an air stable mesophases. However, the upper limit is 0.4 mole for iodine in order to obtain stable and homogenous samples. After this point, the further increase in the iodine concentration leads to precipitation of iodine, and stable liquid crystalline mesophases cannot be formed.

After incorporation of redox couple, the mesophases remain 2D hexagonal with a unit cell parameter *a* of 43.5, 45.5, and 45.1 Å for the LiI-I<sub>2</sub>-xH<sub>2</sub>O-C<sub>12</sub>EO<sub>10</sub>, LiI-LiCl-I<sub>2</sub>-xH<sub>2</sub>O-C<sub>12</sub>EO<sub>10</sub>, and LiI-LiBr-I<sub>2</sub>-xH<sub>2</sub>O-C<sub>12</sub>EO<sub>10</sub> systems, respectively, see **Figure 4.29** and **4.30**. The first diffraction line shifts to lower angles and the d-spacing values increase with the increasing salt concentration.

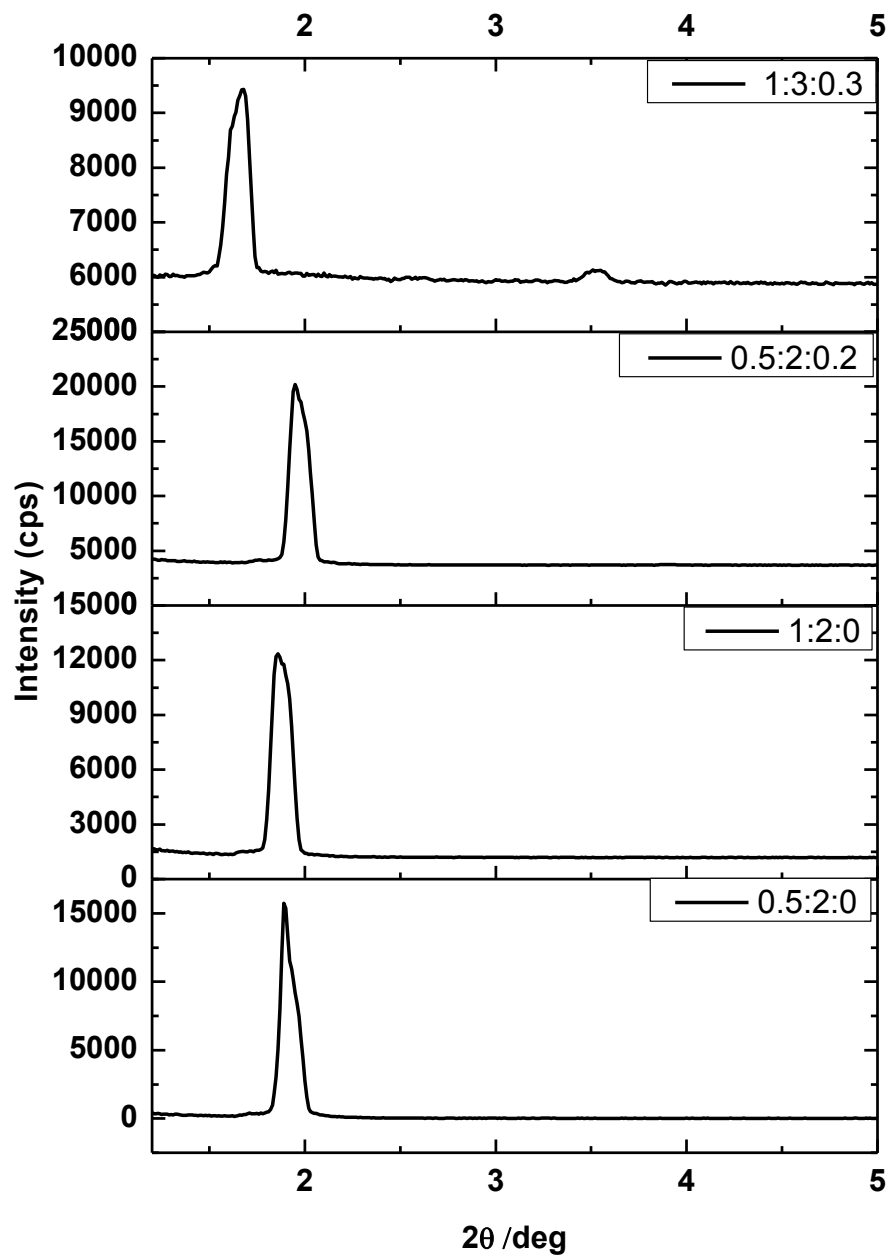


**Figure 4.29.** The XRD patterns at small angles of  $\text{LiCl-LiI-I}_2\text{-xH}_2\text{O-C}_{12}\text{EO}_{10}$  system with  $\text{LiCl}:\text{LiI}:\text{I}_2$  mole ratios per mole of surfactant in the inset.

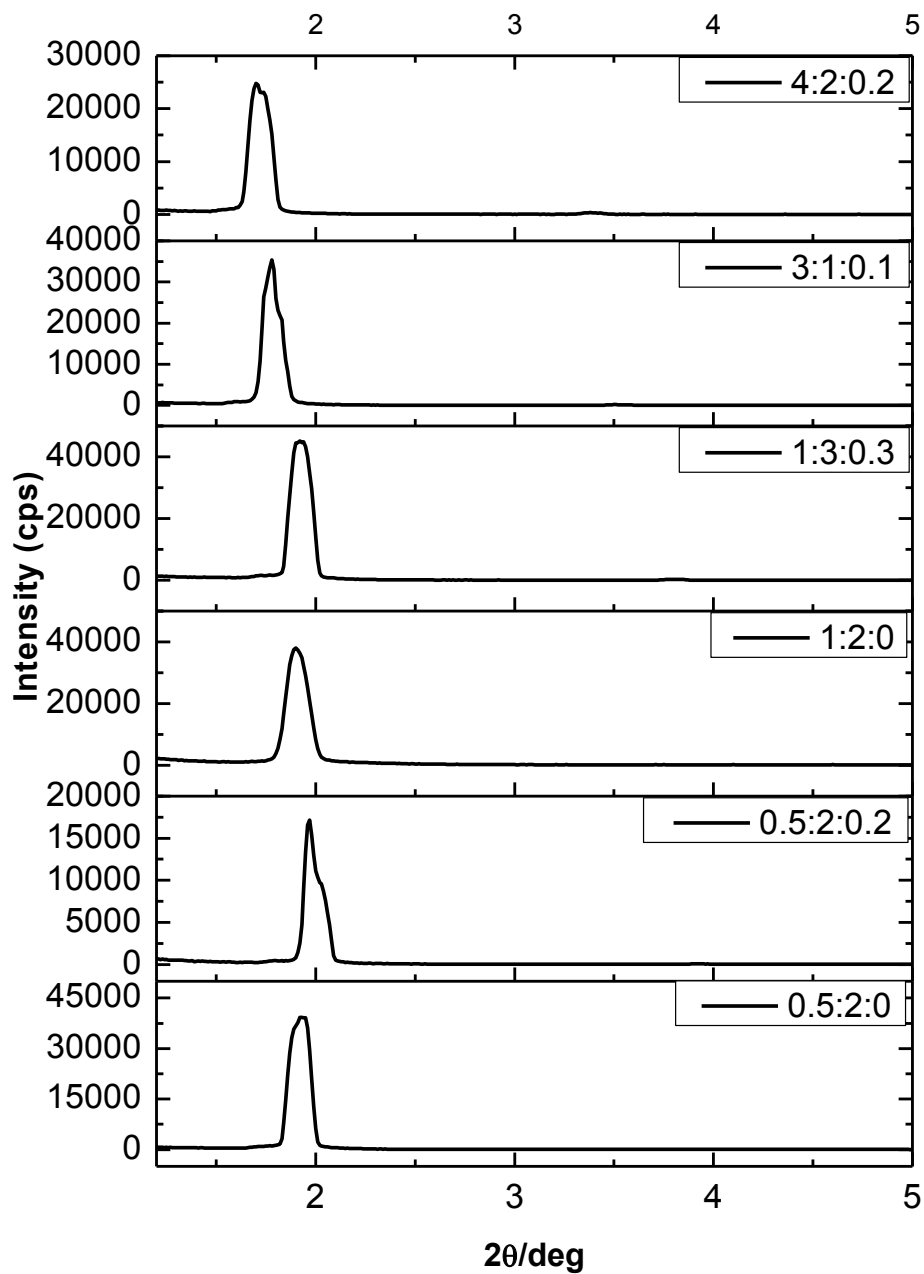


**Figure 4.30.** The XRD patterns at small angles of LiBr-LiI-I<sub>2</sub>-xH<sub>2</sub>O-C<sub>12</sub>EO<sub>10</sub> system with LiBr:LiI:I<sub>2</sub> mole ratios per mole of surfactant in the insets.

Sometimes it is hard to observe the second diffraction line. For this reason, POM images were also used to assign the hexagonal phase, see **Figure 4.31**. The

cubic phases give dark images under the POM and the hexagonal phase usually transforms to a cubic phase at higher salt concentrations.



**Figure 4.31.** The POM images of  $2.0\text{LiI}-0.2\text{I}_2-x\text{H}_2\text{O}-\text{C}_{12}\text{EO}_{10}$ ,  $2.0\text{LiI}-0.5\text{LiCl}-0.2\text{I}_2-x\text{H}_2\text{O}-\text{C}_{12}\text{EO}_{10}$ , and  $2.0\text{LiI}-0.5\text{LiBr}-0.2\text{I}_2-x\text{H}_2\text{O}-\text{C}_{12}\text{EO}_{10}$  samples from left to right.

All samples display similar fan-texture, which is characteristic for 2D hexagonal mesophase. The XRD and POM data together prove that incorporation of the iodide/triiodide redox couple does not disturb the LLC mesophase of the  $\text{LiCl}-x\text{H}_2\text{O}-\text{C}_{12}\text{EO}_{10}$ , and  $\text{LiBr}-x\text{H}_2\text{O}-\text{C}_{12}\text{EO}_{10}$  systems up to 0.4 salt to surfactant mole ratio. Moreover, the LLC mesophase remains hexagonal up to this limit.

#### 4.3.1. FT-IR and Raman Spectroscopic Investigations of the $\text{Li(X)-I}_2-x\text{H}_2\text{O}-\text{C}_{12}\text{EO}_{10}$ Systems

In order to have a better understanding of the impact of anions and iodine on the phase behavior of the systems, the FT-IR spectra were recorded at different salt concentrations. Increase in the mole ratio of salt species leads to an increase in the intensity of  $\nu\text{-OH}$  band at around  $3100\text{-}3700\text{ cm}^{-1}$ , see **Figure 4.32**. It indicates that the water amount kept in the mesophase is proportional to the salt concentration. Ions in the LLC mesophase are surrounded with water molecules, but excess water evaporates. Thus, the interaction between the ions and the water keeps ions in the mesophase. For this reason, the amount of water in the mesophase is related to the amount of salt. In the mesophase, most of the water molecules are in the form of hydration water; therefore the salt species cannot be directly detected in the

FT-IR spectra. The increase in the salt concentration does not cause a shift in the position of the maxima of  $\nu$ -OH band. However,  $\nu$ -CO stretching band of the surfactant head groups at around  $1100\text{ cm}^{-1}$  red-shift with increasing salt concentration because of the increase in the salt-surfactant interactions.

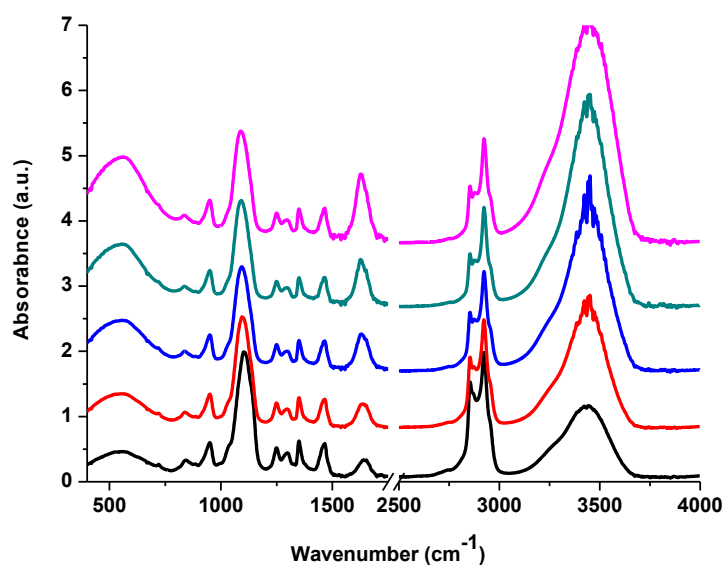


**Figure 4.32.** The FT-IR spectra of the  $\text{LiI}\cdot x\text{H}_2\text{O}\cdot\text{C}_{12}\text{EO}_{10}$  samples with different salt/surfactant mole ratios, from bottom to top 1.0, 2.0, 3.0, 4.0 and 5.0.

The water content of the mesophase also strongly depends on the choice of anion. **Figure 4.33** shows the FT-IR spectra of various samples under a 23% RH at RT. The  $\nu$ -OH stretching region, at around  $3500\text{ cm}^{-1}$ , shows that the  $\text{LiI}\cdot\text{LiBr}\cdot\text{I}_2\cdot x\text{H}_2\text{O}\cdot\text{C}_{12}\text{EO}_{10}$  and  $\text{LiI}\cdot\text{LiCl}\cdot\text{I}_2\cdot x\text{H}_2\text{O}\cdot\text{C}_{12}\text{EO}_{10}$  systems retain more water than  $\text{LiI}\cdot\text{I}_2\cdot x\text{H}_2\text{O}\cdot\text{C}_{12}\text{EO}_{10}$  systems with the same salt to surfactant mole ratios. Moreover, the red-shifted  $\nu$ -OH stretching frequencies in the LiBr and LiCl systems are also evidence for the stronger interactions between the water and  $\text{Br}^-/\text{Cl}^-$  ions, relative to the interaction between the  $\text{I}^-$  ion and water.

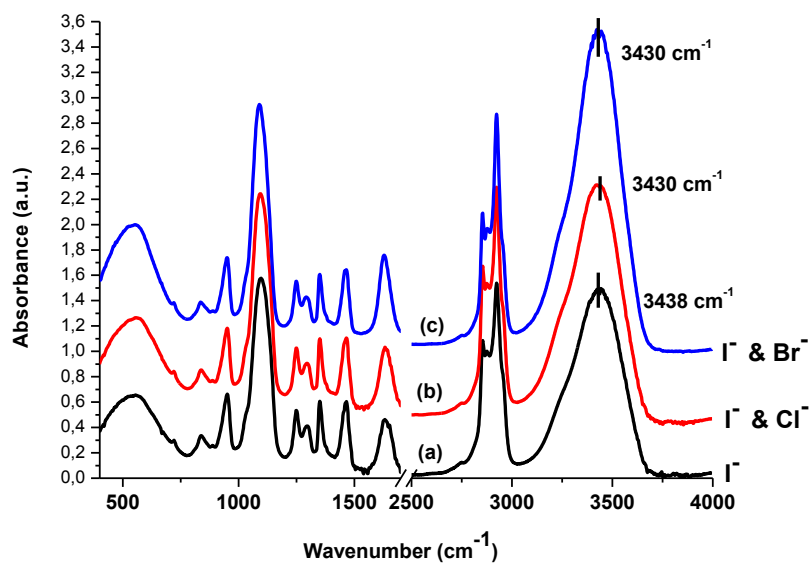


**Figure 4.33.** The FT-IR spectra of samples with compositions: (a)  $2.0\text{LiI}-0.2\text{I}_2-x\text{H}_2\text{O}-\text{C}_{12}\text{EO}_{10}$ , (b)  $2.0\text{LiI}-0.5\text{LiCl}-0.2\text{I}_2-x\text{H}_2\text{O}-\text{C}_{12}\text{EO}_{10}$ , and (c)  $2.0\text{LiI}-0.5\text{LiBr}-0.2\text{I}_2-x\text{H}_2\text{O}-\text{C}_{12}\text{EO}_{10}$ .

**Figure 4.34** shows the micro-Raman spectra of the  $\text{LiI}-\text{I}_2-x\text{H}_2\text{O}-\text{C}_{12}\text{EO}_{10}$ ,  $\text{LiI}-\text{LiCl}-\text{I}_2-x\text{H}_2\text{O}-\text{C}_{12}\text{EO}_{10}$ , and  $\text{LiI}-\text{LiBr}-\text{I}_2-x\text{H}_2\text{O}-\text{C}_{12}\text{EO}_{10}$  samples with the same salt to surfactant mole ratios. The peak, at  $117\text{ cm}^{-1}$ , corresponds to the symmetric stretching mode of triiodide ion, and it indicates the formation of the  $\text{I}_3^-$  ion in the liquid crystalline media.

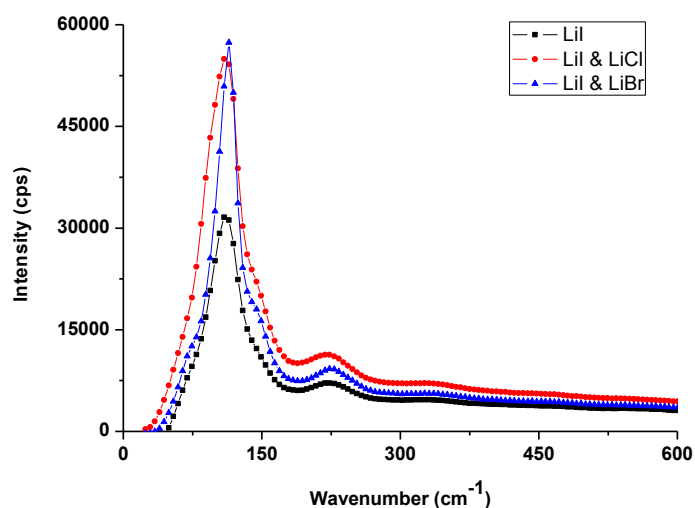


**Figure 4.34.** Raman spectra of the samples with compositions:  $2.0\text{LiI}-0.2\text{I}_2-x\text{H}_2\text{O}-\text{C}_{12}\text{EO}_{10}$ ,  $2.0\text{LiI}-0.5\text{LiCl}-0.2\text{I}_2-x\text{H}_2\text{O}-\text{C}_{12}\text{EO}_{10}$ , and  $2.0\text{LiI}-0.5\text{LiBr}-0.2\text{I}_2-x\text{H}_2\text{O}-\text{C}_{12}\text{EO}_{10}$  from bottom to top.

The UV-vis spectra of the same samples with the same salt compositions were also recorded, see **Figure 4.35**. In order to make comparison, the samples were coated as thin films on quartz substrates with the same spin rate. The peak at 246 nm and peaks at 246 and 291 nm correspond to iodide and triiodide ions, respectively, in the liquid crystalline media.

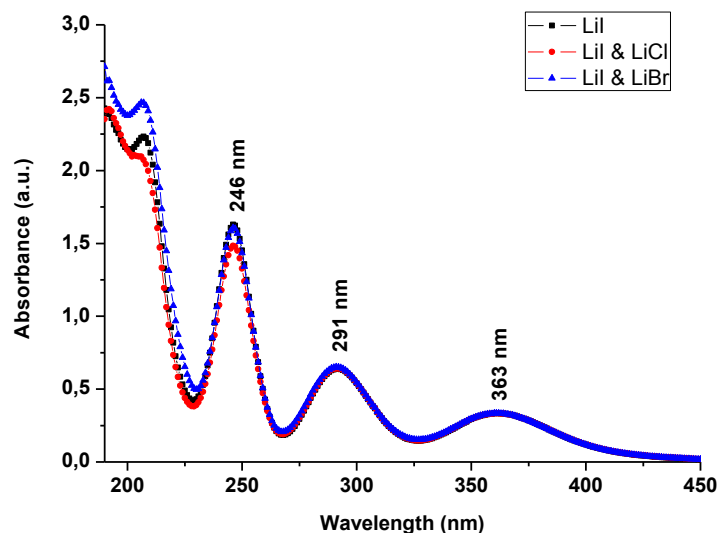


**Figure 4.35.** UV-vis spectra of the samples with compositions:  $2.0\text{LiI}-0.2\text{I}_2-x\text{H}_2\text{O}-\text{C}_{12}\text{EO}_{10}$ ,  $2.0\text{LiI}-0.5\text{LiCl}-0.2\text{I}_2-x\text{H}_2\text{O}-\text{C}_{12}\text{EO}_{10}$ , and  $2.0\text{LiI}-0.5\text{LiBr}-0.2\text{I}_2-x\text{H}_2\text{O}-\text{C}_{12}\text{EO}_{10}$ .

Although the samples have the same mole ratio of LiI, the ratio of iodide to triiodide absorbance ( $A_{\text{I}^-}/A_{\text{I}_3^-}$ ) changes among the systems. The highest  $A_{\text{I}^-}/A_{\text{I}_3^-}$  value is obtained from the  $\text{LiI}-x\text{H}_2\text{O}-\text{C}_{12}\text{EO}_{10}$  as 1.53, and it is calculated as 1.42 and 1.37 from the  $\text{LiI}-\text{LiCl}-x\text{H}_2\text{O}-\text{C}_{12}\text{EO}_{10}$  and  $\text{LiI}-\text{LiBr}-x\text{H}_2\text{O}-\text{C}_{12}\text{EO}_{10}$  systems, respectively. This demonstrates that the presence of another anion in the LLC media diminishes the conversion of  $\text{I}^-$  to  $\text{I}_3^-$  and the equilibrium constant (equation 1) shifts toward reactants. The conversion of the iodide to triiodide also reduced due to the formation of polyhalides such as  $\text{I}_2\text{Cl}^-$  and  $\text{I}_2\text{Br}^-$  with the addition of second salt into the mesophase.

#### 4.4. LLC Mesophases as Gel Electrolyte for Dye-Sensitized Solar Cells

The  $\text{LiI}/\text{I}_2$  couple that forms the  $\text{I}_3^-$  ion is very important for solar cell applications. The LLC media may serve as an electrolyte for ionic conductivity

and also source for the redox couple in a dye sensitized solar cell. Lithium iodide is a very stable salt, and it provides required iodide anions and lithium cations in order to increase conductivity of the electrolyte. Water-based gel electrolytes have widely been studied in order to overcome solvent problems such as electrolyte leakage, evaporation and degradation of the current collectors in the dye sensitized solar cell (DSSC). The photovoltaic performance of the LLC mesophases as electrolyte in the DSSCs has been investigated by recording I-V curves.

The DSSCs were fabricated as stated in **Section 3.3**. Ru-based N719 dye was used as synthesizer on a TiO<sub>2</sub> electrode. The gel electrolyte (solution phase of our LiI LLC mesophase) was dropped onto the dye coated TiO<sub>2</sub> electrode and kept at 80° C for 1 hour in order to ensure sufficient penetration of gel into pores of the TiO<sub>2</sub> electrode (anode). A Pt coated FTO was used as a counter electrode, and placed onto the gel-containing working electrode. For a comparison purpose, the DSSCs were fabricated using the same procedure, only electrolyte was replaced before measurements.

**Table 4.3.** Photovoltaic characteristics of various DSSCs based on different gel electrolytes.

Salt	Solvent	I <sub>sc</sub> (mA)	V <sub>oc</sub> (V)	FF	Efficiency (%)
LiI	Water	1.74	0.42	0.58	0.51
LiI & LiCl	Water	0.27	0.39	0.64	0.08
LiI & LiBr	Water	0.64	0.38	0.65	0.19
LiI	Acetonitrile	1.74	0.32	0.50	0.33
Liquid	Acetonitrile	3.66	0.44	0.28	0.53

**Figure 4.36** compares the I-V curves for the DSSCs employing different water-based gel electrolytes, prepared by using the LLC mesophases of different salt systems. Both open-circuit voltage (V<sub>oc</sub>) and short-circuit current (I<sub>sc</sub>) values are highest in the 2.0LiI-0.2I<sub>2</sub>-xH<sub>2</sub>O-C<sub>12</sub>EO<sub>10</sub> gel electrolyte. Addition of the second salt into the media significantly lowers V<sub>oc</sub> and I<sub>sc</sub> values resulting in 63% and 84% decrease in the efficiency of the cell in the LiBr and LiCl containing electrolytes, respectively, compared to that of only LiI containing electrolyte, see **Table 4.3**.

As discussed before, the addition of the second salt into LLC mesophase decreases the conversion of iodide to triiodide, see **Section 4.3.1**. And reduction in the concentration of triiodide anion causes significant decreases in the efficiency of the cell. The resistances of the electrolytes also play a significant role in the efficiency of the cells. Conductivity has been determined to be 0.27, 0.26 and 0.03  $\text{mS cm}^{-1}$  for LiI, LiI & LiCl and LiI & LiBr containing gel electrolytes, respectively by using AC impedance spectroscopy. The highest efficiency of LiI containing electrolyte is related to its higher conductivity when compared to other electrolytes.

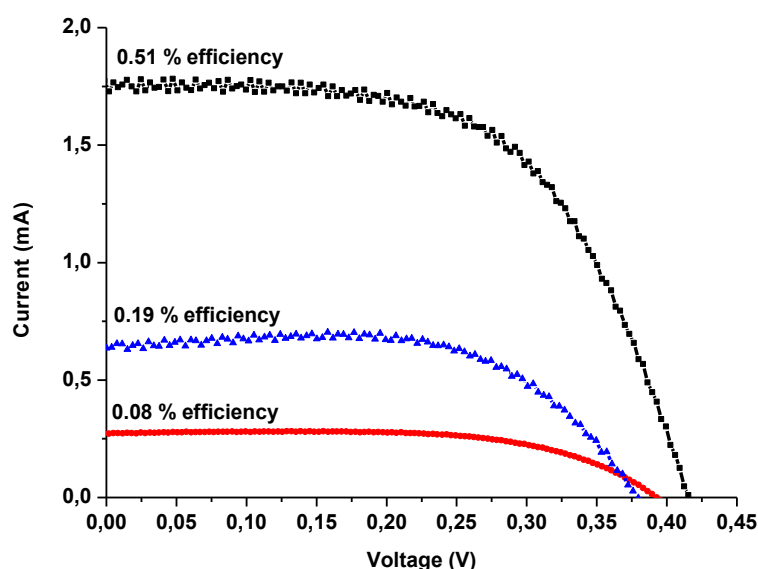


**Figure 4.36.** I-V curves for the DSSCs employing different kinds of electrolytes under 1 sun illumination ( $\text{AM1.5}$ ,  $100 \text{ mW cm}^{-2}$ )  $2.0\text{LiI}-0.2\text{I}_2-x\text{H}_2\text{O}-\text{C}_{12}\text{EO}_{10}$ ,  $2.0\text{LiI}-0.5\text{LiBr}-0.2\text{I}_2-x\text{H}_2\text{O}-\text{C}_{12}\text{EO}_{10}$ , and  $2.0\text{LiI}-0.5\text{LiCl}-0.2\text{I}_2-x\text{H}_2\text{O}-\text{C}_{12}\text{EO}_{10}$  from top to bottom.

The lower efficiency for LiI & LiCl and LiI & LiBr containing gel electrolytes can be related to formation less favorable redox couples such as  $\text{I}^-/\text{I}_2\text{Br}^-$  and  $\text{I}^-/\text{I}_2\text{Cl}^-$ . As discussed in the UV-vis part, the formation of polyhalides in the LLC media may diminish the conversion of  $\text{I}^-$  into  $\text{I}_3^-$  so the efficiency of the solar cell decreases.

Acetonitrile was used as solvent during the preparation of LLC mesophase in order to understand the effect of water on the efficiency of electrolytes. **Figure 4.37** shows the I-V curve of gel electrolytes prepared by  $\text{LiI}-\text{I}_2-x\text{H}_2\text{O}-\text{C}_{12}\text{EO}_{10}$  system using either water or acetonitrile as the solvent.

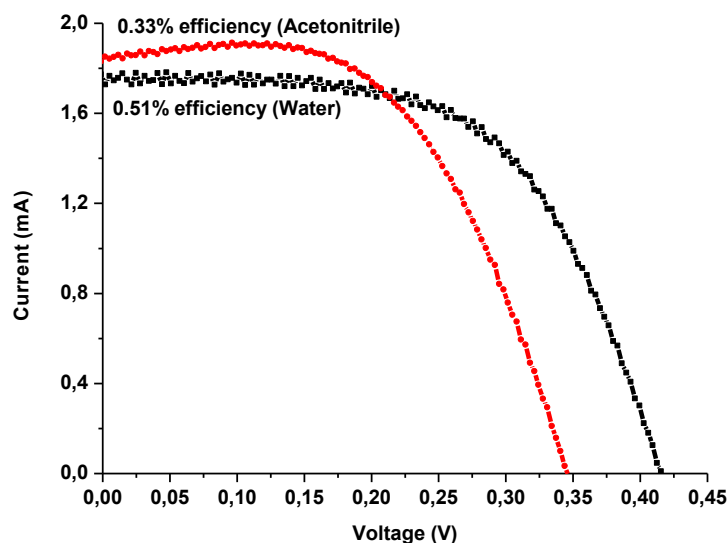


**Figure 4.37.** I-V curves of the DSSCs by employing water-based and acetonitrile-based of electrolytes under 1 sun illumination (AM1.5, 100 mW cm<sup>-2</sup>) using the LiI-I<sub>2</sub>-xH<sub>2</sub>O-C<sub>12</sub>EO<sub>10</sub> system.

Although the photocurrent increases with the addition acetonitrile in the media, the fill factor and V<sub>oc</sub> values of the cell diminishes, resulting a 35% decrease in the efficiency. The enhancement in the V<sub>oc</sub> values of water-based gel electrolyte can possibly be related to a positive shift in the redox potential of iodide/triiodide redox couple. This positive shift in the redox potential was reported before as a main reason of the enhancement of V<sub>oc</sub> by other groups.<sup>80, 90</sup>

**Figure 4.38.** displays the I-V curves of a water-based gel electrolyte made by using the LiI-I<sub>2</sub>-xH<sub>2</sub>O.C<sub>12</sub>EO<sub>10</sub> samples under various sun levels. Both V<sub>oc</sub> and I<sub>sc</sub> values decrease with reducing sun level, however, the efficiency of the cell increases. The efficiency ( $\eta$ ) is calculated according to following formula:

$$\eta = V_{oc} \times I_{sc} \times FF / I_0$$

where *FF* is the fill factor and *I*<sub>0</sub> is the intensity of the simulated sunlight impinging on the solar cell.

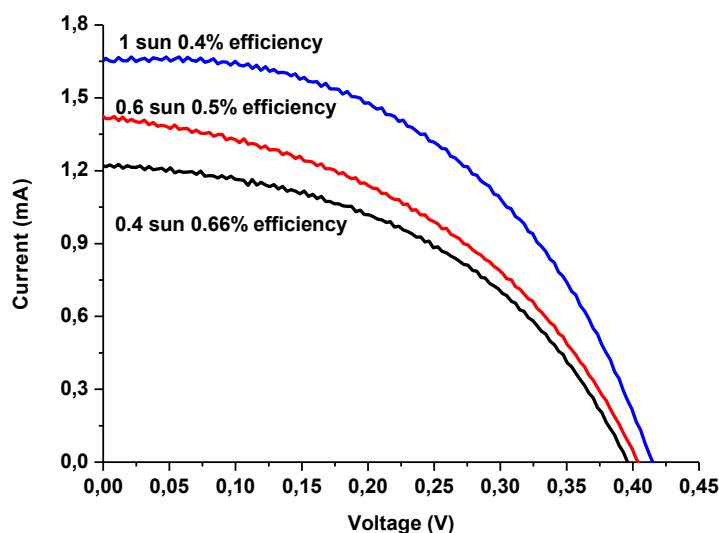


**Figure 4.38.** I-V curves for the DSSCs by employing the water-based LiI-I<sub>2</sub>-xH<sub>2</sub>O-C<sub>12</sub>EO<sub>10</sub> gel electrolyte under illumination of different sun levels.

The stability of the water-based gel electrolytes was investigated by comparing the I-V curves after being stored for 24 and 96 hours, see **Figure 4.39**. The DSSCs were stored under dark conditions at RT and 25% RH.

**Table 4.4.** Photovoltaic characteristics of various DSSCs based on LiI-I<sub>2</sub>-xH<sub>2</sub>O-C<sub>12</sub>EO<sub>10</sub> gel electrolyte at different time intervals.

Time	I <sub>sc</sub> (mA)	V <sub>oc</sub> (V)	Light	FF	Efficiency (%)
Immediate	1.74	0.42	1 Sun	0.58	0.51
24 hours	1.60	0.41	1 Sun	0.62	0.49
96 hours	1.56	0.42	1 Sun	0.48	0.38

The efficiency of the cells decreases to 0.38% 4 days later from its initial efficiency of 0.51%, see **Table 4.4**. The main reason of this reduction is the decrease in photocurrent since the water in the electrolyte can cause desorption of dye molecules from the TiO<sub>2</sub> electrode surface. The cells were not sealed before aging and during the measurements; therefore there may be a solvent leakage over time. This can be another reason of the photocurrent and efficiency decrease.

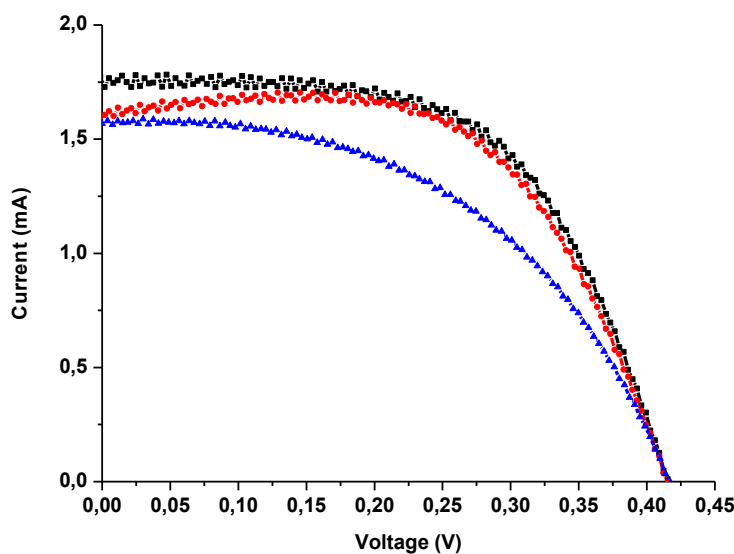


**Figure 4.39.** I-V curves for the DSSCs by employing the water-based  $\text{LiI-I}_2\text{-xH}_2\text{O-C}_{12}\text{EO}_{10}$  gel electrolyte recorded immediately, after 24 hours, and 4 days later from top to bottom.

The fill factor of the cell also decreases after 4 days, see **Table 4.4**. The increase of the series resistance can probably be responsible for the reduction of the fill factor. This can be related to poor contact between the FTO and Pt-coated counter electrodes due to oxidation at counter electrode in time.

#### 4.5. Future Work

In this study, gel electrolytes made by LLC mesophases of lithium salts and  $\text{C}_{12}\text{EO}_{10}$  systems was characterized by means of spectroscopy, diffraction and microscopy. Moreover, the solar performance of DSSCs that contain these gel electrolytes were investigated by collecting only I-V curves. In order to clarify our perspective on the factors which affect the solar performance of DSSCs, we have to investigate series resistance, electrolyte resistance, desorption of dye molecules from  $\text{TiO}_2$  electrode surface, and redox potential of electrolyte by using different techniques such as electrochemical impedance spectroscopy, intensity-modulated photovoltage spectroscopy (IMVS), intensity-modulated photocurrent spectroscopy (IMPS) etc.

## CHAPTER 5

### 5. CONCLUSION

In this thesis, six different lithium salt- $x\text{H}_2\text{O}$ -pluronics systems have been investigated by means of spectroscopy, microscopy and diffraction in order to clarify the self-assembly process of surfactants into liquid crystalline mesophases. It has been shown that the  $\text{Li}(\text{X})$  salts ( $\text{X} = \text{Cl}^-$  or  $\text{NO}_3^-$ ) can be used to form LLC mesophases with pluronics, (tri-block copolymers, P65, P85, P103, and P123) in a broad range of salt concentration. The LLC mesophases are ordered up to nearly 25.0 salt to surfactant mole ratio. The concentrated solutions of lithium salts act as the solvent component of the mesophase, and it organize the surfactant molecules into hexagonal and cubic mesophases. The salt/surfactant range of the hexagonal mesophase depends on the anion, and follows the Hofmeister series. The  $\text{LiCl}$  containing systems display a hexagonal mesophase in a broader range of the salt concentration than those of  $\text{LiNO}_3$  containing ones. The higher structure making character of  $\text{Cl}^-$  ions keeps more hydration water molecules, and so the curvature of the hexagonal mesophase increases and as a result covers a broader range in the phase diagram. Construction of the phase diagram of each system is necessary to fully understand the phase behavior of these new mesophases.

Here, we proposed a new gel electrolyte made up of  $\text{Li}(\text{X})\text{-}x\text{H}_2\text{O}\text{-C}_{12}\text{EO}_{10}$  LLC mesophases for a dye-sensitized solar cell. The  $\text{I}/\text{I}_3^-$  redox couple can be incorporated into the LLC mesophases of the  $\text{LiI}\text{-}x\text{H}_2\text{O}\text{-C}_{12}\text{EO}_{10}$  systems up to 0.3 iodine/surfactant mole ratio and those of 0.4 mole ratio for the  $\text{LiI}\text{-LiCl}\text{-}x\text{H}_2\text{O}\text{-C}_{12}\text{EO}_{10}$  and  $\text{LiI}\text{-LiBr}\text{-}x\text{H}_2\text{O}\text{-C}_{12}\text{EO}_{10}$  samples without disturbing the mesophase. In the LLC media, some  $\text{I}^-$  is converted into  $\text{I}_3^-$  ion that the concentration of the latter can be increased by the addition of  $\text{I}_2$  into the LLC media. The XRD patterns and POM images clearly showed that the above mixtures form stable LLC mesophases in a very broad salt concentration. Overall the  $\text{LiI}$ ,  $\text{LiCl}\text{-LiI}$ , and  $\text{LiBr}\text{-LiI}$  with  $\text{I}_2$  and non-ionic surfactants form stable LLC mesophases with high ionic conductivity. The solar cell performance of the gel electrolytes made using LLC mesophases were measured by recording I-V curves. The highest efficiency was obtained from the LLC mesophases of the  $\text{LiI}\text{-I}_2\text{-}x\text{H}_2\text{O}\text{-C}_{12}\text{EO}_{10}$  system as 0.51%, which is comparable with the commonly used liquid electrolyte ( $\text{I}/\text{I}_3^-$  in acetonitrile) in a similar cell.

Further optimizations are necessary to improve the solar cell performance using the LLC gel-electrolytes.

## BIBLIOGRAPHY

1. S. A. Hudson, and P. M. Maitlis, "Calamitic metallomesogens: metal-containing liquid crystals with rodlike shapes," *Chemical Reviews*, vol. 93, no. 3, pp. 861-885, 1993.
2. P. J. Collings, M. Hird, "Introduction to liquid crystals: chemistry and physics," *CRC Press/Llc*, vol. 1, 1997.
3. D. Demus, "Plenary lecture: One hundred years of liquid-crystal chemistry: Thermotropic liquid crystals with conventional and unconventional molecular structure," *Liquid Crystals*, vol. 5, no. 1, pp. 75-110, 1989.
4. S. Sergeyev, P. Wojciech, and Y. H. Geerts, "Discotic liquid crystals: a new generation of organic semiconductors," *Chemical Society Reviews*, vol. 36, no. 12, pp. 1902-1929, 2007.
5. S. T. Hyde, "Identification of lyotropic liquid crystalline mesophases," *Handbook of Applied Surface and Colloid Chemistry*, 299, 2001.
6. L. A. Madsen, T. J. Dingemans, M. Nakata, and E. T. Samulski, "Thermotropic biaxial nematic liquid crystals," *Physical Review Letters*, vol. 92, no. 14, pp. 145505, 2004
7. P. Alexandridis, U. Olsson, and B. Lindman, "Structural polymorphism of amphiphilic copolymers: Six lyotropic liquid crystalline and two solution phases in a poly (oxybutylene)-b-poly (oxyethylene)-water-xylene system," *Langmuir*, vol. 13, no.1, pp. 23-3, 1997.
8. S. S. Funari, M. C. Holmes, and G. J.T. Tiddy, "Intermediate lyotropic liquid crystal phases in the C16EO6/water system," *The Journal of Physical Chemistry*, vol. 98, no.11, pp. 3015-3023, 1994.

9. M. U. Araos, and G. G. Warr, "Self-assembly of nonionic surfactants into lyotropic liquid crystals in ethylammonium nitrate, a room-temperature ionic liquid," *The Journal of Physical Chemistry B*, vol. 109, no. 30, 14275-14277, 2005.
10. P. Alexandridis, U. Olsson, and B. Lindman, "A record nine different phases (four cubic, two hexagonal, and one lamellar lyotropic liquid crystalline and two micellar solutions) in a ternary isothermal system of an amphiphilic block copolymer and selective solvents (water and oil)," *Langmuir*, vol. 14, no. 10, pp. 2627-2638, 1998.
11. B. J. Forrest, and L. W. Reeves, "New lyotropic liquid crystals composed of finite nonspherical micelles," *Chemical Reviews*, vol. 81, no.1, pp. 1-14, 1981.
12. K. Tsujii, "Surface activity: principles, phenomena, and applications," *San Diego: Academic Press*, pp. 17-42, 1998.
13. J. N. Israelachvili, Jacob N, "Intermolecular and surface forces: revised third edition," *Academic press*, 2011.
14. C. Tanford, "The Hydrophobic Effect: Formation of Micelles and Biological Membranes, 2<sup>nd</sup> Edition," *J. Wiley*, 1980.
15. V. S. Marinov, and H. Matsuura, "Raman spectroscopic study of temperature dependence of water structure in aqueous solutions of a poly (oxyethylene) surfactant," *Journal of Molecular Structure* vol. 610, no.1, 105-112, 2002.
16. K. Holmberg, J. B. JoEnsson, B. Kronberg, & B. E. Lindman, "Surfactants and polymers in aqueous solution," *John Wiley & Sons*, 2003.
17. Forrest, Bruce J., and Leonard W. Reeves. "New lyotropic liquid crystals composed of finite nonspherical micelles" *Chemical Reviews*, vol. 81, pp. 1-14, 1981.

18. G. Cevc, and H. Richardsen, "Lipid vesicles and membrane fusion," *Advanced Drug Delivery Reviews*, vol. 38, no. 3, pp. 207-232, 1999.
19. G. J. de AA. Soler-Illia, C. Sanchez, B. Lebeau, & J. Patarin, "Chemical strategies to design textured materials: from microporous and mesoporous oxides to nanonetworks and hierarchical structures," *Chemical Reviews*, vol. 102, no. 11, pp. 4093-4138, 2002.
20. H. Kunieda, and K. Shinoda, "Evaluation of the hydrophile-lipophile balance (HLB) of nonionic surfactants. I. Multisurfactant systems," *Journal of Colloid and Interface Science*, vol. 107, no. 1, pp. 107-121, 1985.
21. H. Kunieda, and K. Shinoda, "Conditions to produce so-called microemulsions: factors to increase the mutual solubility of oil and water by solubilizer," *Journal of Colloid and Interface Science*, vol. 42, no. 2, pp. 381-387, 1973.
22. H. Kunieda, and K. Shinoda, "Phase behavior in systems of nonionic surfactant/water/oil around the hydrophile-lipophile-balance-temperature (HLB-temperature)," *Journal of Dispersion Science and Technology*, vol. 3, no. 3, pp. 233-244, 1982.
23. R. Dong, and H. Jingcheng, "Complex fluids of poly (oxyethylene) monoalkyl ether nonionic surfactants," *Chemical Reviews*, vol. 110, no. 9 pp. 4978, 2010.
24. T. L. Greaves, and C. J. Drummond, "Ionic liquids as amphiphile self-assembly media," *Chemical Society Reviews*, vol. 37, no.8, pp. 1709-1726, 2008.
25. M. J. Hollamby, K. Trickett, A. Mohamed, J. Eastoe, S.E. Rogers, and R. K. Heenan, "Surfactant Aggregation in CO<sub>2</sub>/Heptane Solvent Mixtures," *Langmuir*, vol. 25, no. 22, pp. 12909-12913, 2009.

26. J. Liu, B. Han, G. Li, Z. Liu, J. He, G. Yang, "Solubility of the non-ionic surfactant tetraethylene glycol n-laurel ether in supercritical CO<sub>2</sub> with n-pentanol," *Fluid Phase Equilibria*, vol. 187, pp. 247-254, 2001.
27. C. Seguin, J. Eastoe, R. Clapperton, R. K. Heenan, and I. Grillo, "Alternative non-aqueous water-miscible solvents for surfactants," *Colloids and Surfaces A: Physicochemical and Engineering Aspects*, vol. 282, pp. 134-142, 2006.
28. C. Seguin, J. Eastoe, R. K. Heenan, and I. Grillo "Controlling aggregation of nonionic surfactants using mixed glycol media," *Langmuir*, vol. 23, no. 8, pp. 4199-4202, 2007.
29. T. Wörnheim, and A. Jönsson, "Phase diagrams of alkyltrimethylammonium surfactants in some polar solvents," *Journal of Colloid and Interface Science*, vol. 125, no. 2, 627-633, 1988.
30. R. Strey, R. Schomacker, D. Roux, F. Nallet, and U. Olsson, "Dilute lamellar and L<sub>3</sub> phases in the binary water–C<sub>12</sub>E<sub>5</sub> system" *Journal of the Chemical Society, Faraday Transactions*, vol. 86, no. 12, pp. 2253-2261, 1990.
31. J. S. Clunie, J. F. Goodman, and P. C. Symons, "Phase equilibria of dodecylhexaoxyethylene glycol monoether in water," *Trans. Faraday Soc.*, vol. 65, pp. 287-296, 1969.
32. K. Shinoda, "Thermodynamic aspects of nonionic surfactant—Water systems," *Journal of Colloid and Interface Science*, vol. 34, no. 2, pp. 278-282, 1970.
33. D. J. Mitchell, G. J. T. Tiddy, T. Bostock, and M. P. McDonald, "Phase behaviour of polyoxyethylene surfactants with water. Mesophase structures and partial miscibility (cloud points)" *J. Chem. Soc., Faraday Trans. 1*, vol. 79, no. 4, pp. 975-1000, 1983.

34. H. Saito, "Solution Properties of Nonionic Surfactant Aqueous Solutions and Their Relations with Foam Property," *Nippon Kagaku Zasshi*, vol. 92, pp. 223-226, 1971.
35. J. C. Lang, and R. D. Morgan, "Nonionic surfactant mixtures. I. Phase equilibria in CE–HO and closed-loop coexistence," *The Journal of Chemical Physics*, vol. 73, pp. 5849, 1980.
36. E. S. J. Rudolph, J. H. Hangeveld, T. W. de Loos, A. J. de Swaan, "Phase behaviour of water + nonionic surfactant systems: experiments and modelling applying the Peng–Robinson equation of state with the Wong–Sandler mixing rules and the UNIQUAC  $g^E$ -model," *Fluid Phase Equilibria*, vol. 173, no. 1, pp. 81-96, 2000.
37. Y. Nibu, and T Inoue, "Phase behavior of aqueous mixtures of some polyethylene glycol decyl ethers revealed by DSC and FT-IR measurements," *Journal of Colloid and Interface Science*, 205, no.2, pp. 305-315, 1998.
38. Y. Nibu, and T Inoue, "Solid-liquid phase behavior of binary mixture of tetraethylene glycol decyl ether and water" *Journal of Colloid and Interface Science*, vol. 205, no.2, pp. 231-240, 1998.
39. H. Evans, D. J. Tildesley, and C. A. Leng, "Theories of cloud-curve phase separation in non-ionic alkyl polyoxyethylene micellar solutions," *J. Chem. Soc., Faraday Trans. 2*, vol. 83, no. 8, pp. 1525-1541, 1987.
40. M. Parrinello, and A. Rahman, "Crystal structure and pair potentials: A molecular-dynamics study," *Physical Review Letters*, vol. 45, no. 14, pp. 1196-1199, 1980.
41. Y. Nibu, T. Suemori, and T. Inoue, "Phase behavior of binary mixture of heptaethylene glycol decyl ether and water: Formation of phase compound in solid phase," *Journal of Colloid and Interface Science*, vol. 191, no.1 pp. 256-263, 1997.

42. F. Hofmeister, *Arch. Exp. Pathol. Pharmacol*, vol. 24, pp. 247-260, 1888.
43. M. G. Cacace, E. M. Landau, and J. J. Ramsden, "The Hofmeister series: salt and solvent effects on interfacial phenomena," *Quarterly Reviews of Biophysics*, vol. 30, no. 3, pp. 241-277, 1997.
44. K. Weckström, and M. Zulauf, "Lower consolute boundaries of a poly (oxyethylene) surfactant in aqueous solutions of monovalent salts" *J. Chem. Soc., Faraday Trans. 1*, vol. 81, no.12, pp. 2947-2958, 1985.
45. Zheng, LiQiang, H. Minamikawa, K. Harada, T Inoue, and G. G. Cernik, "Effect of inorganic salts on the phase behavior of an aqueous mixture of heptaethylene glycol dodecyl ether," *Langmuir* vol. 19, no.25, pp. 10487-10494, 2005.
46. K. S. Sharma, S. R. Patil, and A. K. Rakshit, "Study of the cloud point of C<sub>12</sub>E<sub>n</sub> nonionic surfactants: effect of additives," *Colloids and Surfaces A: Physicochemical and Engineering Aspects*, vol. 219, no. 1, pp. 67-74, 2003.
47. T. Inoue, Y. Yokoyama, and L. Q. Zheng, "Hofmeister anion effect on aqueous phase behavior of heptaethylene glycol dodecyl ether," *Journal of Colloid and Interface Science*, vol. 274, no.1, pp. 349-353, 2004.
48. Ö. Çelik, and Ö. Dag, "A new lyotropic liquid crystalline system: oligo (ethylene oxide) surfactants with [M(H<sub>2</sub>O)<sub>n</sub>]X<sub>m</sub> transition metal complexes," *Angewandte Chemie-International Edition*, vol. 113, no. 20, pp. 3915-3919, 2001.
49. Terminology, I. M. S. Colloidal Surface Chemistry.
50. Y. Wan, and D. Zhao, "On the controllable soft-templating approach to mesoporous silicates," *Chemical Reviews*, vol. 107, no. 7, pp. 2821, 2007.
51. M. G. Kanatzidis, "Beyond silica: nonoxidic mesostructured materials," *Advanced Materials*, vol. 19, no. 9, pp. 1165-1181, 2007.

52. J. S. Beck, J. C. Vartuli, W. J. Roth, M. E. Leonowicz, C. T. Kresge, K. D. Schmitt, E. W. Sheppard, "A new family of mesoporous molecular sieves prepared with liquid crystal templates," *Journal of the American Chemical Society*, vol. 114, no. 27, pp. 10834-10843, 1992.
53. C. T. Kresge, M. E. Leonowicz, W. J. Roth, J. C. Vartuli, and J. S. Beck, "Ordered mesoporous molecular sieves synthesized by a liquid-crystal template mechanism," *Nature*, vol. 359, no. 6397, pp. 710-712, 1992.
54. Wan, Ying, and Dongyuan Zhao, "On the controllable soft-templating approach to mesoporous silicates," *Chemical Reviews*, vol. 107, no.7, pp. 2821, 2007.
55. G. S. Attard, J. C. Glyde, and C. G. Göltner, "Liquid-crystalline phases as templates for the synthesis of mesoporous silica" *Nature*, vol. 378, no. 6555, pp. 366-368, 1995.
56. D. E. De Vos, M. Dams, B. F. Sels, P. A. Jacobs, "Ordered mesoporous and microporous molecular sieves functionalized with transition metal complexes as catalysts for selective organic transformations," *Chemical Reviews*, vol. 102, no. 10, pp. 3615, 2002.
57. H. İ. Okur, Y. Türker, and Ö. Dag, "Synthesis of Stable Mesostructured Coupled Semiconductor Thin Films: meso-CdS-TiO<sub>2</sub> and meso-CdSe-TiO<sub>2</sub>" *Langmuir*, vol. 26, no. 1, pp. 538-544, 2009.
58. Y. Türker, and Ö. Dag, "Synthesis of mesostructured metal sulfide films using [M(H<sub>2</sub>O)<sub>n</sub>](NO<sub>3</sub>)<sub>2</sub>: P85 (M = Cd (II) and Zn (II)) liquid crystalline mesophases," *Journal of Materials Chemistry*, vol. 18, no. 29, pp. 3467-3473, 2008.
59. A. F. Demirörs, B. E. Eser, and Ö. Dag, "Liquid Crystalline Mesophases of Pluronics (L64, P65, and P123) and Transition Metal Nitrate Salts ([M(H<sub>2</sub>O)<sub>6</sub>](NO<sub>3</sub>)<sub>2</sub>)," *Langmuir*, vol. 21, no.9, pp. 4156-4162, 2005.

60. C. Albayrak, A. M. Soylu, and Ö. Dag "Lyotropic Liquid-Crystalline Mesophases of  $[\text{Zn}(\text{H}_2\text{O})_6](\text{NO}_3)_2\text{-C}_{12}\text{EO}_{10}\text{-CTAB-H}_2\text{O}$  and  $[\text{Zn}(\text{H}_2\text{O})_6](\text{NO}_3)_2\text{-C}_{12}\text{EO}_{10}\text{-SDS-H}_2\text{O}$  Systems," *Langmuir*, vol. 24, no. 19, pp. 10592-10595, 2008.
61. Ö. Dag, S. Alayoğlu, and I. Uysal, "Effects of Ions on the Liquid Crystalline Mesophase of Transition-Metal Salt: Surfactant ( $\text{C}_n\text{EO}_m$ )," *The Journal of Physical Chemistry B*, vol. 108, no. 25, pp. 8439-8446, 2004.
62. C. Albayrak, G. Gülten, and Ö. Dag, "Phase Separation in Liquid Crystalline Mesophases of  $[\text{Co}(\text{H}_2\text{O})_6]\text{X}_2$ : P65 Systems ( $\text{X} = \text{NO}_3^-$ ,  $\text{Cl}^-$ , or  $\text{ClO}_4^-$ )," *Langmuir*, vol. 23, no.2, pp. 855-860, 2007.
63. Y. Akdoğan, Ç. Üzümlü, Ö. Dag, and N. Coombs, "Synthesis of solid solutions of  $\text{Cd}_{1-x}\text{Zn}_x\text{S}$  nanocrystals in the channels of mesostructured silica films," *Journal of Materials Chemistry*, vol. 16, no. 21, pp. 2048-2055, 2006.
64. C. Karakaya, T. Yurdanur, Ö. Dag, "Assembly of Molten Transition Metal Salt-Surfactant in a Confined Space for the Synthesis of Mesoporous Metal Oxide-Rich Metal Oxide-Silica Thin Films," *Chemistry of Materials*, vol. 23, no. 12, pp. 3062-3071, 2011.
65. C. Tura, N. Coombs, and Ömer Dag, "One-pot synthesis of CdS nanoparticles in the channels of mesostructured silica films and monoliths," *Chemistry of Materials*, vol. 17, no.3, pp. 573-579, 2005.
66. Ö. Dag, O. Samarskaya, N. Coombs & A. G.Ozin "The synthesis of mesostructured silica films and monoliths functionalised by noble metal nanoparticles" *Journal of Materials Chemistry*, vol. 13, no.2, pp. 328-334, 2003.

67. C. Albayrak, A. M. Soylu, and Ö. Dag, "The role of charged surfactants in the thermal and structural properties of lyotropic liquid crystalline mesophases of  $[\text{Zn}(\text{H}_2\text{O})_6](\text{NO}_3)_{(2)}\text{-C}_n\text{EO}_m\text{-H}_2\text{O}$ " *Journal of Colloid and Interface Science*, vol. 341, no. 19, pp.109-116, 2010.
68. C. Albayrak, N. Özkan, and Ö . Dag, "Origin of Lyotropic Liquid Crystalline Mesophase Formation and Liquid Crystalline to Mesostructured Solid Transformation in the Metal Nitrate Salt– Surfactant Systems" *Langmuir*, vol. 27, no. 3, pp. 870-873, 2010.
69. C. Albayrak, A. Cihaner, and Ö.Dag, "A New, Highly Conductive, Lithium Salt/Nonionic Surfactant, Lyotropic Liquid-Crystalline Mesophase and Its Application" *Chemistry-A European Journal*, vol. 18, no.14, pp. 4190-4194, 2012.
70. C. Albayrak, "New Solvents for Surfactant Self-assembly: Molten Hydrated Salts and Concentrated Aqueous Electolyte Solutions", Doctor of Philosophy Thesis, *Bilkent University*, 2013.
71. C. Albayrak, G. Barım, Ö. Dag, "Lyotropic Liquid Crystal to Soft Mesocrystal Transformation in the Hydrated Salt-Surfactant Mesophases", *Chemistry-A European Journal*, (submitted).
72. R. Q. Song, and H. Cölfen, "Mesocrystals-Ordered nanoparticle superstructures," *Advanced Materials*, vol. 22, no. 12, pp. 1301-1330, 2010.
73. H. Cölfen, and S. Mann, "Higher-order organization by mesoscale self-assembly and transformation of hybrid nanostructures," *Angewandte Chemie - International Edition*, vol. 42, no.21, pp. 2350-2365, 2003.
74. H. Cölfen, and M. Antonietti, "Mesocrystals: inorganic superstructures made by highly parallel crystallization and controlled alignment," *Angewandte Chemi - International Edition*, vol. 44, no. 35, pp. 5576-5591, 2005.

75. C. Albayrak, G. Barım, Ö. Dağ, "Effect of Hygroscopicity of Salts on the Formation of Lyotropic Liquid Crystalline Mesophases," *Langmuir* (submitted).
76. J. H. Seinfeld, and S. N. Pandis, "Atmospheric chemistry and physics: from air pollution to climate change," *Wiley-Interscience*, 2012.
77. B. O'regan, and M. Grfitzeli. "A low-cost, high-efficiency solar cell based on dye-sensitized," *Nature*, vol. 353, pp. 24, 1991.
78. A. Yella, H. W. Lee, and H. N. Tsao, "Porphyrinsensitized solar cells with cobalt (II/III)-based redox electrolyte exceed 12% efficiency," *Science*, vol. 334, no. 6065, pp. 629-634, 2011.
79. S. R. Raga, E. M. Barea, and F. F.-Santiago, "Analysis of the Origin of Open Circuit Voltage in Dye Solar Cells," *The Journal of Physical Chemistry Letters*, vol. 3, no.12, pp. 1629-1634, 2012.
80. S. J. Park, K. Yoo, J. Y. Kim, J. Y. Kim, D. K. Lee, B. S. Kim, H. Kim, J. H. Kim, J. Cho, and M. J. Ko, "Water-Based Thixotropic Polymer Gel Electrolyte for Dye-Sensitized Solar Cells," *ACS Nano*, 2013.
81. Y. S. Jung, B. Yoo, M. K. Lim, S. Y. Lee, K. J. Kim "Effect of Triton X-100 in water-added electrolytes on the performance of dye-sensitized solar cells," *Electrochimica Acta*, vol. 54, no. 26, pp. 6286-6291, 2009.
82. J. N. de Freitas, A. F. Nogueira, and M. A. De Paoli, "New insights into dye-sensitized solar cells with polymer electrolytes," *Journal of Materials Chemistry*, vol. 19, no. 30, pp. 5279-5294, 2009.
83. C. L. Chen, H. Teng, and Y. L. Lee, "In Situ Gelation of Electrolytes for Highly Efficient Gel-State Dye-Sensitized Solar Cells," *Advanced Materials*, vol. 23, no. 36, pp. 4199-4204, 2011.

84. G. Boschloo, and A. Hagfeldt. "Characteristics of the iodide/triiodide redox mediator in dye-sensitized solar cells," *Accounts of Chemical Research*, vol. 42, no. 11, pp. 1819-1826, 2009.
85. S. Pelet, J. E. Moser, and M. Grätzel "Cooperative effect of adsorbed cations and iodide on the interception of back electron transfer in the dye sensitization of nanocrystalline TiO<sub>2</sub>," *The Journal of Physical Chemistry B*, vol. 104, no. 8, pp. 1791-1795, 2000.
86. M. Corti, C. Minero, and V. Degiorgio, "Cloud point transition in nonionic micellar solutions," *The Journal of Physical Chemistry*, vol. 88, no.2, pp. 309-317, 1984.
87. Mizuno, Masagi, Jiro Tanaka, and Issei Harada "Electronic spectra and structures of polyiodide chain complexes," *The Journal of Physical Chemistry*, vol. 85, no.13, pp. 1789-1794, 1981.
88. R. Guidelli, and G. Piccardi, "The dissociation constant of I<sub>3</sub><sup>-</sup> in the voltammetric behaviour of the iodine-iodide couple," *Electrochimica Acta*, vol. 12, no. 8, pp. 1085-1095, 1967.
89. L. I. Katzin, and E. Gebert, "The Iodide-Iodine-Triiodide Equilibrium and Ion Activity Coefficient Ratios," *Journal of the American Chemical Society*, vol. 77, no. 22, pp. 5814-5819, 1955.
90. Zhu, Kai, Song-Rim Jang, and Arthur J. Frank, "Effects of water intrusion on the charge-carrier dynamics, performance, and stability of dye-sensitized solar cells," *Energy & Environmental Science*, vol. 5, no. 11, pp. 9492-9495, 2012.